REPORT NO.
UCB/EERC-83/15
JULY 1983

EARTHQUAKE ENGINEERING RESEARCH CENTER

SEISMIC BEHAVIOR OF ACTIVE BEAM LINKS IN ECCENTRICALLY BRACED FRAMES

by

KEITH D. HJELMSTAD
EGOR P. POPOV

Report to the National Science Foundation

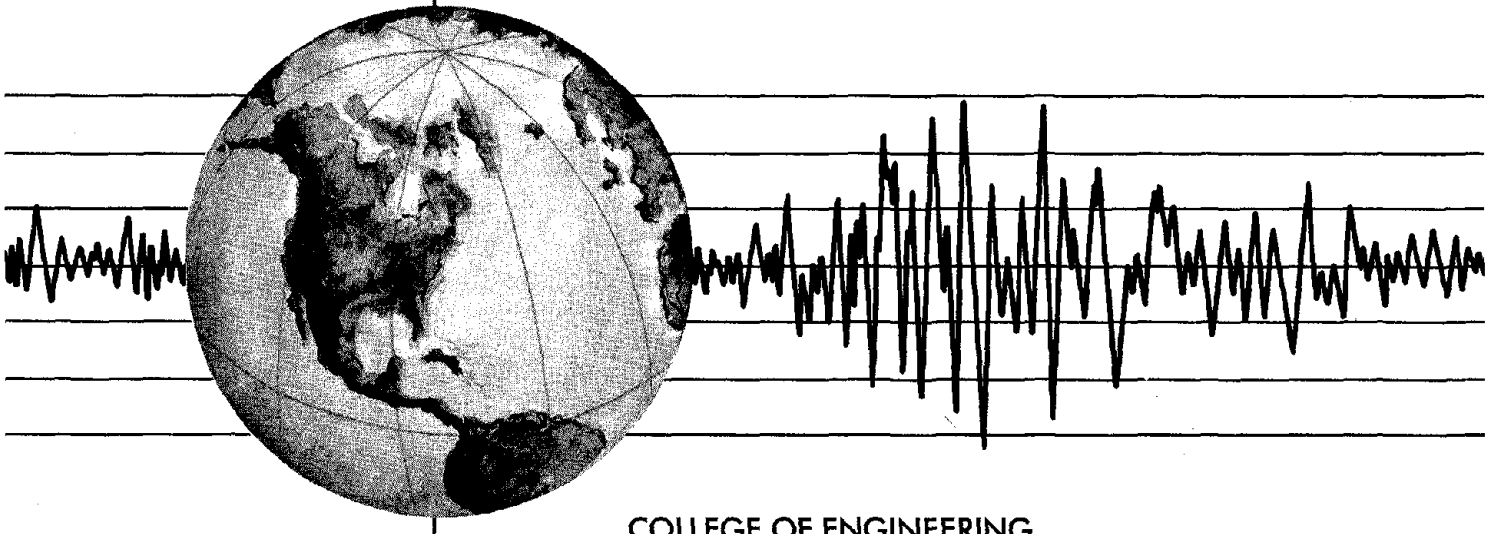

COLLEGE OF ENGINEERING

UNIVERSITY OF CALIFORNIA · Berkeley, California

For sale by the National Technical Information Service, U.S. Department of Commerce, Springfield, Virginia 22161.

See back of report for up to date listing of EERC reports.

SEISMIC BEHAVIOR OF ACTIVE BEAM LINKS IN ECCENTRICALLY BRACED FRAMES

by

Keith D. Hjelmstad
Assistant Research Engineer
University of California, Berkeley

and

Egor P. Popov
Professor of Civil Engineering
University of California, Berkeley

Report to
National Science Foundation

Report No. UCB/EERC - 83/15
Earthquake Engineering Research Center
University of California
Berkeley, California

July 1983

Abstract

An eccentrically brace frame is a structural framing system in which the axial forces in the bracing members are transferred either to other braces or to columns through shear and bending in a short beam segments called *active links.* The active link acts as a fuse, dissipating large amounts of input energy upon lateral overloading of the structure. Eccentrically braced frames are well suited for use in seismic regions because they can possess both a high elastic stiffness and good ductility.

Experimental research performed on models of eccentrically braced frames has clearly shown that the behavior of the active link elements dominates the behavior of the structure. While these experiments have demonstrated the good global behavior of the framing system they have not provided an adequate evaluation of the inelastic behavior of the active links, especially as regards the web buckling phenomenon. Furthermore, rigorous analytical tools for the inelastic analysis of the active link elements, and therefore eccentrically braced frames, appear to be lacking. These two important topics relating to active links in eccentrically braced frames are treated in this report.

In the first part of the report the results of an experimental study of the behavior of active links are presented. The study includes fifteen tests on full sized active links, which were performed to determine the general response characteristics of this type of element, especially as regards the buckling and post-buckling behavior. An effort is made to determine how much energy dissipation capacity an active link has, how the energy dissipation capacity is affected by the web buckling phenomenon, and how it can be extended through the introduction of transverse web stiffeners.

The second part of the report concerns the elasto-plastic analysis of eccentrically braced frames, with emphasis on accurately modeling the active link elements. Two analytical models are developed for this purpose. The first model employs the three dimensional equilibrium equations of a continuum, which are subsequently constrained through the introduction of a

kinematic hypothesis. The choice of kinematic hypothesis employed here accounts for warping of the cross section due to transverse shear. The elasto-plastic constitutive equations are treated with a viscoplastic model in a penalty approach. An iterative finite element procedure is used to solve the nonlinear problem.

The second model is developed entirely in terms of stress resultant quantities and their conjugate strain measures. The elasto-plastic constitutive equations are again treated using the penalty approach. The problem of describing a suitable plastic flow potential for the I-type cross section, which is typically used for active links, is given special consideration. Again, an iterative finite element solution scheme is employed.

Five numerical examples related to eccentrically braced frames are presented. The first two examples are designed to point out the features of each of the two mathematical models and to compare their differences. The last three examples represent a study of the behavior of three one bay, three story eccentrically braced frames employing different bracing arrangements. The three frames are subjected to cyclic loading and are evaluated with respect to stiffness, ultimate capacity, and member ductility demands.

Finally, an appendix dealing with the effects of warping restraint in thin walled beams is presented. The elastic case is solved in closed form. The elasto-plastic case is considered by employing the numerical solution procedure developed earlier.

Acknowledgements

This report represents the doctoral dissertation of Keith D. Hjelmstad, submitted to the Graduate Division of the University of California, Berkeley in partial satisfaction of the requirements for the degree of Doctor of Philosophy. Professor Egor P. Popov was the research supervisor. Thanks are extended to Professors Robert L. Taylor and Ole H. Hald for serving on the dissertation committee.

The many discussions with Juan C. Simo regarding the developments reported herein have been extremely helpful and are gratefully acknowledged. Helpful discussions with Philip C. Filippou and J. Marcial Blondet are also gratefully acknowledged.

The expert work of Gail Feasell with the preparation of illustrations, and that of Wesely Neighbor in the laboratory is much appreciated.

The authors are grateful for the financial support provided for this investigation by the National Science Foundation under Grant CEE 81-07217, and some support by the American Iron and Steel Institute. Any opinions, findings, conclusions, or recommendations expressed in this report are those of the writers and do not necessarily reflect the views of the sponsors.

Table of Contents

Introduction

Buildings constructed in seismic regions must satisfy two basic design requirements. First, the structure must have controlled drift under normal loading conditions in order to prevent structural and/or non-structural damage. Second, the structure must be safe from collapse in a severe earthquake. A ductile structure with a large elastic stiffness meets these requirements. Unfortunately, such systems are sometimes difficult to realize economically. Moment resisting frames, for example, have excellent ductility capability but tend to be flexible unless member sizes made relatively large and details are made sufficiently stiff. Concentrically braced frames, on the other hand, have high elastic stiffnesses but possess limited ductility capability. The eccentrically braced frame is a hybrid system having features common to both the moment resisting frame and the concentrically braced frame. This system offers the advantage of economy and satisfies the two diverse requirements of stiffness and ductility for seismic design [42,43].

An eccentrically braced frame, two examples of which are shown in Fig. 0.1, is any braced framing system in which the axial forces in a brace are transferred either to another brace or to a column through shear and bending in a short segment of beam called an *active link.* The active link acts as a structural fuse, generally behaving elastically under normal loading conditions, but deforming inelastically upon overloading of the frame. A large amount of energy can be dissipated through inelastic deformation in the active link regions. This energy dissipation mechanism allows for the ductile behavior of eccentrically braced frames.

To put the concept of eccentric bracing into perspective, it is instructive to consider the simple system shown in Fig. 0.2 in the context of the two design requirements given above. The ratio of the height of the structure h, to the breadth L, will be called the aspect ratio h/L. and the ratio of the length of the eccentric element e, to the breadth L, the eccentricity ratio e/L.

The elastic lateral stiffness of the simple frame is shown in Fig. 0.3(a) as a function of the eccentricity ratio for various aspect ratios, keeping all other properties of the structure in the same relative proportions. The stiffness values for each value of the aspect ratio have been normalized by the value of stiffness at $e/L = 1$. It is evident that a large elastic stiffness can be achieved by employing short active links (small e/L). In fact, at $e/L = 0$, the stiffness of the concentrically braced frame is recovered. On the other hand, values of $e/L > 0.5$ show little advantage over the unbraced (moment resisting) frame. The split-K framing system, shown in Fig. 0.3(b), illustrates even more dramatically that the eccentricity ratio must be kept small to achieve high elastic lateral frame stiffness.

When one considers the probable mode of inelastic deformation of the structure, it becomes clear that the smaller is the active link, the greater will be its ductility requirements upon overloading. To see that this statement is true, consider again the simple frame whose collapse mechanism is shown in Fig. 0.4. Geometrical considerations show that the member deformation γ, is related to the structure deformation θ, as

$$\gamma e = \theta L \tag{0.1}$$

Hence, if e/L is small, then γ/θ will be large.

Experimental research on scale models of eccentrically braced frames has shown that the system behaves well when subjected to severe pseudo-static cyclic loading [42,27] and to dynamic loading [49]. These studies have also verified that the demands placed on the active links can be extreme for severe lateral loading. Under these conditions, the active links often experience inelastic web buckling. Previous work on the shear buckling of web plates has focussed on applications to plate girders having thin webs [1,6]. Certain similarities do exist between the buckling of plate girders and the buckling of active links. However, in the former, buckling generally precedes inelasticity, whereas, in the latter, inelasticity almost invariably precedes buckling. Hence, a direct application of plate girder analysis techniques cannot be made.

Two important problems relating to active links in eccentrically braced frames are addressed in this work. The first part of the dissertation is concerned with determining how much energy dissipation capacity is available in an active link, and how that capacity is affected by the inelastic web buckling phenomenon. The second part of dissertation deals with the problem of determining what the magnitude of the inelastic deformations are for an active link which is part of a complex structural system. An estimate of such member ductility demands can be obtained from an inelastic analysis of the system. Motivated by this observation, the second topic examined in this dissertation concerns the inelastic analysis of eccentrically braced frames, with emphasis on an accurate characterization of the inelastic pre-buckling behavior of the active link elements.

The nature of the phenomena involved and the goals of the study have dictated two distinctly different approachs to the problems considered, the first being experimental and the second being analytical. The following paragraphs describe the content of each of the chapters, and the approaches followed in them.

The first three chapters are concerned with the problem of inelastic web buckling of active links subjected to severe cyclic loading. Due to the inherent complexity of this phenomenon, an experimental approach to the problem has been adopted here. The goal of this portion of the study is to obtain data on the general response characteristics of active links with emphasis on buckling and post-buckling behavior. In particular, the extension of energy dissipation capacity through transverse stiffening of the web region is studied. Fifteen full sized active links with various stiffening arrangements have been tested under pseudo-static loading conditions in an effort to achieve these goals.

In Chapter 1 the groundwork of the experimental program is laid. The modeling assumptions are discussed and the testing procedure is described. Chapter 2 gives a chronologically oriented description of each of the fifteen tests. Shear-displacement hysteretic characteristics of each link are presented along with specific observations made during the experiments. General conclusions regarding the behavior of the test specimens are made in Chapter 3, wherein the

quantification of certain important limit states is also made.

Chapters 4 through 7 are concerned with the problem of analyzing eccentrically braced frames having active links which are stiffened against buckling. An accurate analysis of such frames relies upon proper modeling of the active links. Hence, the developments are slanted toward the analysis of the elastic and inelastic, pre-buckling behavior of active links. Inasmuch as active links are likely to experience moderately large deformations, second order theories are considered. Material behavior is assumed to be perfectly elasto-plastic.

Chapter 4 gives an introduction to the analysis of active links and a brief account of some previous efforts in this direction. Comments are confined mostly to applications involving the analysis of eccentrically braced frames. In Chapter 5, a model of active link behavior is developed starting from a three dimensional continuum theory and subsequently constraining it by introducing a kinematic hypothesis. The specific kinematic hypothesis employed, first considered in [45] for problems of elastic stability, is able to account for the warping of the cross section which necessarily accompanies transverse shearing. A viscoplastic penalty approach to the problem of modeling elasto-plastic material behavior is employed. A Finite Element discretization of the domain is used in conjunction with a Newton-Raphson iteration scheme to solve the nonlinear problem. Since the model is able to discern phenomena which are local to the cross section of the member it has been called a "local approach".

A simpler model, developed entirely in terms of stress resultants and their conjugate strain measures, is presented in Chapter 6. Again, a viscoplastic penalty approach to the elasto-plastic constitutive equations is used. The problem of describing the yield potential of an I-beam, suitable for use in this approach, is given special consideration. The solution algorithm is similar to the one used in Chapter 5.

Finally, five example applications are presented in Chapter 7. The first two examples are designed to show the characteristics of the two analytical models developed in Chapters 5 and 6. The second example has the specific purpose of assessing the suitability of the stress resultant model for use in the analysis of eccentrically braced frames. This assessment is accomplished

by comparing the results obtained with the stress resultant model with those obtained using the local approach. The last three examples represent a study of three single bay, three story eccentrically braced frames subjected to cyclically applied loading. Some comments are made regarding the inelastic behavior of the frames studied.

Motivated by earlier work [43] which idealized the I-beam as a sandwich construction, an appendix is presented which generally treats the problem of warping restraint in thin walled members. It is felt that the thin walled approximation is more appropriate for the I-section than is the sandwich idealization.

It is emphasised that the experimental and analytical portions of the present work treat different aspects of the active link problem. The analytical procedures developed are not able to characterize the inelastic web buckling phenomenon studied in the experiments. Hence, the correlations made between the experiments and analytical results are circumspect.

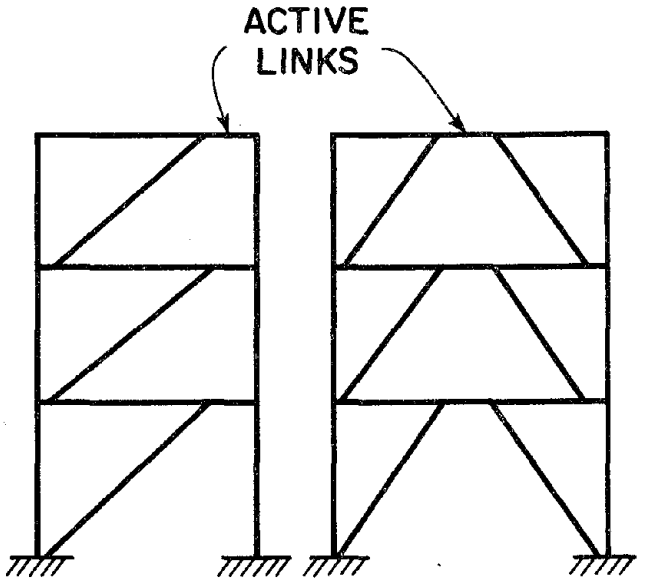

Fig. 0.1 Typical Eccentrically Braced Frames

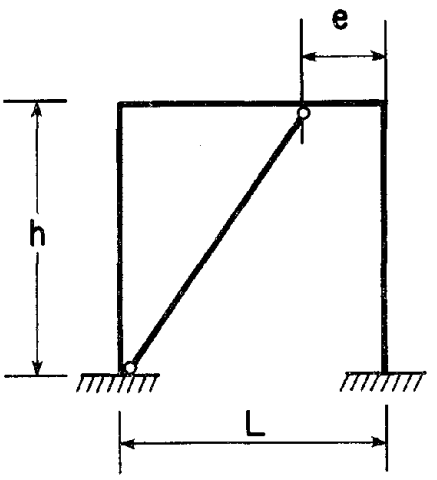

Fig. 0.2 Simple Eccentrically Braced Frame

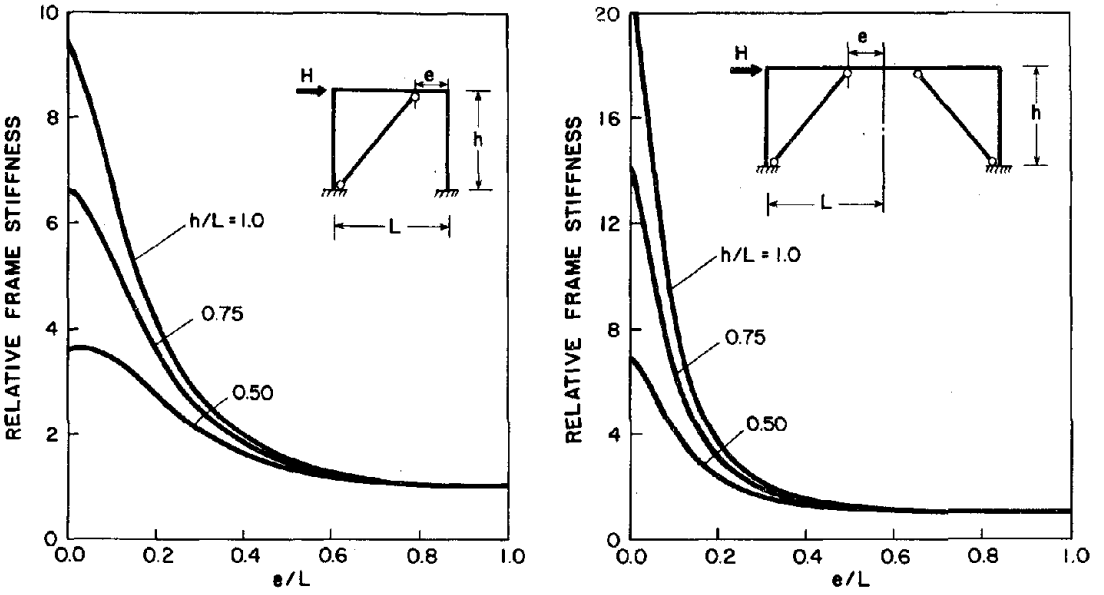

(a) Single Diagonal Brace

(b) Split-K Brace

Fig. 0.3 Variation of Elastic Lateral Stiffness with e/L for Two Simple Frames Employing Different Bracing Arrangements

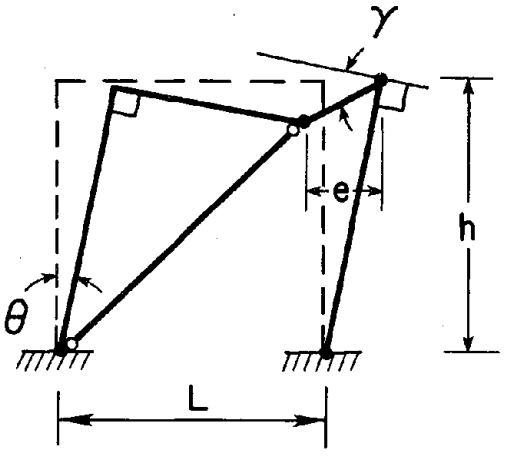

Fig. 0.4 Collapse Mechanism of Simple Eccentrically Braced Frame

Chapter 1

Experimental Program

1.0. Introduction

The tasks in an experimental investigation are first to model as accurately as possible the physical domain of the problem and then to excite the model in an appropriate way. It is seldom feasible to model a complete structure due to physical limitations of excitation apparati, limits of resolution of response measurement devices, and difficulties associated with measuring internal force quantities. Furthermore, it is not practical to test an entire structure to determine the local behavior of certain of its elements. In these cases, testing of an isolated part of the structure provides an attractive alternative. This approach has been adopted in the present study.

Past research on eccentrically braced frames has been devoted to experimental investigations of one-third scale, three story, one bay frames [27,43]. While these tests have demonstrated the good behavior of eccentrically braced frames under severe cyclic loading and have yielded valuable data on the global response of such frames, they have not provided an adequate evaluation of the local behavior of the active link elements. The need for better information regarding the inelastic prebuckling and postbuckling behavior of active links motivated the experimental investigation reported herein.

1.1. Modeling of Active Links

The isolation of an element of a structure requires that certain surfaces which are in the interior of the global domain must serve as boundaries of the isolated domain. Constraints imposed at these boundaries should model as closely as possible the expected state in the prototype structure. For the purpose of the present investigation, the model was extracted from two possible prototype configurations as shown in Fig. 1.1. The fully welded, heavy end plates

imposed the following boundary constraints on the test specimens: (1) Warping of the cross section was totally restrained at both ends of the link, and (2) the flanges were held fixed at both ends of the link.

Since the link beam will generally be either adjacent to a region of beam with low shear (and a correspondingly small amount of warping) or welded to a column flange, warping restraint will generally exist in real applications. Such warping restraint is generally localized and thus should not significantly affect overall link response. The effects of warping restraint are treated analytically in Appendix I.

It is good design practice to stiffen a beam at the point of application of a concentrated load (such as that occuring at a brace-beam intersection) to prevent local failures due to web crippling. Hence, fixity of the flanges at the ends of the test specimens closely represents the situation commonly found in practice.

Localizing the specimen for testing purposes precludes modeling the interaction between the element and the global system. In reality, peculiarities in the element force-deformation relationships cause the internal forces to redistribute throughout the structure. Such a redistribution of forces means that the input to each element is changed. This feedback mechanism has not been considered here. It is felt that this global problem is better handled analytically.

In view of the preceding argument, the imposed loading was chosen to be radial and had the following characteristics: (1) Constant resultant shear, (2) linearly varying bending moment, reaching equal end moments and vanishing at midspan, and (3) zero net axial force. The acceptability of these loading assumptions is clearly application dependent. Judgement should be used in extrapolating the results to situations which significantly depart from the conditions of these tests.

The testing system, designed to impart the aforementioned conditions, is shown schematically in Fig. 1.2(a). The load was transferred from the actuator to the specimen via a rigid L-shaped member which slid on three Teflon-coated supports. Frictional forces induced at the supports were determined to be negligible in comparison with the resolution of the load

measuring devices. The specimens were bolted securely to the testing apparatus through the end plates. The side arm was provided to ensure system stability. Loads were monitored in the side arm throughout the tests and were generally found to be negligible. A photograph of the testing system is shown in Fig. 1.2(b).

1.2. Loading History

The ultimate goal of this research is to make inferences about the behavior of active links in eccentrically braced frames under the influence of earthquake-type actions. The deformations experienced by any given active link depend upon the link's constitution, the structure topology, and the excitation history. This investigation aims at gaining an understanding of the action-deformation properties of active link type elements in a general sense. To this end, structure topology and excitation history have been simplified. Once active link behavior has been explicated, the more general problem of eccentrically braced frame response to earthquake groundmotion can be approached analytically.

All specimens were subjected to quasi-statically applied cycles of relative end displacement in the plane of the specimen's web. This loading program consisted of one cycle at a displacement magnitude of one half inch and two cycles each at displacement magnitudes of one inch, one and a half inches, two inches, etc. until failure of the specimen occurred. Each test was preceded by linear range cycling to determine the elastic response of each link. Failure was defined as substantial loss of load carrying capacity. Material and inertial effects arising from the dynamic nature of earthquake loading were neglected in this test program.

For future reference each cycle consisted of two displacement excursions from a point of zero load, one in a northerly direction (N) and one in a southerly direction (S). The north half cycle always preceded the south half cycle.

1.3. The Test Specimens

The test specimens were chosen to model, in full size, link beams likely to be encountered in real applications. Some of the important properties of each of the fifteen specimens are summarized in Table 1.1, which lists the section used, the length of the specimen[†], the dimensionless ratios a/t_w and α (described below), and the sizes of each of the panel zones.

Specimen	Section	Length (in)	$\frac{a}{t_w}$	α	Longitudinal Panel Zone Dimensions	
					No.	(inches - E to W)
1	W18×40	28.0	53.6	1.27	1	28.0
2	W18×40	28.0	44.0	1.27	2	14.0, 14.0
3	W18×40	28.0	28.9	1.27	3	9.33, 9.33, 9.33
4	W18×40	28.0	21.4	1.27	4	7.0, 7.0, 7.0, 7.0
5	W18×40	28.0	33.8	1.27	3	8.5, 11.0, 8.5
6	W18×40	28.0	-	1.27	3	11.2, 8.4, 8.4
7	W18×35	28.0	28.0	0.85	3	9.33, 9.33, 9.33
8	W18×60	36.0	40.1	1.17	1	36.0
9	W18×40	36.0	37.4	0.98	3	12.0, 12.0, 12.0
10	W16×26	36.0	57.0	0.71	1	36.0
11	W18×35	36.0	52.3	0.66	1	36.0
12	W12×22	36.0	43.2	0.37	1	36.0
13	W16×26	36.0	44.7	0.71	3	12.0, 12.0, 12.0
14	W18×35	36.0	36.3	0.66	3	12.0, 12.0, 12.0
15	W12×22	36.0	-	0.37	3	6.0, 24.0, 6.0

Table 1.1 Test Specimen Properties

The quantity a/t_w is the ratio of the smallest dimension of the largest panel zone(s), a, to the thickness of the web, t_w. This ratio is useful in characterizing the buckling limit state of an active link. In these tests, only Specimens 5, 6, and 15 had unequally spaced stiffeners. Values of a/t_w are not reported for either Specimen 6, in which the value of a is not known due to the presence of a gusset plate, or for Specimen 15, in which the largest panel zone was not critical from the standpoint of web buckling.

[†] excluding the end plates

For the test configuration employed in the present investigation the equilibrium equation $2M = LV$ holds, where M is the absolute value of the moment at both ends of the specimen, L is the length of the specimen, and V is the transverse shear force. Inspired by this equation, we define the dimensionless ratio α as

$$\alpha = \frac{2M^*}{L\,V_0} = \frac{\sigma_0}{\tau_0}\,\frac{h}{L}\,\frac{\Omega_f}{\Omega_w} \tag{1.1}$$

where M^* is the plastic moment of the flanges alone and V_0 is the fully plastic shear of the section, given respectively by

$$M^* = \sigma_0 h b t_f$$

$$V_0 = \tau_0 h t_w \tag{1.2}$$

In these equations, h is the distance between the centroids of the two flanges, b is the flange width, t_f is the flange thickness, t_w is the web thickness, σ_0 is the yield stress in tension, τ_0 is the yield stress in pure shear, L is the length of the link, and Ω_f and Ω_w are the gross areas of the flanges and web, respectively. The index α can be used as a rough guide in describing the behavior of active links. Active links having values of $\alpha > 1$ are likely to yield predominantly in shear. Such links will often be called *shear links*. Active links having values of $\alpha < 1$ will generally be subject to moment-shear interaction. For lack of a better name, these links will often be called *bending links*.

Section Properties.- The geometric properties of the five sections used are given in Table 1.2, in which d is the section depth, t_w is the web thickness, b is the flange width, t_f is the flange thickness, I is the moment of inertia, Ω is the area, and κ is the shear coefficient, an expression for which can be found in [2].

Material Properties.- The ability of an active link to dissipate energy depends strongly on the mechanical properties of the material. The material must be highly ductile in order to withstand the large inelastic deformations required of it. In general, the low strength carbon steels

Section	d (in)	t_w (in)	b (in)	t_f (in)	I (in^4)	Ω (in^2)	κ
W12×22	12.31	0.266	4.000	0.415	154	6.37	0.478
W16×26	15.70	0.263	5.484	0.356	312	7.85	0.496
W18×35	17.69	0.324	5.906	0.378	475	9.95	0.541
W18×40	17.88	0.314	5.985	0.521	605	11.52	0.457
W18×60	18.28	0.422	7.563	0.681	978	17.44	0.408

Table 1.2 Test Specimen Section Properties

are preferred in applications requiring such high ductility. All specimens in this investigation were fabricated from ASTM A36 steel.

The initial properties of the material in the test specimens were determined by uniaxial tension tests on coupons extracted from the flanges and webs of the beam stock for each section size; one coupon being taken from each flange, and two from the web. The results of these tests are summarized in Table 1.3, in which σ_0 is the yield stress, σ_u is the ultimate stress, ϵ_{sh} is the strain at the onset of strain hardening, ϵ_u is the strain corresponding to σ_u, and E is Young's modulus. All of the material used in the experimental program exhibited the typical behavior shown in Fig. 1.3, consisting of a stiff elastic range followed by a plastic plateu and finally a region of strain hardening. Values given in the table represent averages of duplicate coupon tests. Except for the W12×22, the tests gave reasonably consistent results. The cyclic material properties, which can be quite different from the virgin properties, will undoubtedly dominate the response of cyclically loaded links. The monotonic material properties do, however, provide good reference values for comparisons between specimens.

End Connection Details.- It was not the purpose of this investigation to explore the effects of the end connection details. All of the connections were moment resisting, and were

Specimen		σ_0	σ_u	ϵ_{sh}	ϵ_u	E
Section	Location	ksi	ksi	in/in	in/in	ksi
W12×22	web	55.5	68.3	0.021	0.16	29700
	flange	42.4	63.4	0.025	0.24	29800
W16×26	web	48.3	67.2	0.026	0.24	30150
	flange	49.7	68.9	0.018	0.21	30100
W18×35	web	46.7	68.9	0.020	0.20	28650
	flange	41.4	63.7	0.022	0.21	28600
W18×40	web	39.5	60.1	0.018	0.22	28300
	flange	35.0	58.5	0.014	0.24	28000
W18×60	web	44.4	68.4	0.019	0.21	28600
	flange	38.9	66.6	0.013	0.24	29200

Table 1.3 Test Secimen Material Properties

designed to develop forces somewhat greater than the full plastic capacity of the member so as to allow for strain hardening effects. It is emphasized that integrity of the connections is extremely important for the active link regions of eccentrically braced frames. A brittle failure of a connection could destroy the ductile behavior of an eccentrically braced frame.

Each of the test specimens employed one of the connection types shown in Fig. 1.4, and described below:

Type 1: The Type 1 connection shown in Fig. 1.4(a) employs full penetration welds of the flanges and web to the end plate. The flange welds were made using cope holes and backup bars.

Type 2: The Type 2 connection shown in Fig. 1.4(b) employs fillet welds all around the flanges and web.

Type 3: The Type 3 connection shown in Fig. 1.4(c) employs full penetration welds with cope holes and backup bars for the flanges, as in the Type 1 connection. In the web region, a thick gusset plate was first fillet welded to the end plate and subsequently fillet welded to the web.

Specimens 1 through 5 had Type 1 connections at both ends, Specimen 6 had a Type 2 connection at one end and a Type 3 at the other, and the remaining specimens had exclusively Type 2 connections.

Transverse Stiffeners.- Transverse stiffeners were employed in these tests to prevent, or at least delay, inelastic buckling of the webs of the active links. No effort was made in the present investigation to determine the optimal size required of the stiffener to perform its function. Transverse stiffeners for all specimens employing them were 0.375 in. thick, cut flush with the flanges, and fillet welded to the web and to both flanges. Intermittent welding was not employed. Stiffeners were always placed in pairs, one on each side of the web.

1.4. Instrumentation and Data Acquisition

The response of each specimen was monitored electronically using a Neff high speed data acquisition system, in conjunction with a Nova computer. Data were read and stored on a hard disc in digital form. After each test, the digitized data were transferred to a CDC6400 mainframe computer using magnetic tape storage. All subsequent data reduction was performed on the CDC6400, using programs written for this special purpose.

Measurement of forces in the specimens was accomplished via load cells located in the loading ram and in the side arm (Fig. 1.2). With these two forces known, the stress resultants at any point in the specimen could be obtained from static equilibrium. Tolerances for the load cells were taken to be ± 1.0 k for the 350 k capacity loading ram load cell and ± 0.5 k for the 125 k capacity side arm load cell. Frictional resistance of the test frame sliding on its Teflon-coated support pedestals was determined to be less than the load cell resolution and was therefore neglected.

Movement of the specimen's loaded end (u_1 , u_2 , and u_3 in Fig. 1.5(a)) was monitored with linear potentiometers for all specimens, each u_i being the average reading of two instruments. Movement of the supported end (u_4 , u_5 , and u_6) was monitored during the testing of Specimen 1 using linear variable differential transformers (LVDT's) and was found to be small

in comparison with the displacement of the loaded end. These measurements were discontinued in subsequent tests. Lateral displacement of the specimen at stiffener locations were measured with linear potentiometers for those specimens that had stiffeners. Additionally, an array (usually 3 by 3) of linear potentiometers was used to monitor out-of-plane displacements of the web. Resolution of the linear potentiometers was ± 0.001 *in.* and that of the LVDT's was ± 0.0001 *in.*

Placement of strain gages and strain gage rosettes varied from specimen to specimen. Fig. 1.5(b) shows typical locations for these gages for a three panel specimen. Flange and stiffener strains were measured with uniaxial SR-4 post yield strain gages (0.25 in. gage length), and web strains were measured with SR-4 post yield strain gage rosettes (0.125 in. gage length). The flange gages were placed at the center of the flange width opposite the flange-web junction. The stiffener gages were placed in pairs, one third of the stiffener width away from the web plate, at the center of the depth of the section. The web rosettes were usually placed in pairs on opposite side of the web at the center of each panel zone. Specimen 1 was an exception, having a three by three array of rosettes. The adhesive used limited maximum strain measurements to values between 5 and 10 percent strain. Strain gage readings were assumed accurate to within 50 microstrain due to neglect of temperature effects.

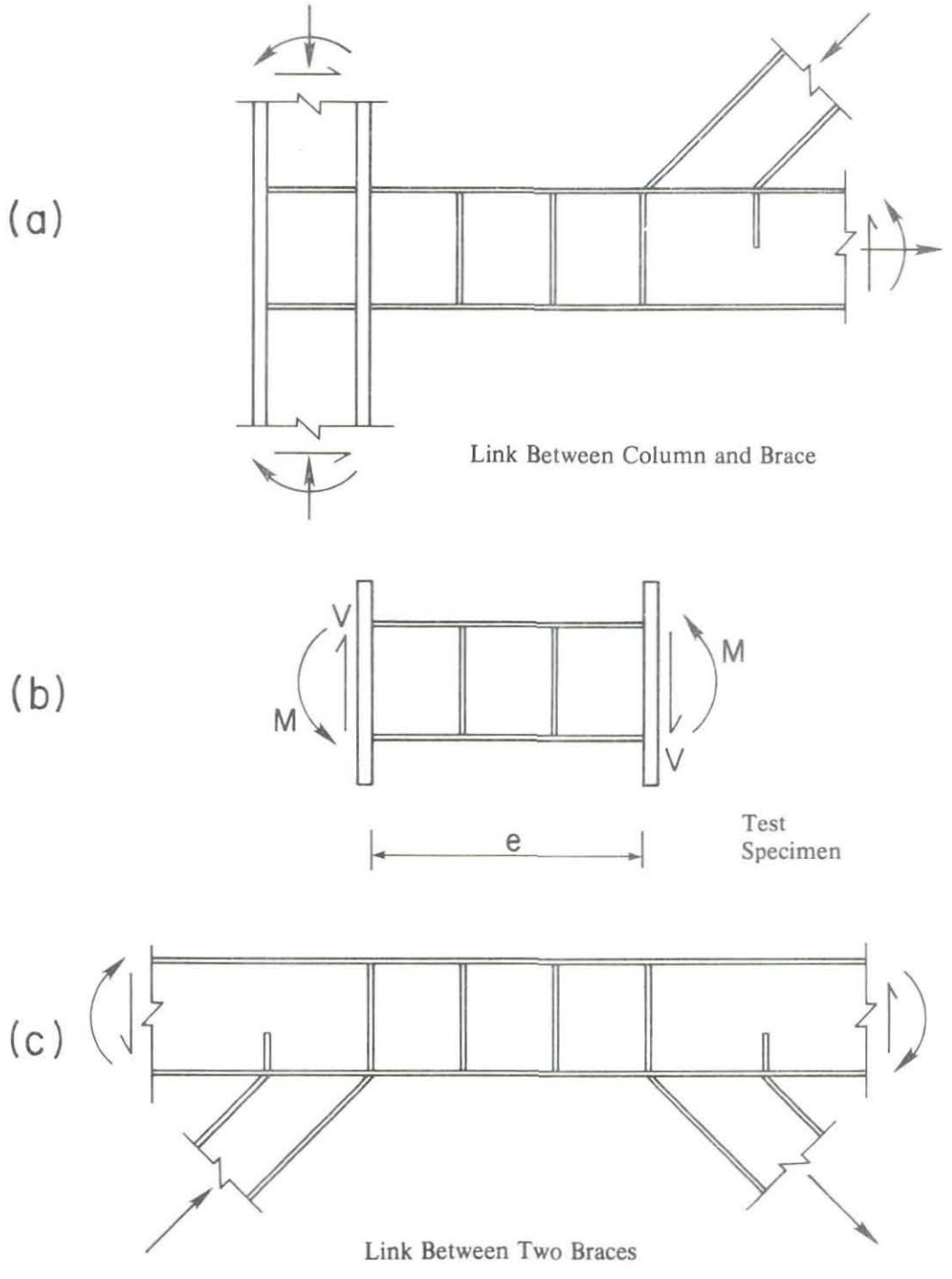

Fig. 1.1 Extraction of Active Link Model From Two Possible Prototype Structures

(a)

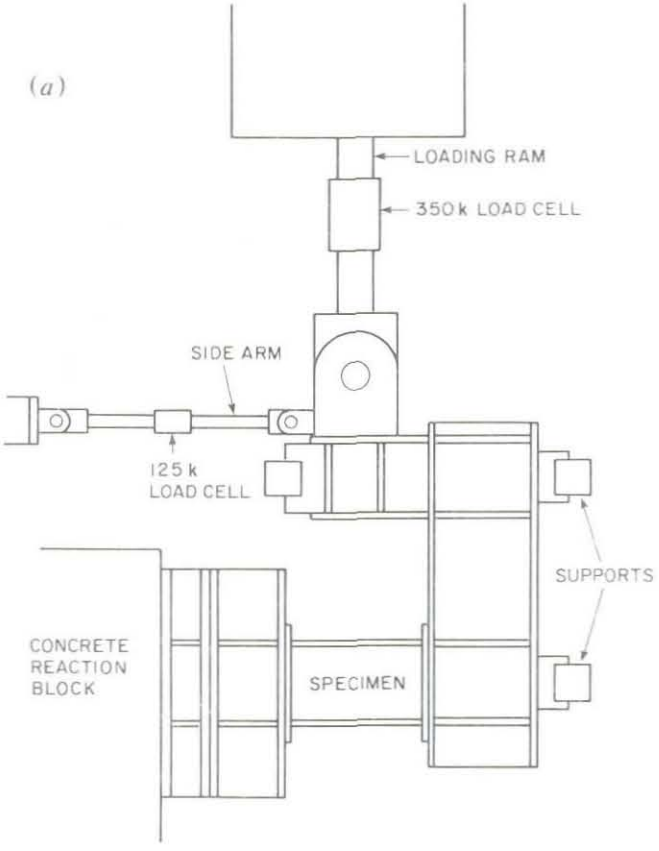

(b)

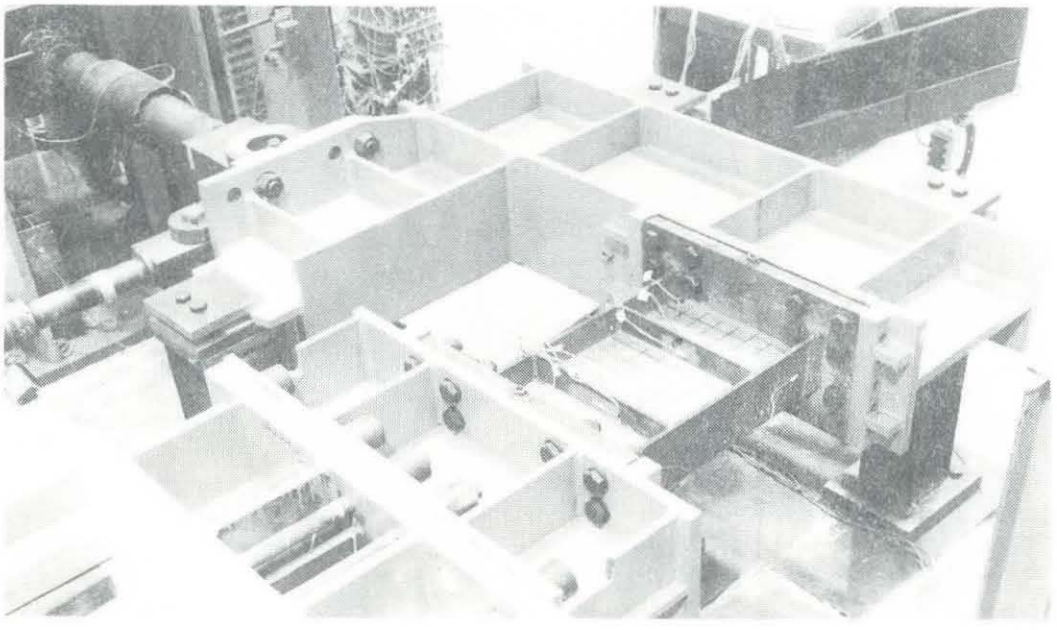

Fig. 1.2 Testing Arrangement

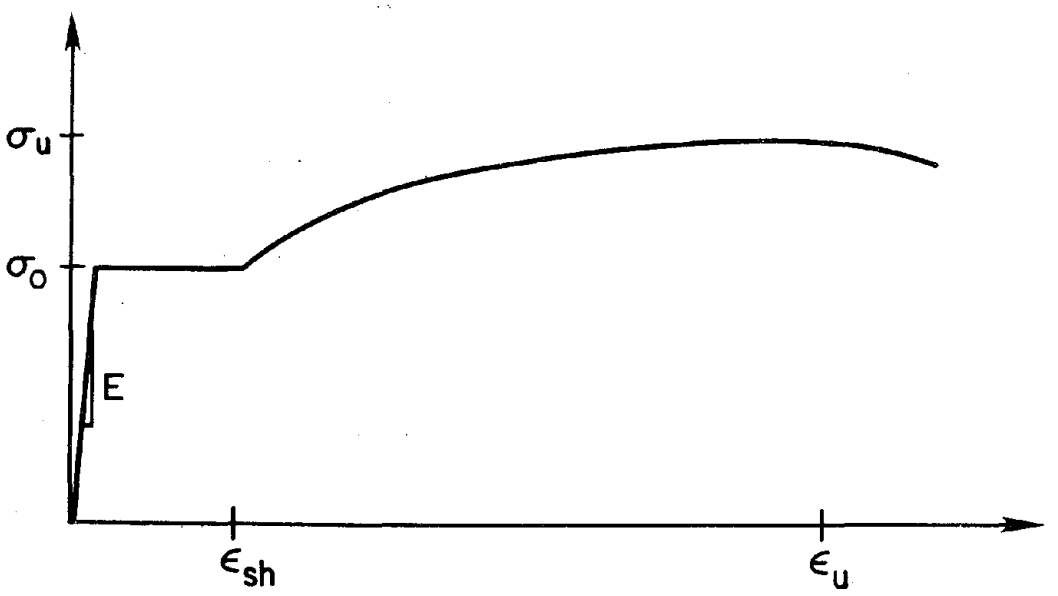

Fig. 1.3 Typical Uniaxial Stress-Strain Curve for Steel used in the Experimental Program

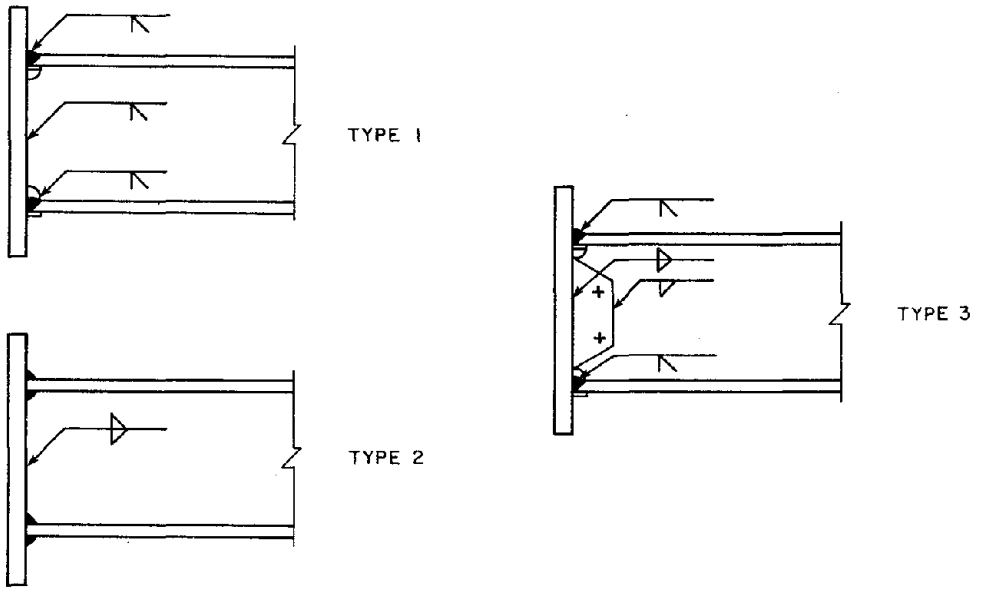

Fig. 1.4 End Connection Details

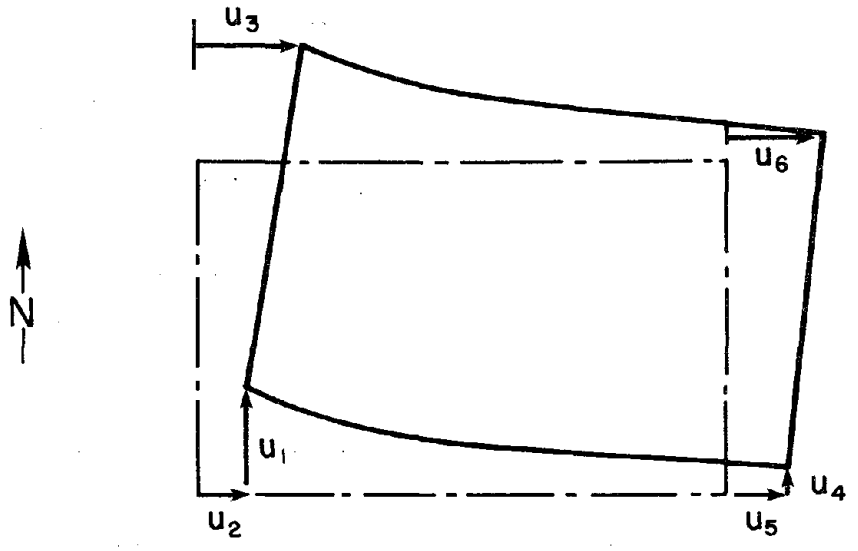

(a) Gross End Displacements

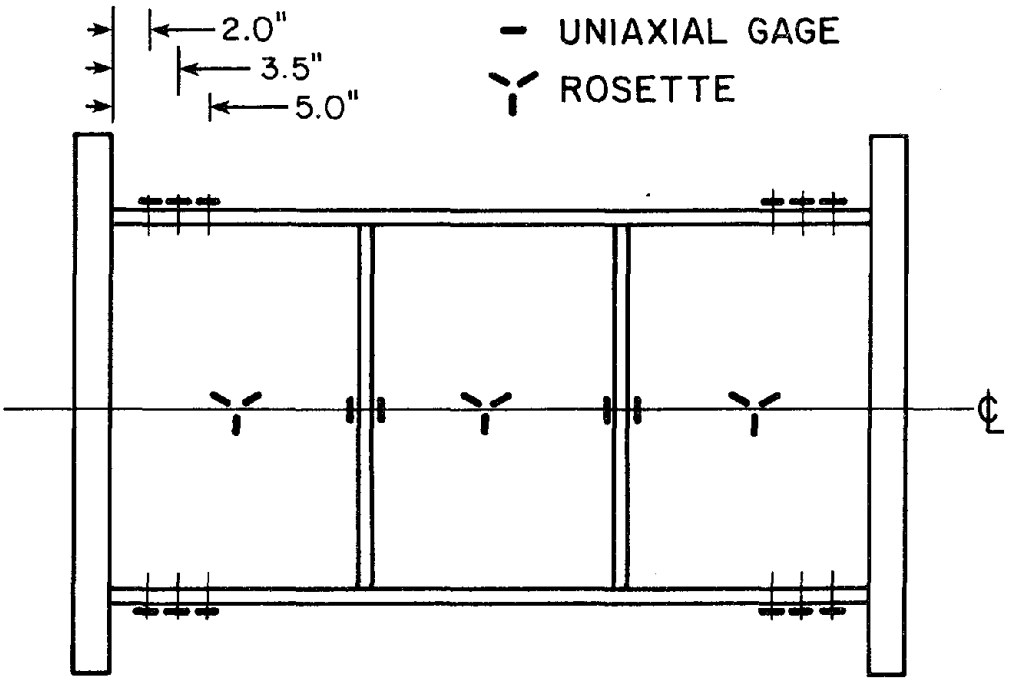

(b) Strain Gage Locations

Fig. 1.5 Measurement of Deformation Response

Chapter 2

The Hysteretic Behavior of Active Links: A Chronological History of the Tests

2.0. Introduction

In this chapter the hysteretic behavior of active links is studied by examining the response of the fifteen test specimens described in the previous chapter. Each of the fifteen tests is presented individually, following the order that the specimens were tested. Some conclusions based on observations of the hysteretic behavior are made, but most generalizations will be presented in Chapter 3.

To facilitate the presentation and discussion of specimen behavior, reference is repeatedly made to the global force-displacement histories (i.e. applied shear force vs. relative end displacement) of each specimen. The following nomenclature and conventions are used in describing the hysteretic behavior of the test specimens: Positive displacements are northerly, negative displacements are southerly, and positive shear force causes positive displacement. An *absolute* displacement is taken to mean displacement relative to the undeformed specimen. A *relative* displacement is taken to mean displacement relative to the most recent unloaded (but not generally unstressed) state as sensed by the load cell in the hydraulic loading ram. Relative displacements are generally a more meaningful measure of the deformation of a specimen. The loading was controlled by specifying absolute displacements. Each cycle consisted of an imposed northerly displacement followed by a southerly one of the same absolute magnitude.

2.1. The Tests

Specimen 1.- Specimen 1 was a shear link (W18×40, 28 inches long) constructed without stiffening the web region. Consequently, it contained a single panel zone 28.0 × 16.9 inches in size[†]. The shorter sides of the panel boundary were fixed to end plates while the longer sides

[†] Panel dimensions are taken to be clear distances without discounting for fillets at welds or web-flange junctions.

were partially restrained by the flanges. The action-deformation relationship recorded for Specimen 1 is shown in Fig. 2.1(a).

The initial loading to +0.5 inch displacement showed a high elastic stiffness followed by a plastic plateau at 117.8 k. A slight amount of strain hardening was noted near the maximum displacement in this virgin excursion. Upon load reversal, an apparent "Bauschinger effect" was exhibited. (As an example in Chapter 7 shows, this so-called "Bauschinger effect" is due, in part, to the distribution of residual inelastic strains over the cross section of the link and not exclusively to the mechanical properties of the material. The resemblance of this geometric effect to the true Bauschinger effect associated with material constitutive behavior has motivated the denomination.) The strains in the web were nearly pure shear during the first cycle and had magnitudes of approximately one percent in both the northerly and southerly excursions measured relative to the undeformed configuration (ie. the southerly excursion had two percent relative strains). The southern leg of the first cycle showed strain hardening at an absolute displacement of -0.1 inches.

Substantial web buckling occurred in cycle 2N (ie. the second cycle in the northerly direction) at a displacement of 0.9 inches relative to the most recent unloaded state. The applied shear force at buckling was 134.9 k, or 1.15 times the yield shear. Buckling in the opposite direction took place at identical load and relative displacement magnitudes. First buckling marked the highest attained load as well as the beginning of significant load carrying capacity degradation. Amplitude of out-of-plane web displacement due to buckling increased with each cycle with maximum values of around 3.0 inches in the latter portions of the test (roughly equal to half the flange width). The hysteretic behavior recorded for Specimen 1 was typical of an active link experiencing cyclic inelastic web buckling. Each cycle exhibited a distinct buckling load followed by a drop in load carrying capacity. The loss in load carrying capacity was subsequently arrested due to the formation of a tension field. Tension field action allowed load losses to be recovered, the buckling load often being surpassed. The cyclic web buckling phenomenon will be discussed in greater detail in Chapter 3.

Tearing of material at the center of the panel occurred upon the first excursion to +2.0 inches absolute displacement as a direct consequence of the distress caused by the cyclic changing of the buckled mode shapes. This tearing severed the tension field which is the predominant load carrying mechanism in a severly buckled link. Cycle 7 was carried out even though severe tearing was already present. A photograph of the failed specimen is shown in Fig. 2.1(b).

Specimen 2.- Specimen 2 was identical to Specimen 1 except for the addition of a transverse stiffener in the center, which created two equal panel zones with dimensions 16.9 × 13.8 inches. The response of this specimen, shown in Fig. 2.2(a), was nearly identical to that of Specimen 1 for the first cycle, confirming the belief that the addition of transverse stiffeners has little effect on the inelastic prebuckling shear behavior of an active link. Generalized yielding occurred at a load of 120.2 k.

The effect of stiffening the web plate was to delay buckling until the second excursion to -1.0 inches absolute displacement. Buckling first occurred in the east panel at a load of 160.5 k and a displacement of 1.74 inches relative to the most recent unloaded state. Substantial out-of-plane web deflection was not noted until the fourth cycle of the test. The smaller panel size helped control the amplitude of web buckling thereby lessening the severity of load carrying capacity degradation of the member upon cycling. The stiffener showed visible distress in the later cycles.

Although the west panel did eventually buckle, it wasn't until late in the loading program that this buckling occurred. Consequently, deformation concentrated in the east panel during most of the test. This behavior was noted to varying degrees in all of the multi-panel links but Specimen 2 provided one of the clearest examples of it. Concentration of deformation puts a higher demand on the material in the buckled panel and is thus considered undesirable.

Due to geometric and material imperfections, one panel in an otherwise symmetrical link is likely to buckle first. We have seen that buckling causes a deterioration in load carrying

capacity. It seem reasonable that the panel which buckled first would limit the load taken by the link, thereby protecting the other panel(s) from buckling. In some cases, however, tension field action in the buckled panel, together with material softening associated with inelastic cycling in the unbuckled panel(s), may lead to buckling elsewhere.

Failure of Specimen 2 occurred in cycle 8 after one excursion to +2.5 inches absolute displacement. The manifestation of failure was tearing at the web-flange junction, a mode of failure characteristic of most of the multi-panel links. The failed specimen is shown in Fig. 2.2(b).

Specimen 3.- Specimen 3 was identical to Specimens 1 and 2 except that it had two equally spaced transverse stiffeners. With two sets of stiffeners, the clear panel sizes were 9.1 × 16.9 inches. Although weld imperfections in the flanges caused premature failure, valuable information was still obtained.

The response of Specimen 3 was similar to that of Specimens 1 and 2 in the pre-buckling range of behavior. The hysteretic loops are shown in Fig. 2.3(a). When the southwest flange weld fractured in cycle 5, no web buckling had been noted. The weld was repaired and the test was resumed. Buckling of the web occurred in the northern leg of cycle 6 at a load of 182.9 k and a relative displacement of 2.96 inches. As can be seen in Fig. 2.3(b), buckling was well distributed among the three panel zones. Shortly after first buckling a second flange weld failure occurred. The test was terminated since evidence of load carrying capacity degradation had already been shown.

Specimen 4.- A further variation on the original theme, Specimen 4 had four equal panel zones of dimension 6.6 × 16.9 inches. As can be seen in Table 1.1, this specimen had the smallest a/t_w ratio of all of the fifteen specimens. The hysteretic behavior is shown in Fig. 2.4(a). One can note a remarkable improvement over the behavior exhibited by Specimen 1. Deformations throughout most of the test were realized through inelastic shearing of the web

region. Web buckling was slight, not occurring until the southern part of cycle 9 at a load of 206.5 k and a relative displacement of 5.0 inches. Failure occurred in cycle 11 by tearing at the web-flange junctions originating in the cope holes in each corner. The failed specimen is shown in Fig. 2.4(b).

The first four specimens show clearly the superior energy dissipation capacity of stiffened links. A stiffened link is able to accomplish energy dissipation through inelastic shearing strains rather than through inelastic web buckling. When buckling is prevented, the inelastic shearing deformations distribute evenly throughout a link causing less intense working of a greater volume of material than the buckling links which tend to have concentrated deformations.

The next two specimens, 5 and 6, represent slight perturbations to the original group. Specimen 5 was tested to examine the effect of having unequal sized panel zones. Specimen 6 was tested to explore the effect of employing an alternative end connection detail. Being of the same stock and length, comparisons with the first four specimens are immediate.

Specimen 5.- Up to this point all panel zones in a link were made to be of equal width. Since, due to the presence of bending as well as shear, not all panels experience the same states of stress, one would expect the exterior panels to be more highly stressed than the interior ones. In fact, it was noted that buckling occurred most severely in an *exterior* panel in Specimens 3 and 4. Specimen 5 was designed to investigate the effect of employing unequal panel zone sizes on the behavior of active links.

The two sets of stiffeners in Specimen 5 were placed so as to form a larger central panel (10.7 × 16.9 in.) and two equal end panels (8.4 × 16.9 in.). The response of this specimen was as shown in Fig. 2.5(a). The initial behavior was, as expected, the same as Specimens 1-4 with initial yielding at 120.8 k. However, buckling of the central panel occurred quite early (cycle 2S) at a load of 171.6 k and relative displacement of 2.93 inches. The behavior was clearly inferior to that of the other three panel specimen (Specimen 3). One might conclude from this test that behavior is not improved by employing an unequal spacing of stiffeners in active links

which yield predominantly in shear. It will be seen that bending links are different in this regard.

Specimen 6.- On a more practical note, Specimen 6 dealt with the problem of end connection detailing, being constructed with a Type 2 connection at the west end and a Type 3 connection at the east end. The two sets of stiffeners were placed so as to form two equal panels (8.2 × 16.9 in.) at the west end with a larger zone for the panel with the thick gusset plate. The response of Specimen 6 is shown in Fig. 2.6(a).

The behavior of this specimen was basically favorable. Buckling of Specimen 6 was most severe in the panel containing the gusset plate with the buckles penetrating to the corners around the gusset as shown in Fig. 2.6(b). The center panel experienced significant buckling also. This favorable distribution of buckling (ie. buckling in more than one panel) slowed degradation of load carrying capacity in the post buckling range. Failure of Specimen 6 was by tearing of the web around the gusset plate.

Although this single test does not provide conclusive evidence, it would appear that end connection details have little effect on the integrity of active links, *provided the connections are fully welded, moment-resisting, and designed to develop the full capacity of the member.*

Specimen 7.- Specimen 7 was constructed from a W18×35 section and consequently had flanges that were considerably more slender than the previous specimens. The purpose of this test was to explore the effect of slender flanges on the buckling behavior of active links which deform predominantly in shear. The width-to-thickness ratio of the flanges was $b/2t_f = 7.8$, which is high for rolled wide flange sections.

Two sets of stiffeners were equally spaced in this specimen creating three panel zones of dimension 9.1 × 16.9 inches. Flange buckling occurred first in cycle 3 at an absolute displacement magnitude of 1.0 inch. These buckles continued to form, increasing in size until cycle 6 when the central web panel buckled at a load and relative displacement of 205.0 k and 3.02

inches respectively. Web buckling, *not* flange buckling, marked the beginning of specimen deterioration. Buckling concentrated in the middle panel where failure finally occurred by peripheral tearing of the web region in cycle 9. The important conclusion from this test is that web buckling is far more debilitating to an active link than is flange buckling. Thus, the former may be a useful limit state whereas the latter might not be.

Specimen 8.- Specimen 8 was fabricated from a W18×60 section and was 36 inches long. Having no stiffeners, it resembled Specimen 1 in that the longest panel dimension had flange boundaries. The panel zone was 8 inches longer than that of Specimen 1 and had a considerably thicker web. The response of Specimen 8 is shown in Fig. 2.8(a).

Generalized yielding of the cross section occurred at a load of 189.0 k. Member behavior was typical of a shear link, showing considerable strain hardening at increasing deformation. Buckling occurred relatively late, happening in the first positive excursion to 1.0 inches absolute displacement. The buckling load was 241.0 k with a corresponding relative displacement of 2.15 inches, well below the maximum load of 257 k achieved in the half cycle prior to buckling.

The buckled shape differed from that of Specimen 1 in that the buckle (and therefore tension field) did not run from corner to corner, as can be seen in Fig 2.8(b). The manifestations of this different buckling mode can be seen in the action-deformation relationship of the member. The effects of different buckling modes on the behavior of the test specimens will be discussed in more detail in Chapter 3, and consequently is not pursued here. Some torsional response of the flanges, induced by web buckling, was evident in the later cycles of the test.

Specimen 9.- Specimen 9 was constructed from the same stock as the first six specimens but it was 36 inches long. With two sets of stiffeners it had three equal panel zones of dimension 11.8 × 16.9 inches. This specimen was designed to provide more information about links in the transition region between bending and shear type behavior. The response history of Specimen 9 is shown in Fig. 2.9(a).

The yield load for this specimen was slightly higher than for the W18×40 specimens at the shorter length. This apparent contradiction may have been caused by an inadvertent initial inelastic pulse in the northerly direction prior to the test. The important point to note is that even though the bending moment was 22% higher in Specimen 9 than in Specimens 1-6, the yield load was roughly the same, indicating little interaction between bending and shear capacity for these lengths.

Buckling of the center panel occurred in cycle 4S at a load and relative displacement of 172 k and 2.66 inches respectively. No flange distress was noted throughout the entire test. Buckling concentrated entirely in the middle panel. The relative contributions to total displacement from the other two panels, as measured by the linear potentiometers stationed at the stiffener locations, decreased as the test progressed.

Specimen 10.- In order to achieve relatively longer links (ie. ones in which bending has a greater effect), sections of lesser depth were used. Specimen 10 was made from a W16×26 section and was 36 inches long. It had no stiffeners, making the panel zone 36.0 × 15.0 inches. With the longer of the panel sides being bounded by flanges, this specimen was similar to Specimens 1 and 8. Response of Specimen 10 is shown in Fig. 2.10(a).

Although this specimen had the most slender web, buckling did not occur until the southerly branch of cycle 2, half a cycle after the point in the loading history where Specimen 1 had buckled. This difference is due to the fact that, since Specimen 10 was more flexible, Specimen 1 experienced more severe inelastic deformations for the same displacement history. Post-buckling behavior of Specimen 10 was nonetheless considerably worse than that of Specimen 1. The reason for poorer performance was clearly due to the inability of the flanges of Specimen 10 to resist the buckling deformations. Specimen 1 had flanges with greater torsional stiffness and had buckling modes which required less resistance of the flanges. Flange rotations were much greater in Specimen 10 (reaching approximately 30 degrees in the later stages of the test) than in Specimen 8 which had a similar buckling mode, again because of the greater torsional

resistance of the flanges in Specimen 8. The sense of flange rotation did not change with cycling. Deterioration of specimen integrity was rapid, ending with material tearing in the middle of the panel. Even though Specimen 10 was clearly a bending link and had relatively slender flanges, no flange distress was noted prior to web buckling. Significant interaction between web and flange buckling fields was noted in the later portion of the test.

Specimen 11.- Another single panel specimen, Specimen 11, was constructed of W18×35 section (the same stock as Specimen 7). With a slightly less slender web and slightly more slender flanges, this specimen had a smaller value of α than did Specimen 10. The response of this specimen was nonetheless similar to that of Specimen 10 and is shown in Fig. 2.11(a).

The yield load of 147 k was identical to the yield load of Specimen 7, its 28 inch counterpart, again showing essentially no moment-shear interaction at these lengths. Buckling behavior was very much like Specimen 10, showing a similar mode shape and the same rapid deterioration. Again, flange distress was not noted before web buckling but interaction between flange and web buckling fields was considerable. Also, flange rotations were large, as evidenced in Fig. 2.11(b). Failure occurred by tearing in the middle of the panel zone.

Specimen 12.- With a value of $\alpha = 0.37$, Specimen 12 was relatively the longest link tested. The absence of stiffeners gave it a single panel zone with dimensions 36.0 × 11.5 inches. The response is shown in Fig. 2.12(a).

Buckling occurred later in this more compact specimen than in the previous two, happening in cycle 4S at a load of 95.8 k and a relative displacement of 2.15 inches. Flange and web buckling interacted to a large extent throughout the test but the buckling fields at opposite ends of the link did not overlap as was the case in previous specimens. The interaction of the two buckling fields at opposite ends of the link was manifested in the form of marked lateral torsional response of the member as seen in Fig. 2.12(b). Deterioration of member properties was not as rapid for this specimen as it was for the previous two.

It should be noted that, by virtue of its size and length, Specimen 12 (and also Specimen 15) was the most flexible among the test specimens. The same absolute displacement history was imposed on all specimens, therefore, the more flexible ones suffered less severe distortions. This difference will be accounted for in Chapter 3 through normalization of the results.

Specimen 13.- The last three specimens were appropriately stiffened versions of the previous three. Specimen 13, the counterpart of Specimen 10, had three panel zones measuring 11.5 × 15.0 inches. The behavior of this specimen was an improvement over Specimen 10 and is shown in Fig. 2.13(a). Web buckling was noted in cycle 4N (as opposed to 2S for Specimen 10) and was accompanied by substantial flange buckling. The delay in web buckling allowed the link to develop the expected flange stability problems. Fig. 2.13(b) shows, however, that web buckling was still dominant. Since the flanges were stiffer in torsion, rotations were confined to the end segments.

Specimen 14.- Specimen 14 was the counterpart of Specimen 11 and had three equal panel zones. Flange distress was substantial prior to web buckling which occurred in cycle 4S. Load carrying capacity did not begin to deteriorate until web buckling had set in. In the advanced stages of the test the northwest flange developed a full wavelength buckle causing the specimen to rotate torsionally at that end. Failure occurred by tearing in the center of both end panels.

Specimen 15.- The counterpart of Specimen 12, Specimen 15 was stiffened 6 inches from each end of the link. The enhanced response of this specimen is shown in Fig. 2.15(a). The presence of the stiffeners effectively precluded the lateral response noted in Specimen 12. Slight flange distress was noted in the first southern excursion to 1.5 inches. Upon cycling to 2.0 inches for the first time, slight web buckling could be seen in the small end panel zones. Shortly thereafter abrupt failure occurred by tearing of the flanges in the heat affected zone of

the welds.

2.2. Summary and Conclusions

Specimens 1 through 4 were designed to determine to what extent the performance of an active link which yields primarily in shear can be improved by stiffening the web against buckling. Since the well stiffened link (Specimen 4) did not buckle until the ninth cycle, the hysteresis loops remained full, the load carrying capacity continually increased due to material strain hardening effects, and far greater member ductilities were achieved before failure occurred.

Specimen 5 had three panel zones, the center one being slightly larger than the outer two. Exhibiting behavior typical of multipanel active links, buckling in Specimen 5 was concentrated in a single panel zone (the center one in this case). The performance of this specimen was found to be inferior to the specimen with three *equal* panel zones (Specimen 3). Based on this test one can conclude that, for active links which yield predominantly in shear, equal sizing of panel zones is optimal.

Specimen 6 had a special end connection consisting of full penetration flange welds and a welded shear tab instead of having all around full penetration welds with cope holes and backup bars for the flange welds (as did Specimens 1-5) or having all around fillet welds (as did Specimens 7-15) for the end connections. Behavior of Specimen 6 was, in general, satisfactory. Buckling was confined mainly to the panel containing the gusset plate. However, substantial buckling of the center panel also occurred, indicating that the size chosen for the panel containing the gusset was appropriate. Specimen 6 was only slightly inferior to Specimen 3.

Specimens 7 through 9 were included to fill out the database and to provide comparisons between the first six specimens and the last six. Specimen 7 was a shorter version of Specimens 11 and 14, exhibiting behavior superior to both. Specimen 9 was a longer version of Specimens 1 through 6 and was inferior to all but Specimen 1. Specimen 8 was cut from a heavier section and showed behavior similar to Specimen 1.

The last six specimens (10-15) were designed to accentuate bending energy dissipation. These tests were paired with one stiffened and one unstiffened specimen in each pair. Specimens 12 and 15 had the greatest contribution of energy dissipation from bending and Specimens 11 and 14 had the least. It can be seen by comparing Specimen 1 (Fig. 2.1) to Specimen 11 (Fig. 2.11) that the longer unstiffened link exhibited a post-buckling behavior having a more rapid deterioration of load carrying capacity than the shorter specimen. Significant flange buckling, accompanying the web buckling, in the longer link was generally responsible for this phenomenon. Flange buckling was often found to induce a significant lateral-torsional buckling of the specimen as a whole, even though both ends were fixed against twisting. The stiffening arrangement used in Specimen 15 (stiffeners placed approximately one flange width away from the end plates) effectively inhibited lateral-torsional buckling.

The following general conclusions can be made based on observations of the hysteretic behavior of the test specimens:

(1) Inelastic shearing is more efficient than inelastic web buckling for energy dissipation.

(2) Stiffening improves the energy dissipation capability of an active link by delaying the onset of inelastic web buckling.

(3) Stiffening slows the degradation of load carrying capacity in an active link by controlling the amplitude of out-of-plane displacement of the web.

(4) Web buckling has a more deleterious effect on the load carrying capacity of a link than does flange buckling. Interaction of web and flange buckling fields causes a more severe degradation of capacity than either of the modes acting alone. Such interaction is most likely to occur in active links having $\alpha < 1$ and has been shown to be important for values as low as $\alpha = 0.37$ in these tests.

(5) The formation of a tension field arrests the drop in load carrying capacity that occurs after web buckling. Within a cycle, the tension field is often able to develop a carrying capacity greater than the initial buckling load.

In the following chapter the conclusions of this chapter will be extended by making further comparisons between the test specimens.

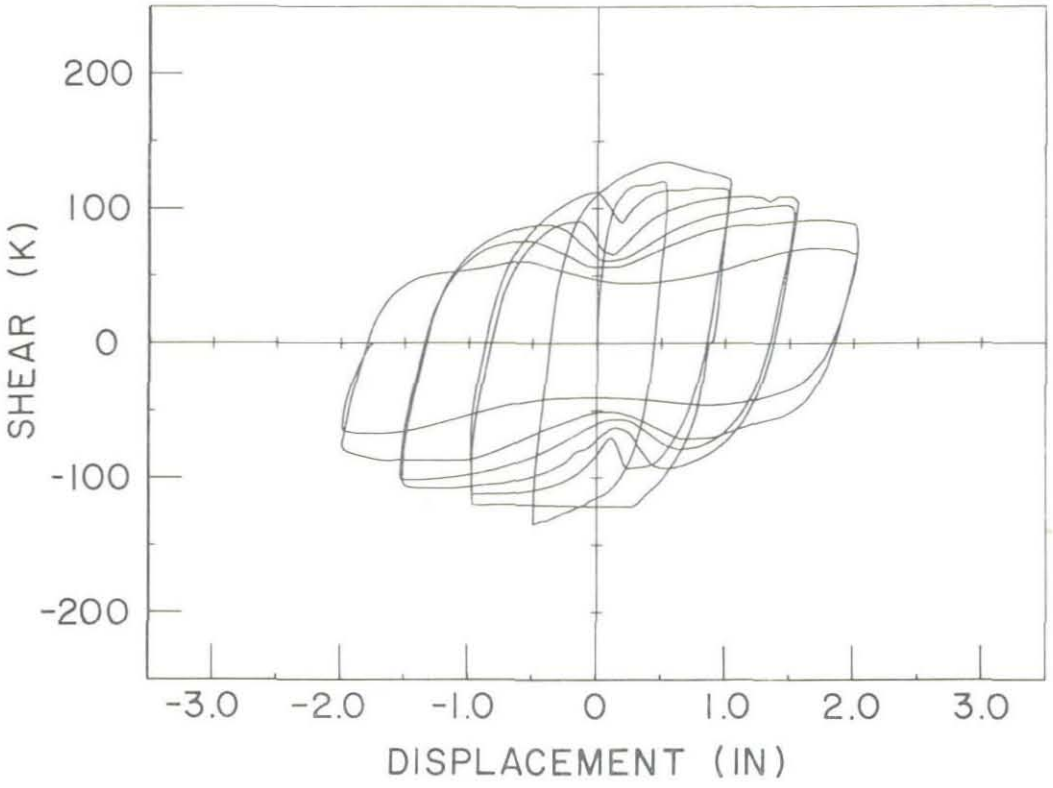

(a) Applied Shear vs. Relative End Displacement

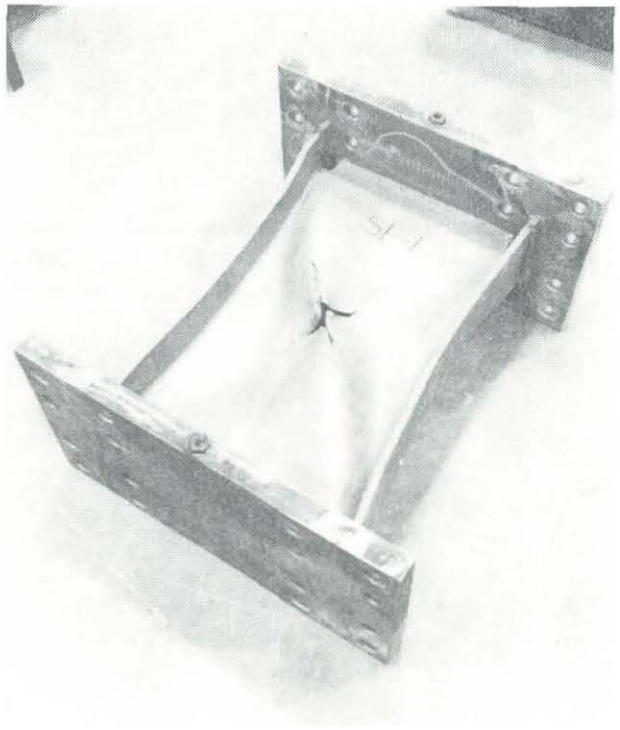

(b) Specimen 1 after Failure

Fig. 2.1 Hysteretic Response of Specimen 1

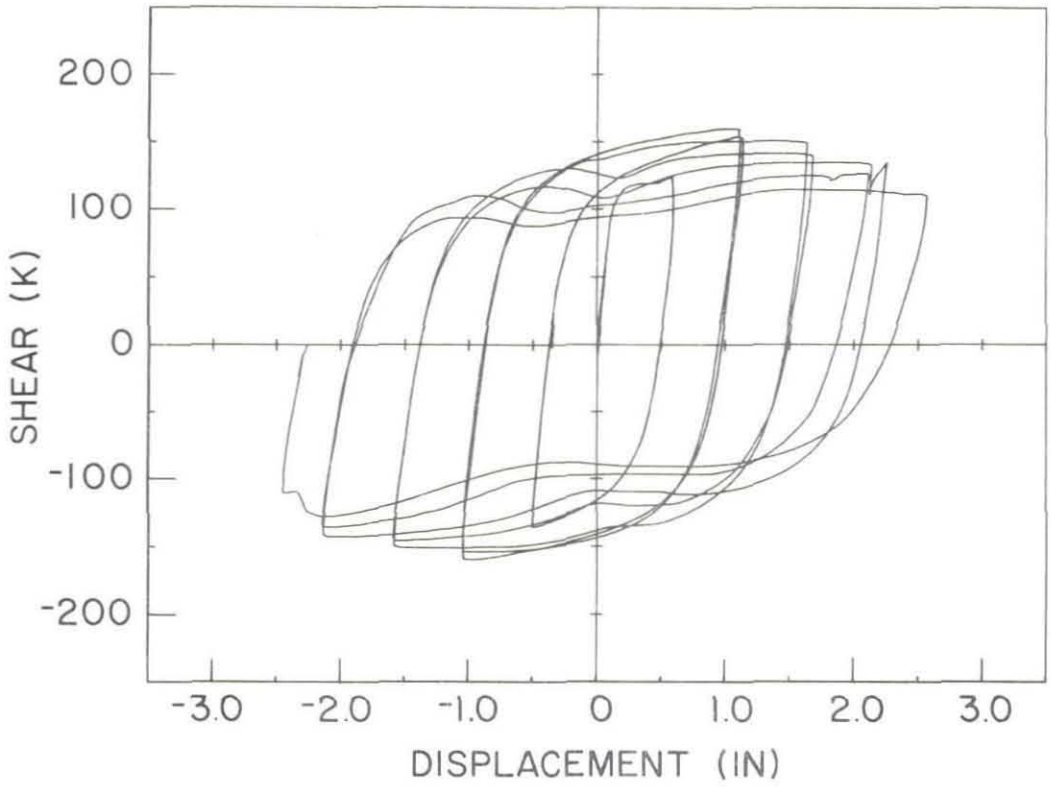

(a) Applied Shear vs. Relative End Displacement.

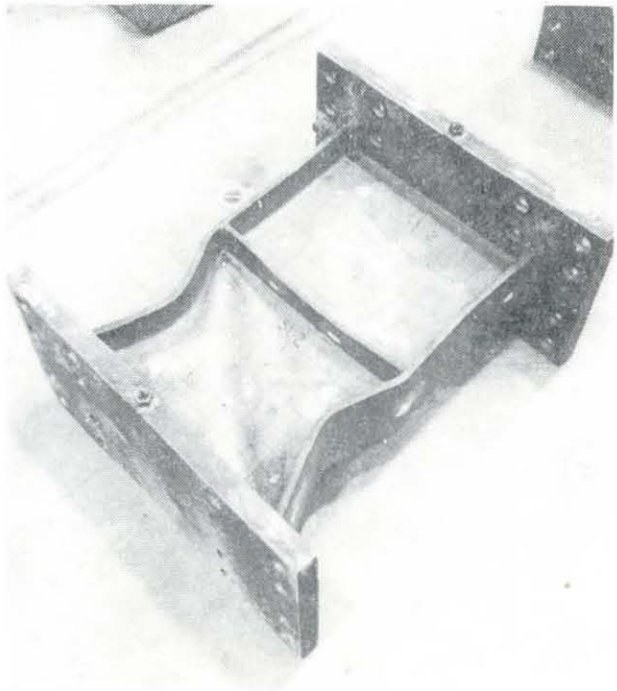

(b) Specimen 2 after Failure

Fig. 2.2 Hysteretic Response of Specimen 2

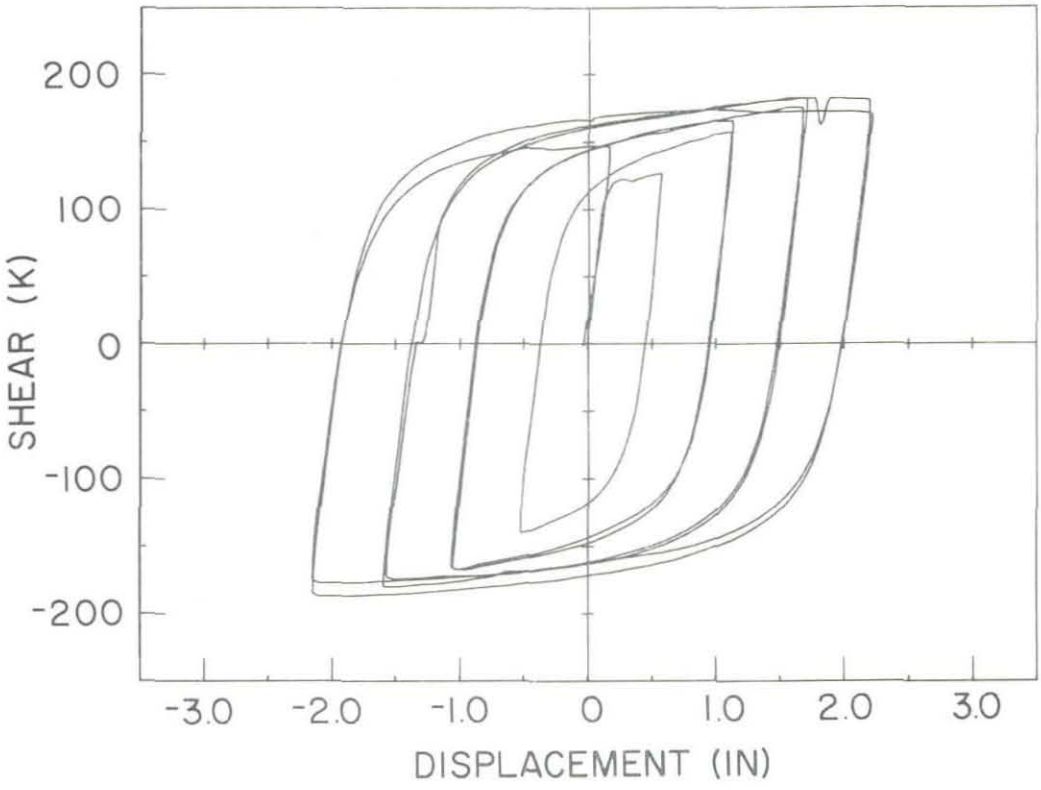

(a) Applied Shear vs. Relative End Displacement

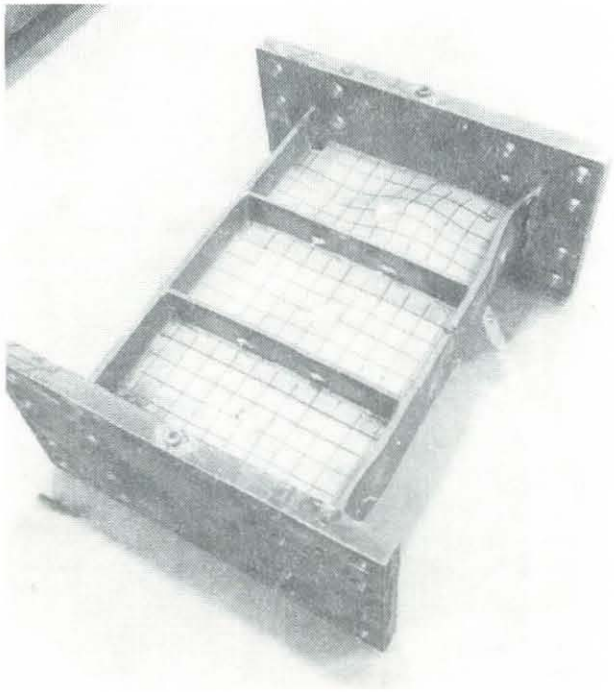

(b) Specimen 3 after Failure

Fig. 2.3 Hysteretic Response of Specimen 3

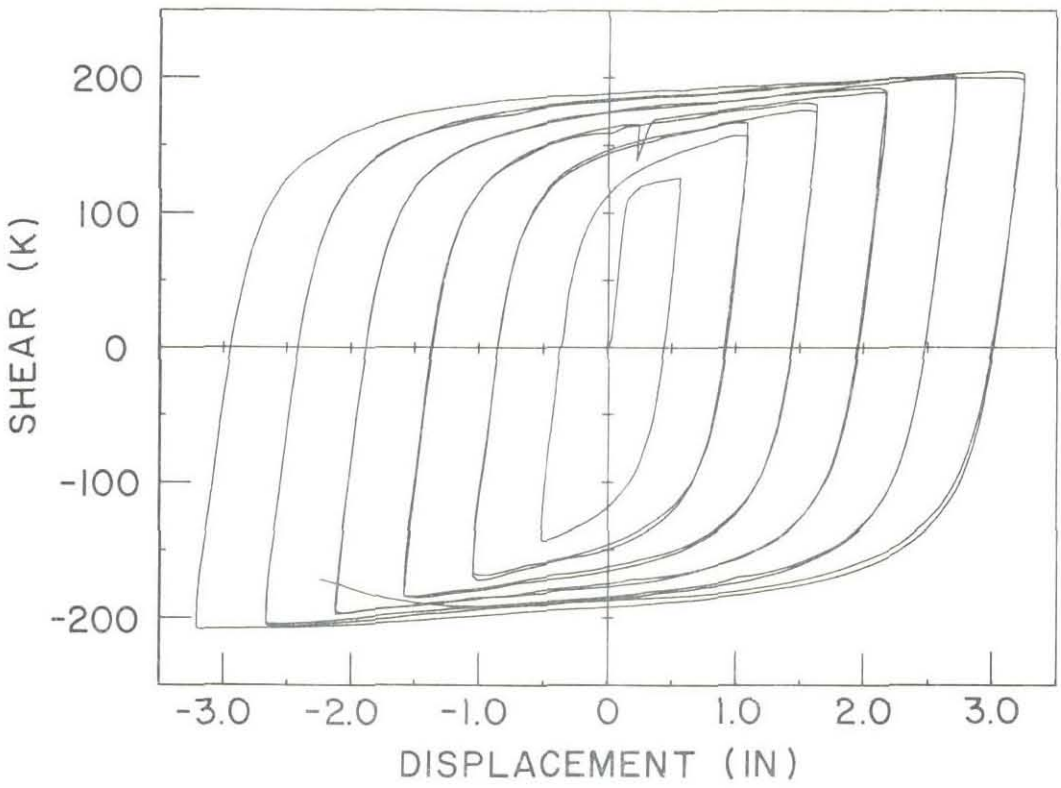

(a) Applied Shear vs. Relative End Displacement

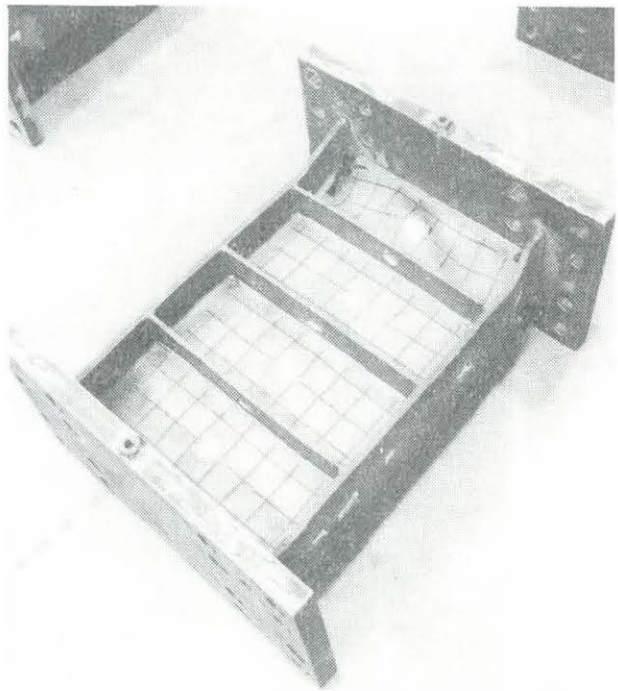

(b) Specimen 4 after Failure

Fig. 2.4 Hysteretic Response of Specimen 4

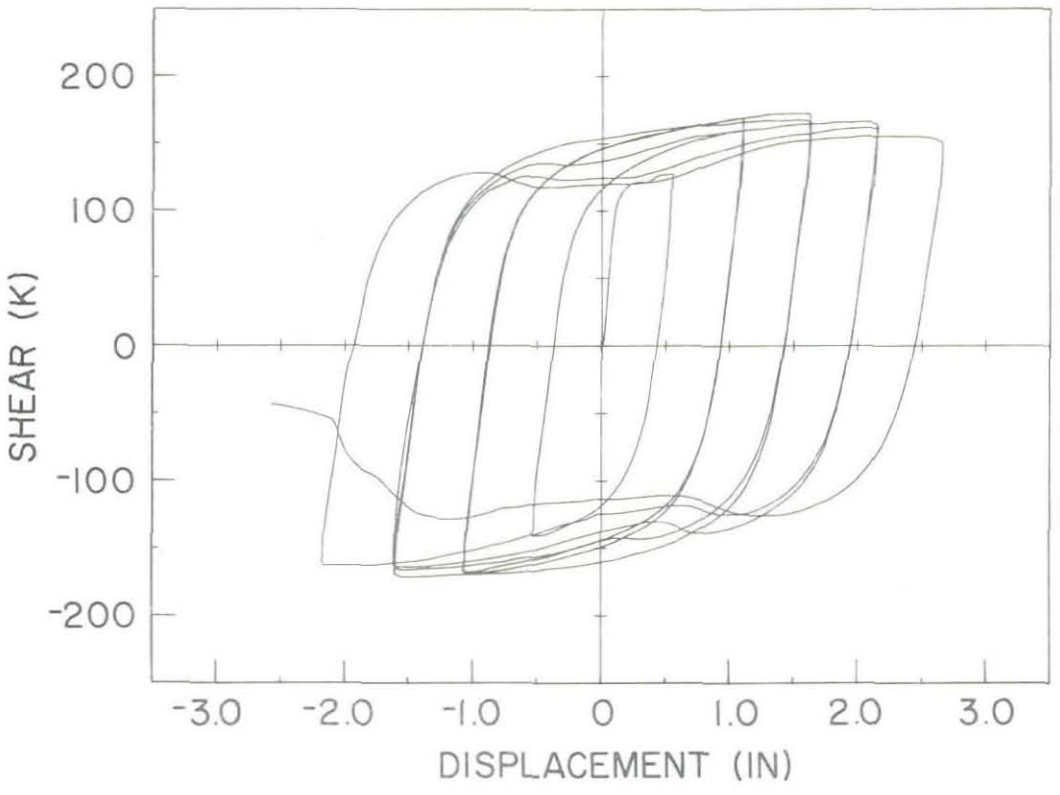

(a) Applied Shear vs. Relative End Displacement

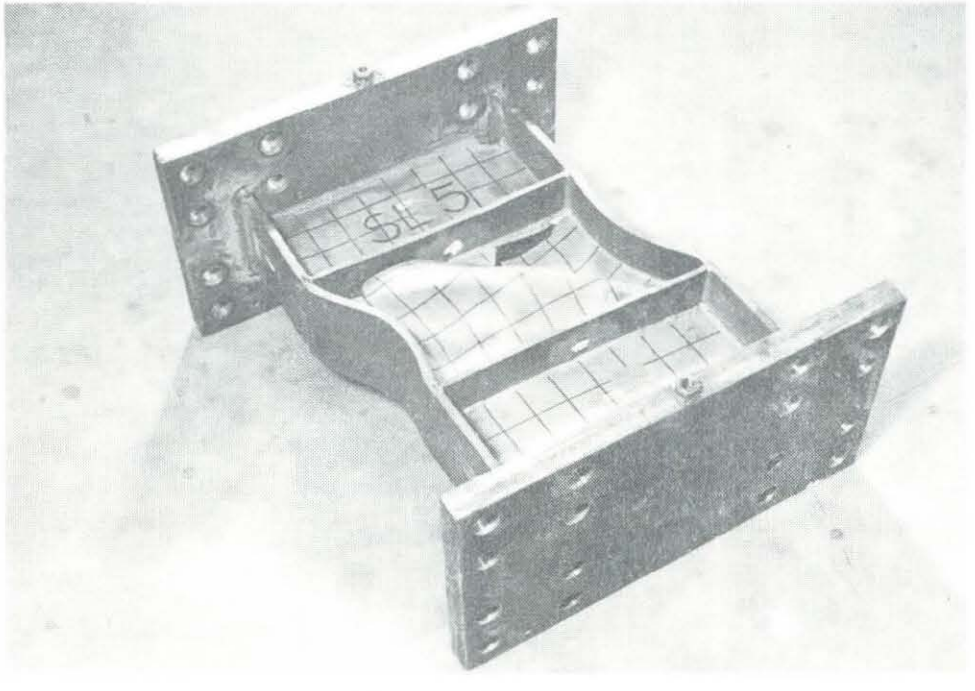

(b) Specimen 5 after Failure

Fig. 2.5 Hysteretic Response of Specimen 5

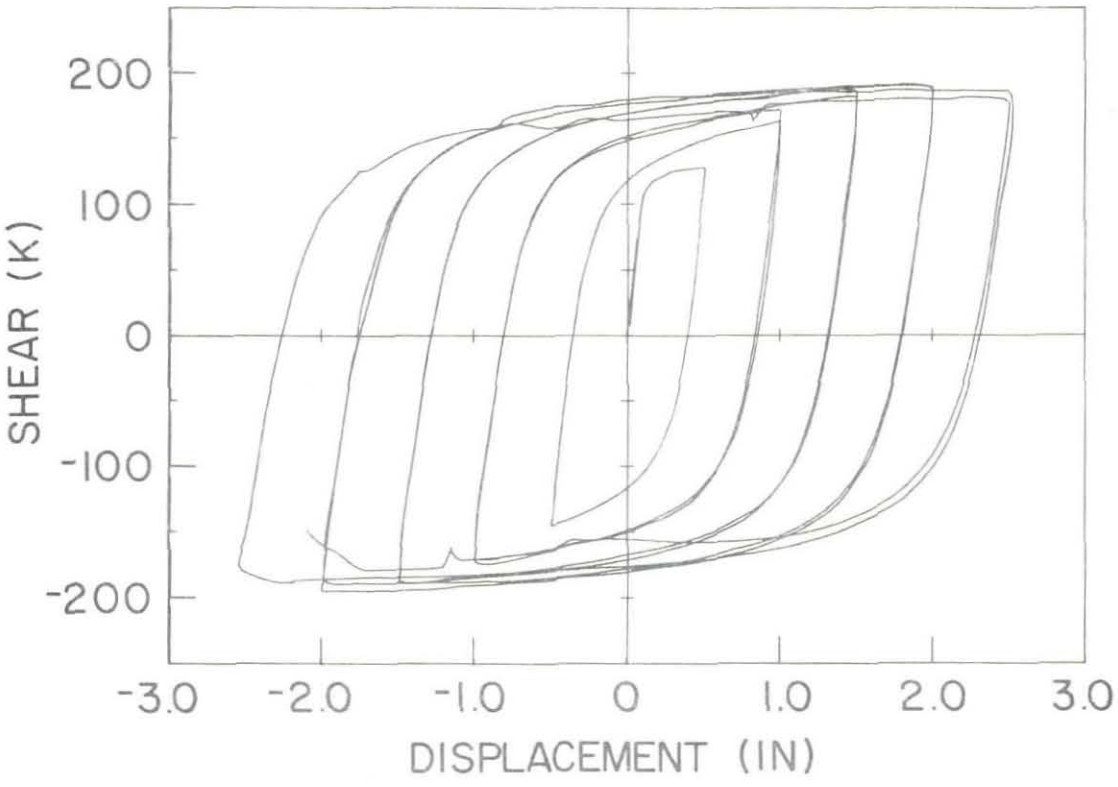

(a) Applied Shear vs. Relative End Displacement

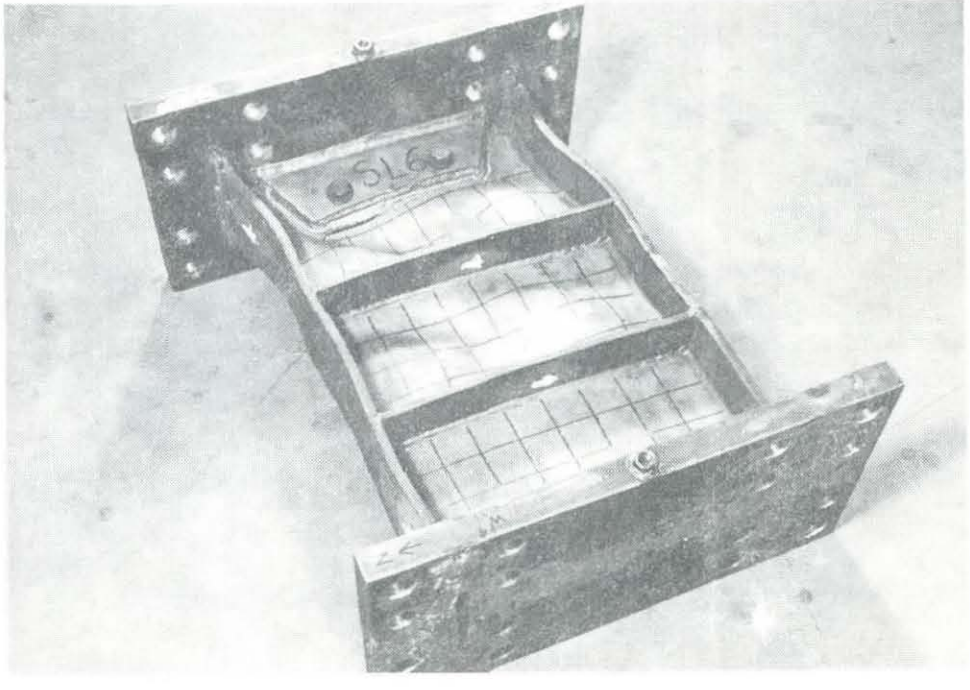

(b) Specimen 6 after Failure

Fig. 2.6 Hysteretic Response of Specimen 6

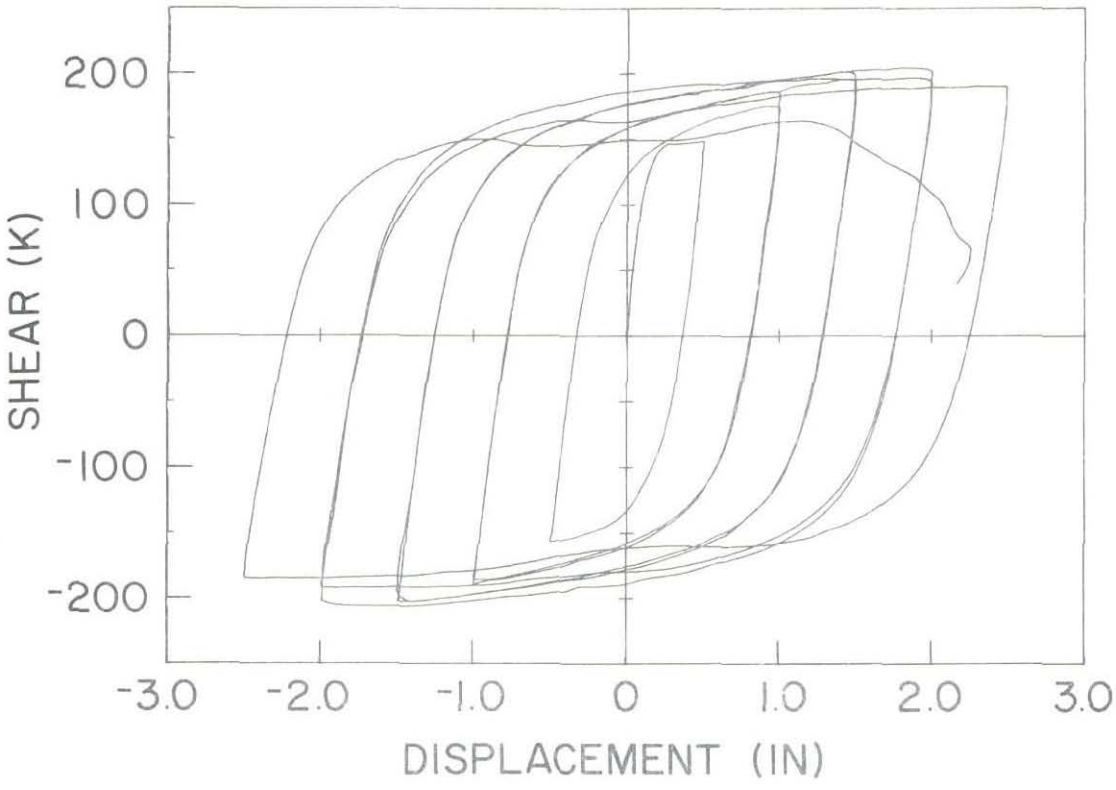

(a) Applied Shear vs. Relative End Displacement

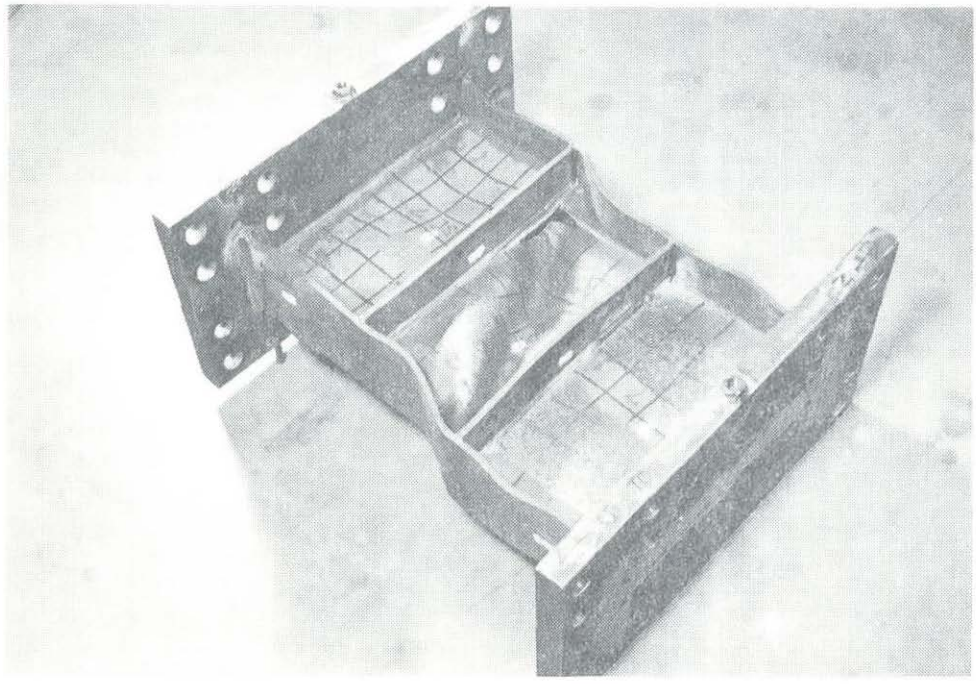

(b) Specimen 7 after Failure

Fig. 2.7 Hysteretic Response of Specimen 7

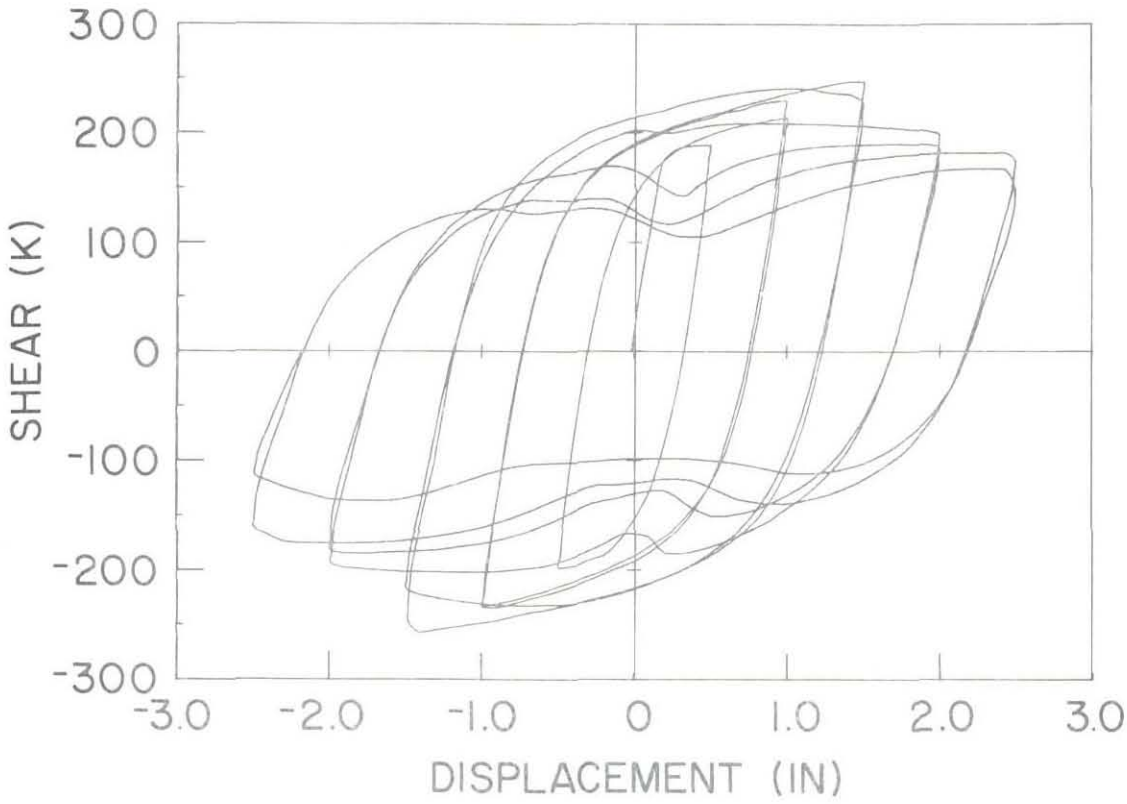

(a) Applied Shear vs. Relative End Displacement

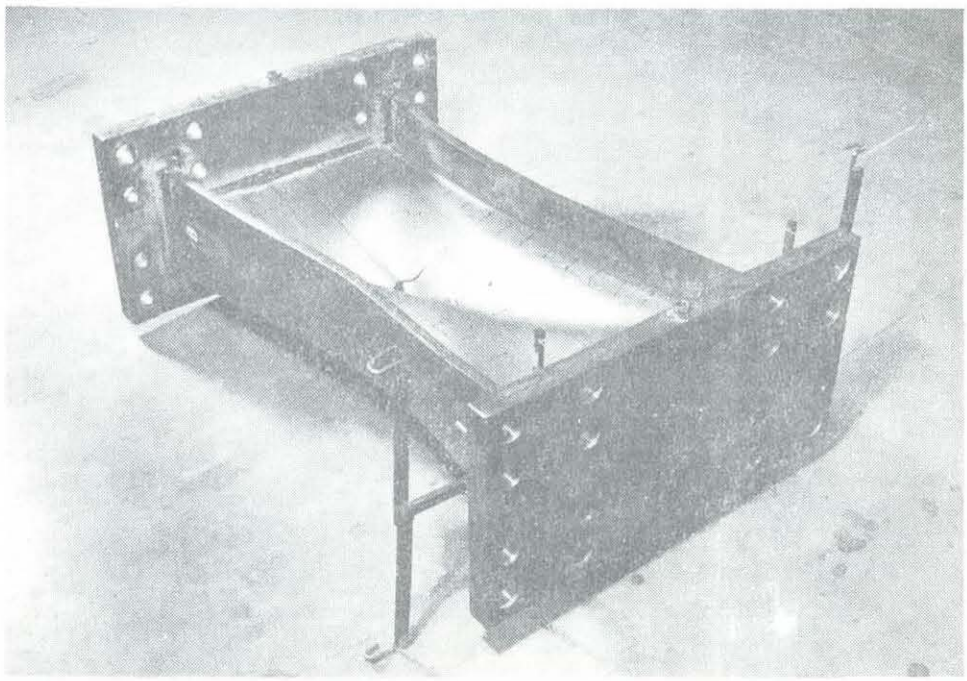

(b) Specimen 8 after Failure

Fig. 2.8 Hysteretic Response of Specimen 8

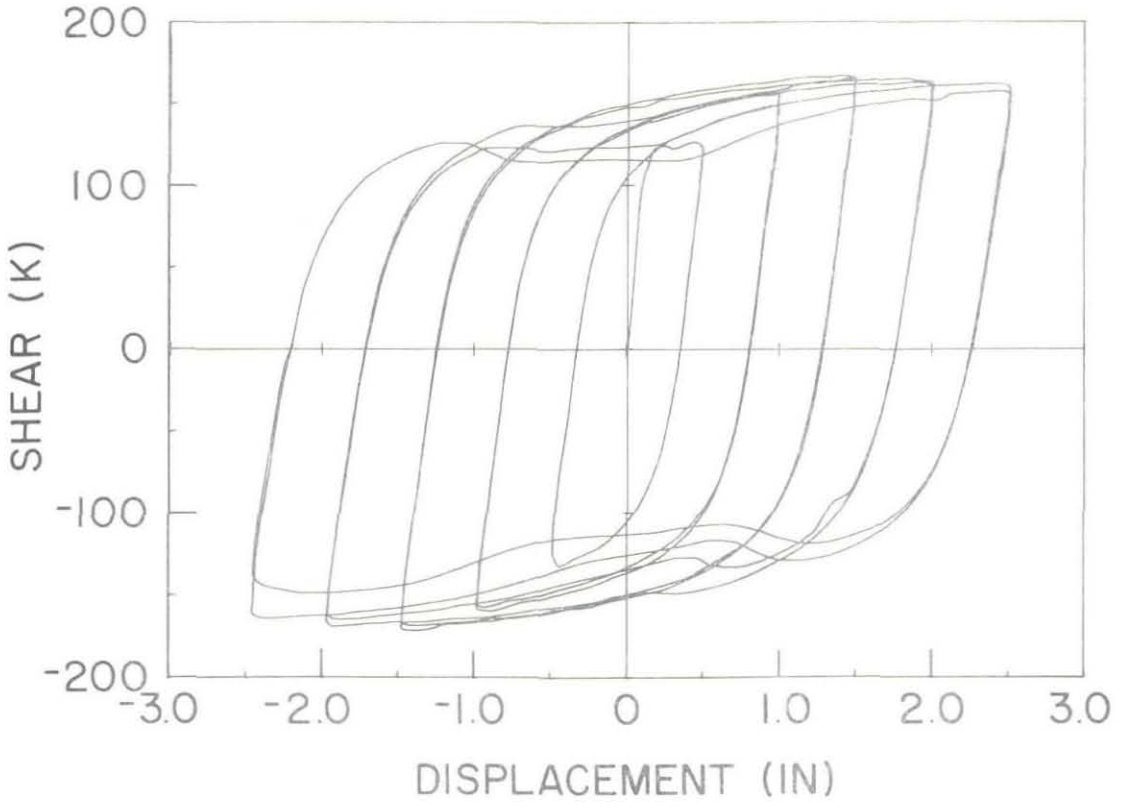

(a) Applied Shear vs. Relative End Displacement

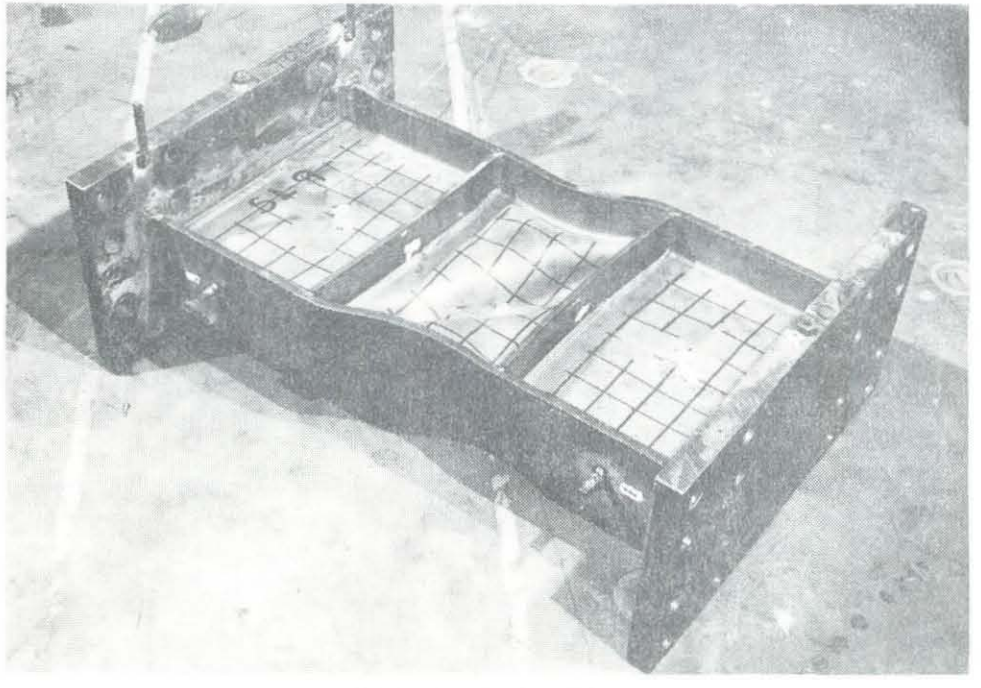

(b) Specimen 9 after Failure

Fig. 2.9 Hysteretic Response of Specimen 9

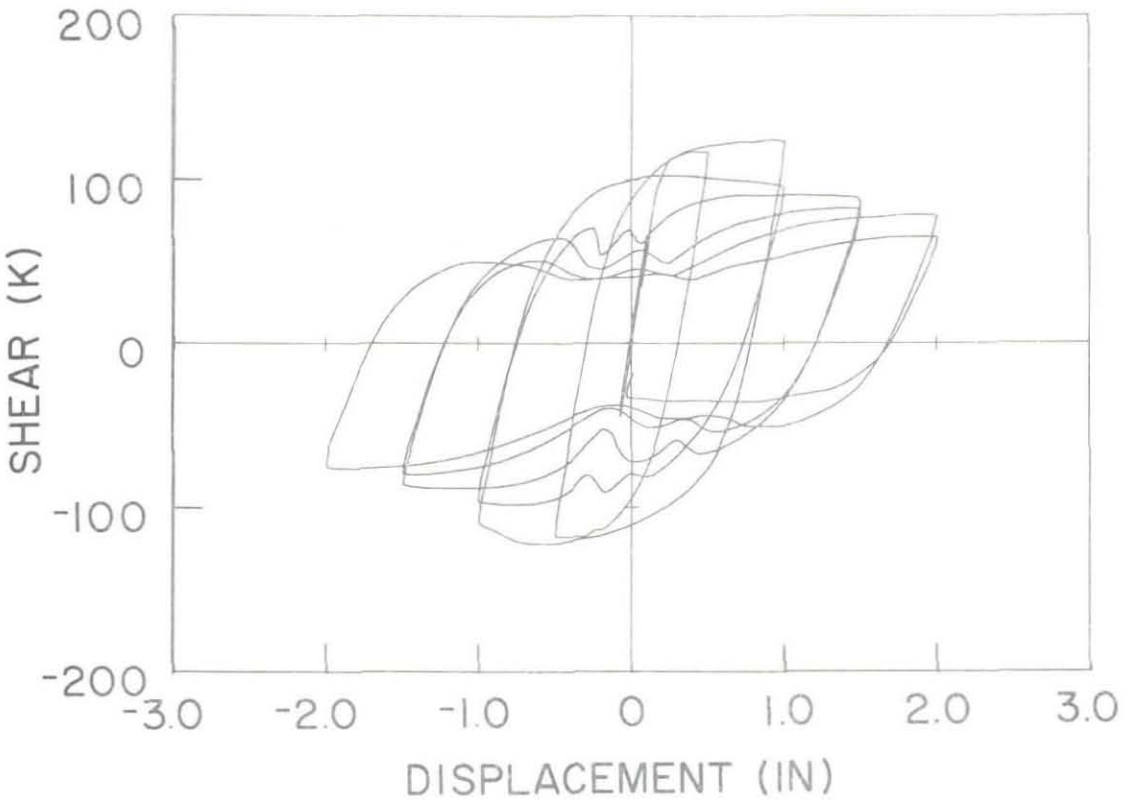

(a) Applied Shear vs. Relative End Displacement

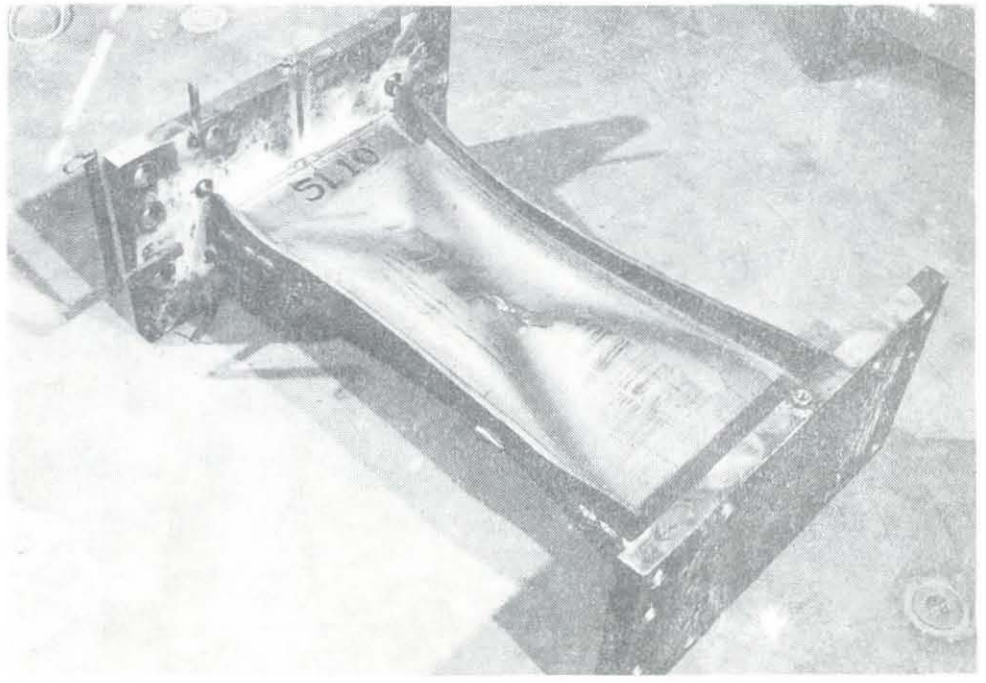

(b) Specimen 10 after Failure

Fig. 2.10 Hysteretic Response of Specimen 10

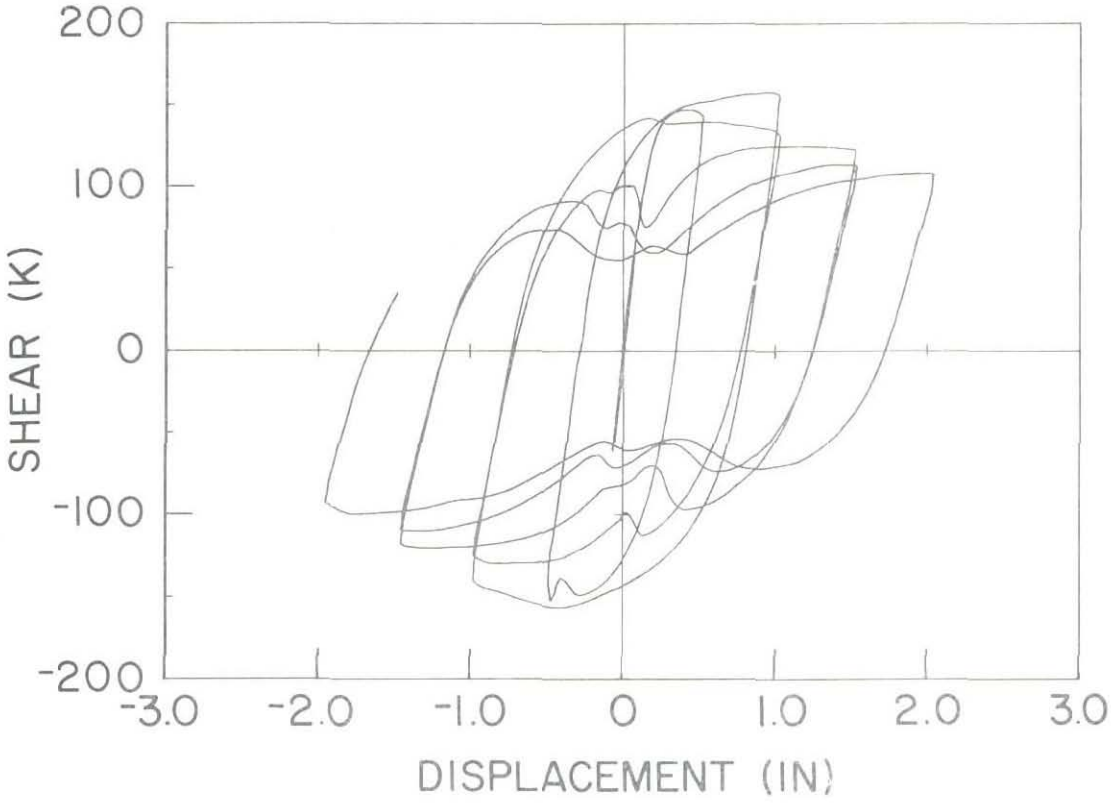

(a) Applied Shear vs. Relative End Displacement

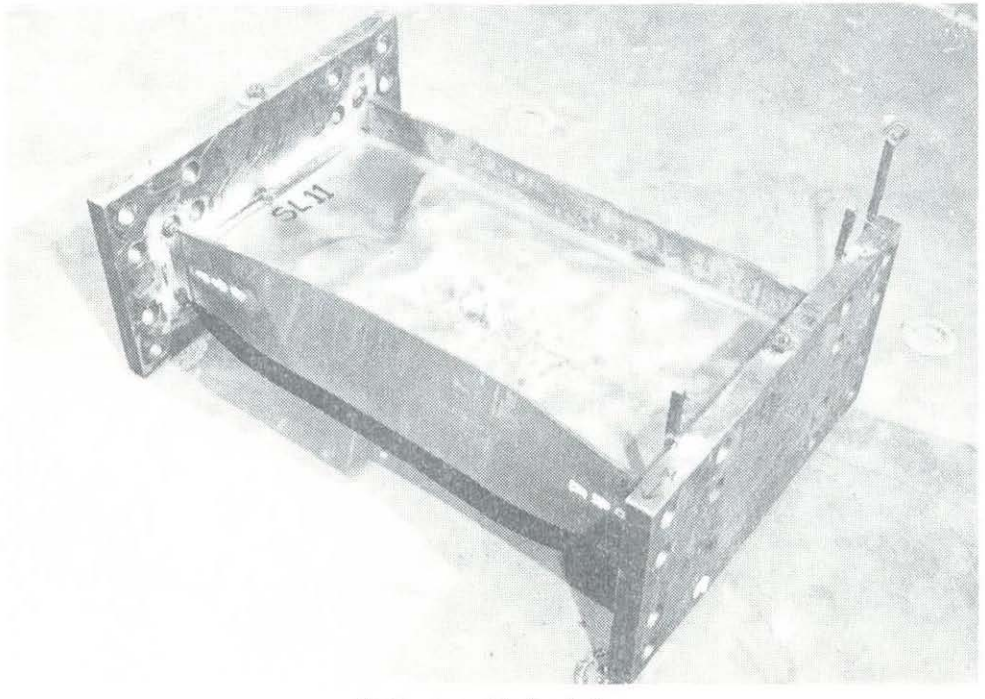

(b) Specimen 11 after Failure

Fig. 2.11 Hysteretic Response of Specimen 11

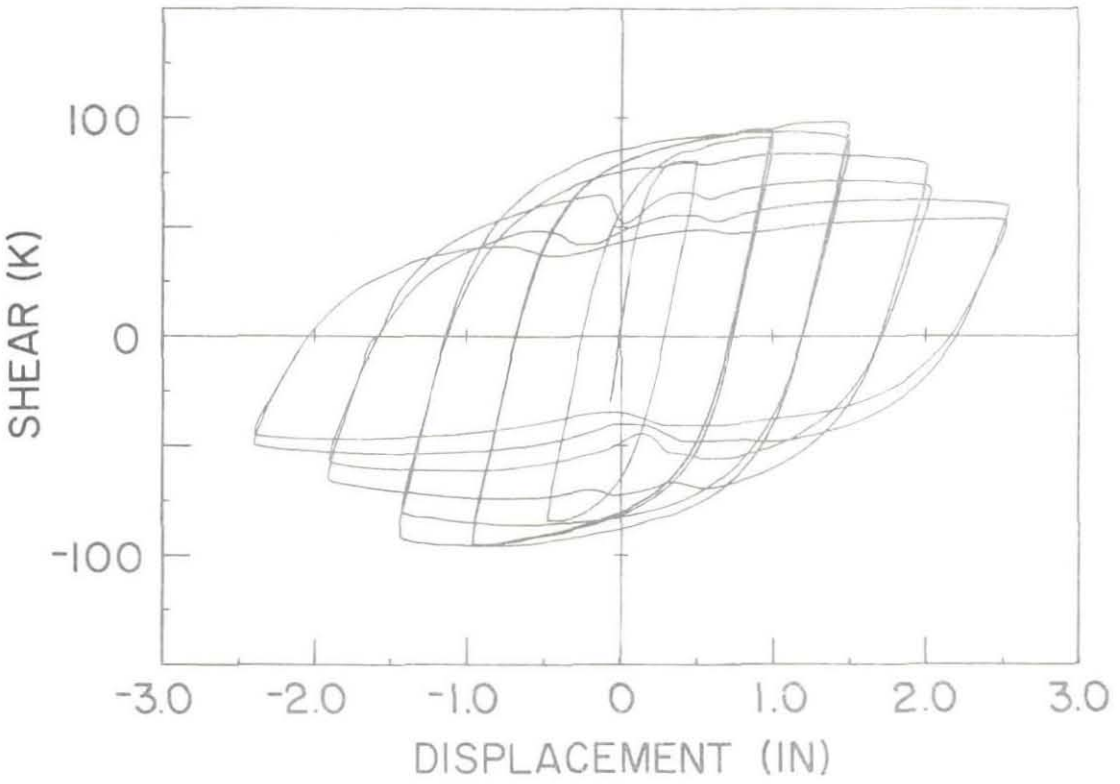

(a) Applied Shear vs. Relative End Displacement

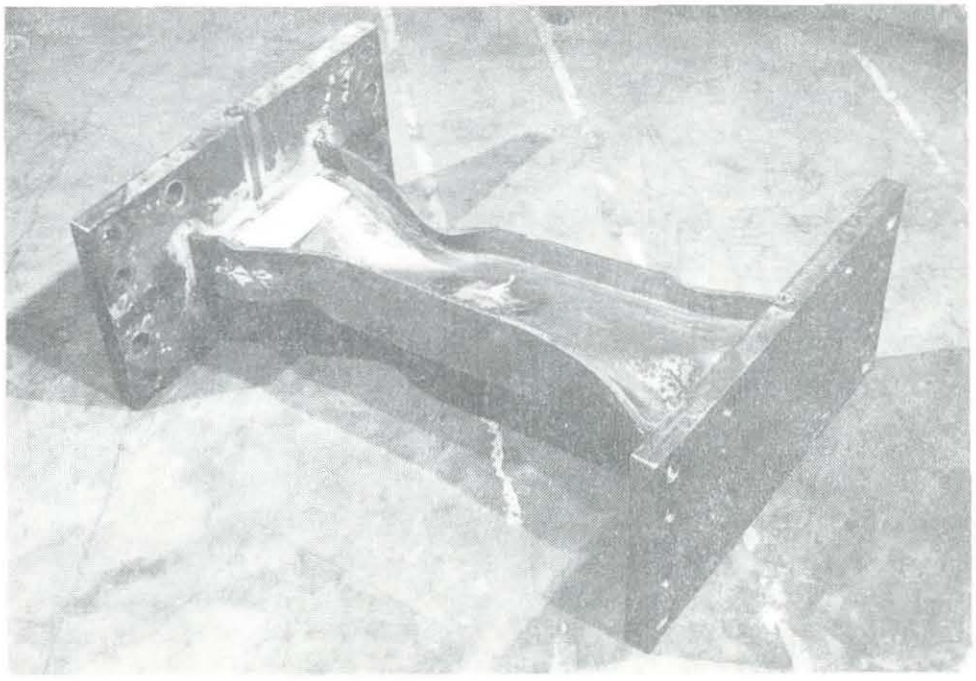

(b) Specimen 12 after Failure

Fig. 2.12 Hysteretic Response of Specimen 12

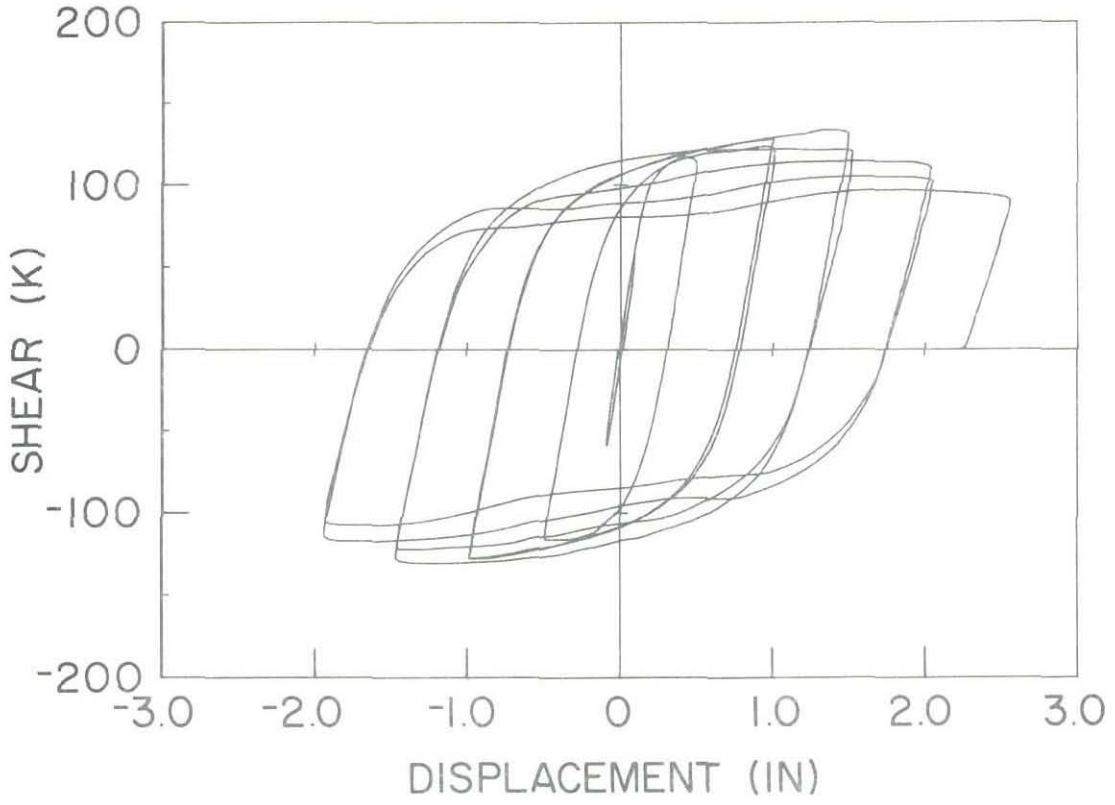

(a) Applied Shear vs. Relative End Displacement

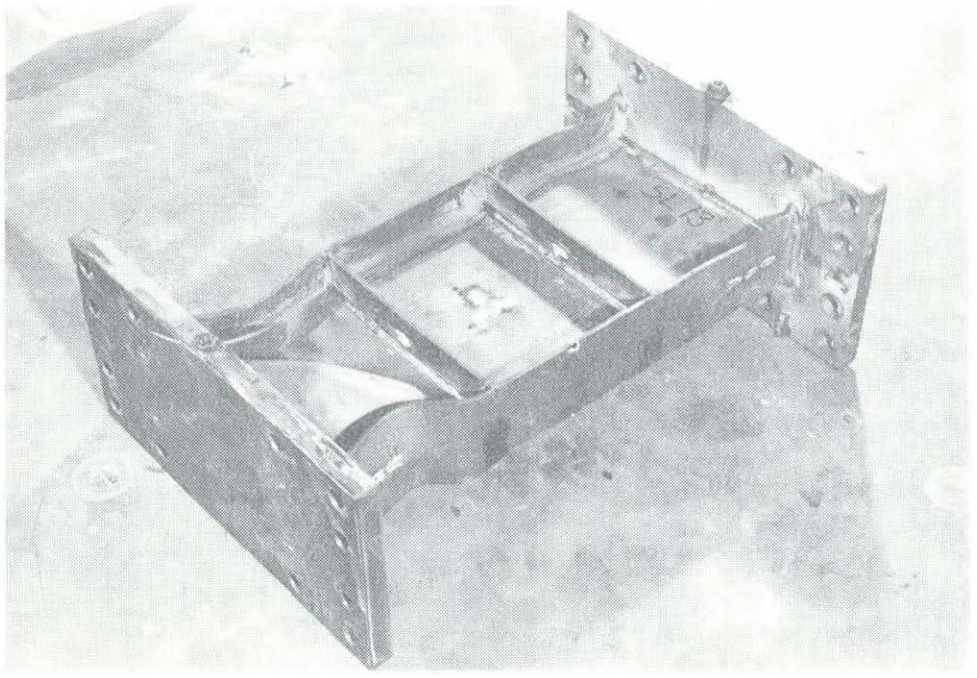

(b) Specimen 13 after Failure

Fig. 2.13 Hysteretic Response of Specimen 13

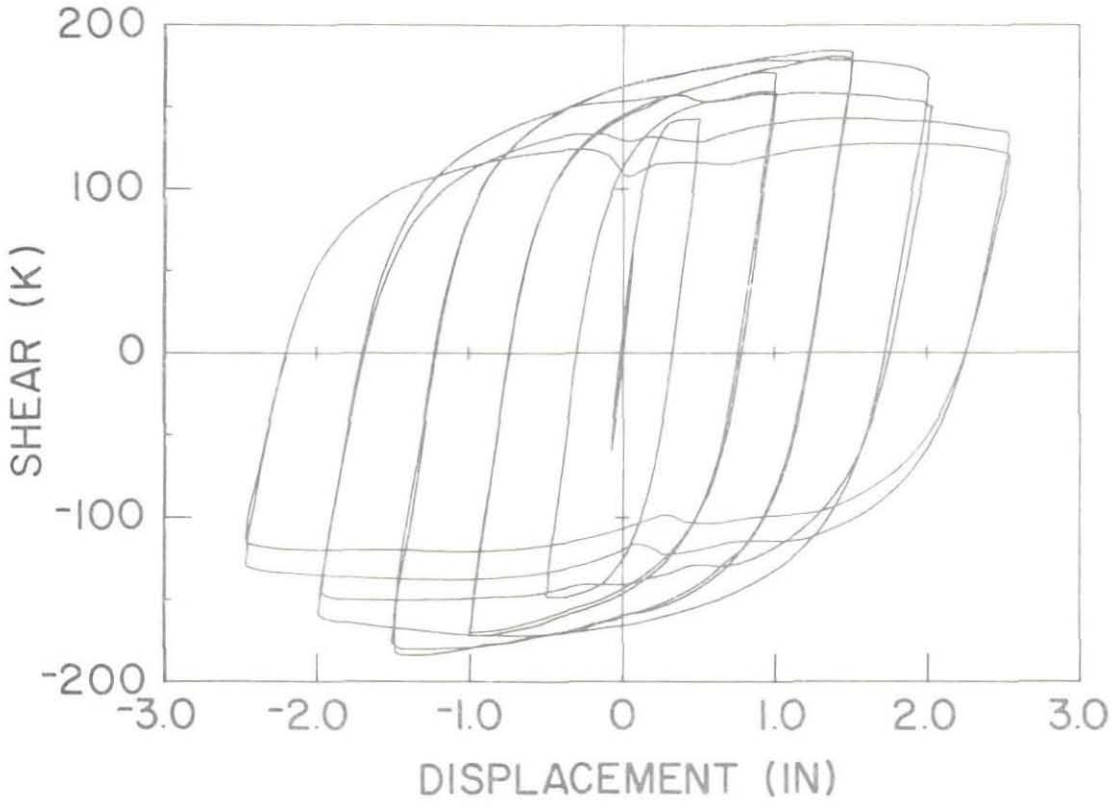

(a) Applied Shear vs. Relative End Displacement

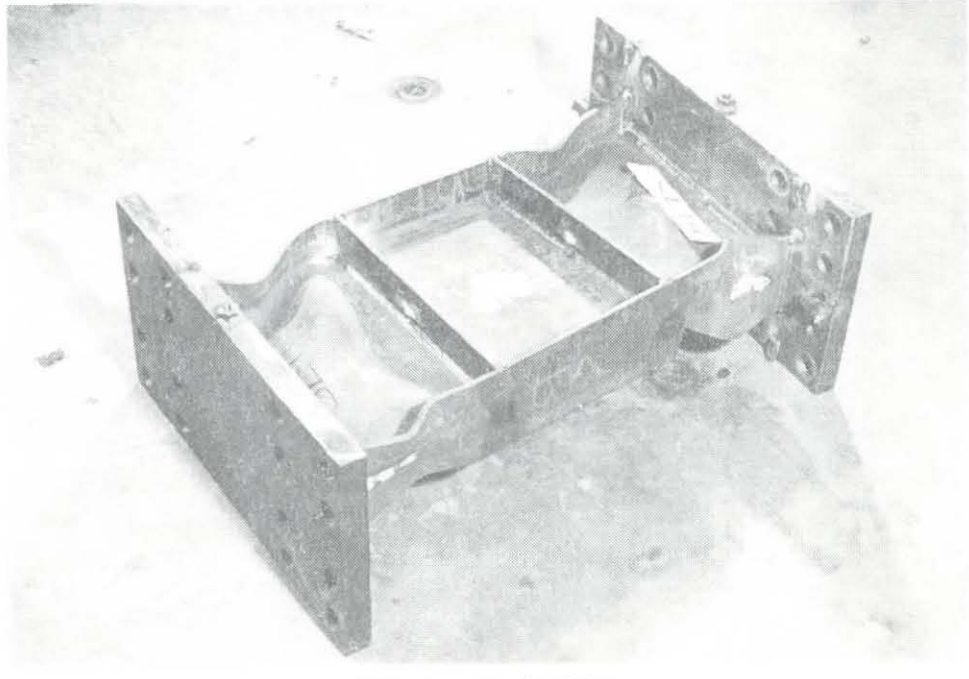

(b) Specimen 14 after Failure

Fig. 2.14 Hysteretic Response of Specimen 14

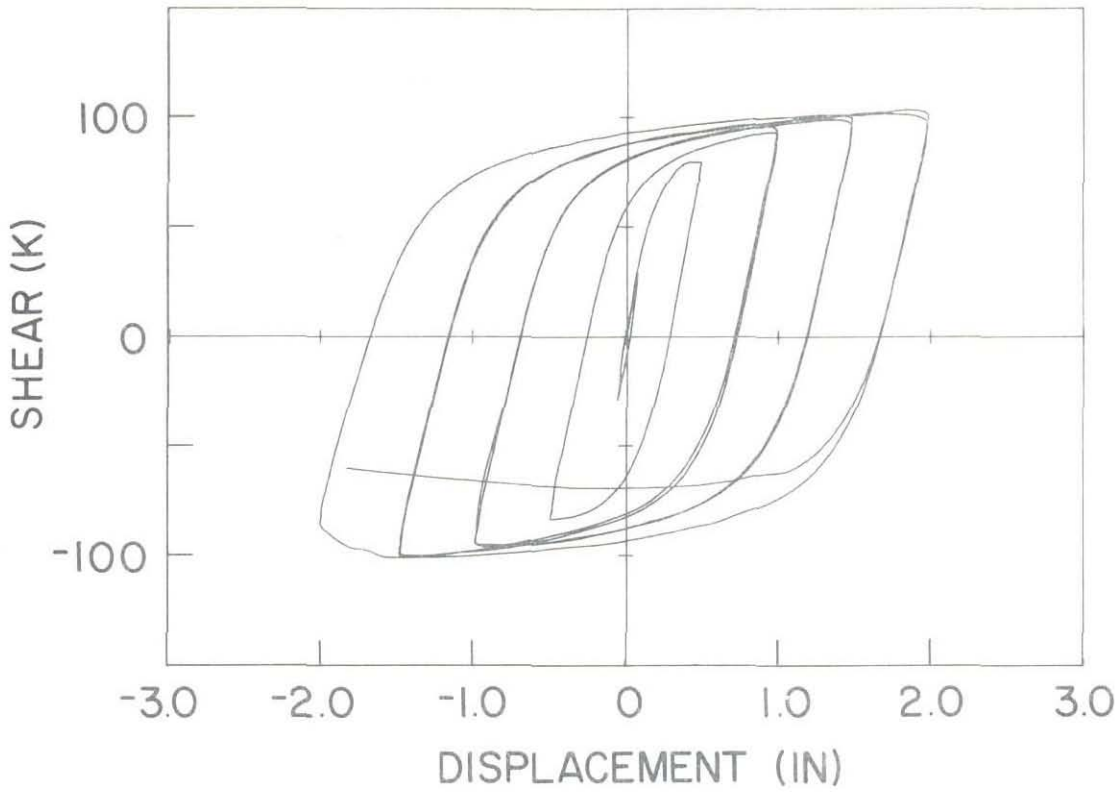

(a) Applied Shear vs. Relative End Displacement

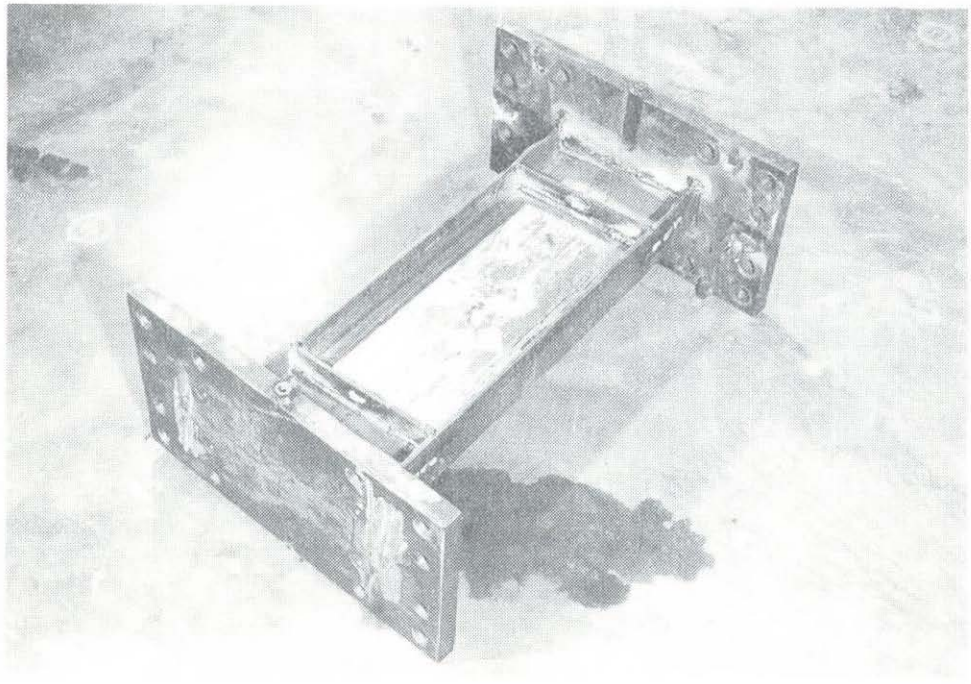

(b) Specimen 15 after Failure

Fig. 2.15 Hysteretic Response of Specimen 15

Chapter 3

General Behavior of Active Links: An Experimental Assessment

3.0. Introduction

In Chapter 2, each of the fifteen tests was described and observations on the hysteretic behavior of active links were noted. Some comparisons were drawn between specimens, and a few general conclusions were made. The present chapter broadens the comparisons already drawn in an effort to make more general statements regarding the behavior of active links. In addition to the action-deformation relationships already presented other data will be introduced to facilitate the discussion.

The response potential of a structural element consists of various modes of behavior which can be identified with certain defined limit states. A schematic representation of this concept is shown in Fig. 3.1 for the case of the active link. These elements can exhibit three different modes of behavior: Elastic, Inelastic Pre-buckling, and Post-buckling. These three modes of behavior are bounded by three limit states: Yield, Buckling, and Failure. This chapter is devoted to explicating the general features of active link behavior, based on experimental evidence. An effort is made to define and, where possible, quantify the limit states. Some comments are made regarding which of the limit states might be appropriate to consider when designing active links.

3.1. Elastic Behavior

Since analytical procedures can accurately characterize the elastic behavior of active links, only a limited amount of data were taken during the tests to experimentally assess this range of behavior. In this section we present some of this data as a means of verifying that the testing apparatus applied the intended excitation. Also given in this section is an analytical expression

for the elastic stiffness of the specimens used in these experiments which will be used in later sections to normalize results.

Verification of Test System.- It is shown in Appendix I that, even in the presence of warping restraint, the constitutive equation for the bending moment is given by

$$M(x) = EI\, k(x) \tag{3.1}$$

where EI is the usual cross sectional bending stiffness and k is the curvature of the beam. We can approximate the curvature as the difference between the longitudinal strains at the extreme fibers divided by the distance between them. The strain at the extreme fibers, in the absence of axial force, is then given as

$$\epsilon_{11}(x, \frac{d}{2}) = \frac{M(x)}{EI}\,\frac{d}{2} \tag{3.2}$$

where d is the section depth.

Specimens 10 through 15 were gaged at three locations on the flanges at each of the four corners of each specimen (Fig. 1.5). The readings obtained from these gages are plotted along with the extreme fiber strains computed from Eq. (3.2) in Fig. 3.2. The two strain distributions presented for each specimen were measured during the initial elastic level cycling of the test. The distributions for each specimen correspond to a northerly excursion and a southerly excursion. The actual data points, which are connected by solid lines, correspond to the gage locations shown in Fig. 1.5. Only the two five inch segments at the ends of each beam are shown in the figure. The dotted lines correspond to strains computed from Eq. (3.2) based upon the known bending moment. It can be seen that the experimentally measured distributions are close to linear and show good symmetry, verifying the expected symmetry and intensity of the imposed loading. The computed results are based on the section properties given in Table 1.2, using a Young's modulus of 29500 ksi.

Elastic Stiffness of Test Specimens.- Because of the high elastic stiffness of the active links and the small but not negligible flexibility of the supports, experimental determination of link stiffness was not accomplished with great accuracy. For this reason, computed, rather than experimentally measured, values of the stiffness are employed in this study (generally for normalization purposes). Under the conditions imposed by the test apparatus, the stiffness, defined as end displacement divided by applied shear, can be expressed as

$$K = \frac{12EI}{L^3}\left(\frac{1}{1+\frac{12EI}{\kappa G\Omega L^2}}\right) \tag{3.3}$$

where EI is the bending stiffness, $\kappa G\Omega$ is the effective shear stiffness, and L is the length of the link. The measurements of the stiffness of Specimen 1, allowing for support flexibility, was found to be within 15 percent of the stiffness computed using Eq. (3.3).

3.2 The Yielding Limit State

A considerable amount of research has been done in an effort to determine the plastic capacity of beams under the action of shear and bending [5,9,10,14,15,21,22,29,30,31]. Usually, an attempt is made to find the collapse load of a cantilever beam subjected to a tip shear using the bounding theorems of perfect plasticity. Extrapolation of the results to general loading conditions is then suggested. Most of the resulting interaction relationships are given in parametric form and are consequently inconvenient in applications. Neal [31] has suggested an approximate interaction relationship between moment and shear which is adopted here because it is explicit. This relationship is given as

$$\left(\frac{|M|-M^*}{M_p-M^*}\right)^2+\left(\frac{V}{V^*}\right)^2=1 \qquad M^* \leqslant |M| \leqslant M_p \tag{3.4}$$

otherwise $V = V^*$ for $|M| \leqslant M^*$, where V^*, M^*, and M_p are given by

$$V^* = \tau_0(d-t_f)t_w \tag{3.5}$$

$$M^* = \sigma_0(d-t_f)(b-t_w)t_f \tag{3.6}$$

$$M_p = \sigma_0 Z \tag{3.7}$$

In these equations τ_0 and σ_0 are the yield stress in pure shear and pure tension respectively; d, b, t_f, and t_w are the section dimensions; and Z is the plastic section modulus. The relationship is symmetric about M=0.

The moment-shear interaction relationship given by Eq. (3.4) is shown in Fig. 3.3 for two values of M^*/M_p which are representative of the sections used in the experiments. Also displayed in the figure are the initial yield interaction points of the test specimens recorded during the virgin excursion, prior to the onset of strain hardening. The actual values of the applied shear at initial yielding is given for each of the test specimens in Table 3.1, which also gives some information pertinent to the buckling limit state. The size of the circle corresponding to each specimen reflects the uncertainty in the material properties obtained from the tension tests. The first nine specimens corroborate the suggested interaction relationship well, whereas the last six seem to indicate less interaction than Eq. (3.4).

The problem of moment-shear interaction will be addressed again in Chapter 6, wherein the effects of axial forces are taken into account.

3.3. Inelastic Pre-Buckling Behavior

During the inelastic pre-buckling stage of behavior an active link functions most effectively as an energy dissipator. The response of active links in this range of behavior is characterized by remarkable cyclic stability of the hysteretic loops (after a small amount of softening following the virgin inelastic excursion). Strain hardening allows the links to sustain increased loads at increased relative deformations. This type of behavior is desirable since it tends to distribute energy dissipation (and damage) more evenly throughout a structure under severe excitation.

In this section, the behavior of the test specimens in the inelastic pre-buckling range of behavior is examined. Energy dissipation is used as a primary means of measuring the performance of the test specimens. Some strain distributions recorded during the tests which point out the differences between the inelastic behavior of short and long links are also presented. Finally, an attempt is made to integrate these strains approximately to obtain displacements for the purpose of qualitatively assessing the applicability of normality flow rules in stress resultant space.

Energy Dissipation.- In order to make comparisons among all of the tests, it is necessary to normalize the energy dissipation. Thus, the energy dissipated in each half cycle has been divided by the energy that an elastic-perfectly plastic system having the same yield load as the virgin specimen would dissipate if going through the same inelastic deformations. The normalized energy, λ, is plotted in Fig. 3.4 versus a normalized measure of maximum deformation (ductility level), μ, for each half cycle. In the normalization process, the following definitions have been utilized:

$$\lambda = \frac{\text{Actual energy dissipated by test specimen}}{\text{Energy dissipated by elastic–plastic system}} \tag{3.8}$$

$$\mu = \frac{v_{max}}{v_y} \tag{3.9}$$

where v_{max} is the maximum relative end displacement, measured from the most recent point of zero load, and v_y is the relative end displacement at initial yield. The information presented in Fig. 3.4 provides a convenient way of viewing and comparing the performance of the fifteen test specimens of the current investigation. No cause and effect relation between λ and μ is suggested.

The following observations on link behavior can be made based upon the data presented in Fig. 3.4:

(1) Active links which yield primarily in shear (shear links) are more effective energy dissipators than are active links that yield predominantly in bending (bending links).

(2) Shear links are able to achieve greater ductilities than are bending links before failure by tearing. However, it is important to keep in mind that shear links will generally have higher ductility demands placed upon them by virtue of structural configuration [11]. This concept was illustrated in the Introduction to this dissertation for a simple case.

(3) Buckling of the web leads to a significant loss of both carrying capacity and energy dissipation capability. This effect is accentuated when flange buckling is also unrestrained. Flange buckling alone has a relatively minor influence on the behavior of the link.

(4) Bending links are less able to benefit from strain hardening than are shear links.

A general observation to be made from Fig. 3.4 is that the point at which λ begins to decrease corresponds to the point of first significant web buckling. (In this context, significant buckling is defined as buckling which causes a noticeable change in the behavior of the test specimen, as evidenced by visual observation of out-of-plane displacement of the web or by gage readings). The subsequent rate of deterioration depends upon specific detailing (most notably panel size), however some deterioration was noted in all cases. This evidence strongly suggests that web buckling is a useful limit state for active link design. An attempt will be made to quantify this important limit state in Section 3.4.

Inelastic Strain Distributions.- Understanding of the global behavior of an element like an active link is often enhanced by knowledge of local behavior. The global action-deformation relationships presented in Chapter 2 capture only an integrated sense of what occurs. The strains measured during the tests lend insight into the evolutionary processes that take place on a local level. Some important experimentally obtained strain distributions for several of the links are presented in this section.

Shear links dissipate energy through inelastic shear straining of the web region. Therefore, it is instructive to see how these shearing strains distribute themselves upon cycling.

Figure 3.5 gives the maximum shearing strains for the northern and southern legs of the first two cycles for Specimen 1. The first cycle shows that, contrary to what elementary beam theory predicts, the maximum shearing strains occurred near the flanges at the center of the link. Each subsequent plot shows strains relative to the previous one (ie. not the total absolute strains). The first buckling cycle (2N) showed a significant redistribution of the shearing strains. One can see that the tension field had begun to form, but was not yet complete in cycle 2N. Upon reversal to cycle 2S buckling was more severe and the shearing strains had evolved more toward a tension field type distribution. Beyond the second cycle strain gage readings were not reliable because of gage failures due to extremely high skin strains in the bent web.

The important straining for longer links is longitudinal normal straining in the flanges due to bending. Figure 3.6 shows the distribution of flange strains for Specimen 10 at the maximum displacement in both directions of the first three cycles of loading. These data are presented in the same manner as that given in Fig. 3.2. In this figure one can see the distribution of curvature at the ends of the beam. Specimens 11 through 15 all showed straining patterns similar to Specimen 10. For most of the specimens during most of the cycles, the plastic action appeared to be confined to the five inch segments shown. The plastic region showed a tendency to grow in some of the specimens due to strain hardening effects. Buckling markedly changed the curvature distribution in all cases (see, for example cycles 3N and 3S of Specimen 10, Fig. 3.6). The buckling cycle for Specimen 10 was cycle 2S.

Strain-Displacement Relationships.- The connection between the local and global measurements of response can be seen in the form of strain-displacement relationships. The results in this section qualitatively corroborate the widely used normality flow rules used in stress resultant plasticity theories.

The end displacement of the links tested in this investigation can be expressed as

$$v(L) = \int_0^L \beta(x)\, dx + \int_0^L \int_0^x k(\xi)\, d\xi\, dx \tag{3.10}$$

where β is the average shear strain over the cross section and k is the curvature.

The first term on the right hand side of Eq. (3.10) gives the portion of displacement due to shearing strains, denoted here by v_{sh}. A numerical quadrature formula was devised with sampling points corresponding to gage locations in the tests to approximately evaluate this integral for Specimens 1 through 4. The results of this integration are shown in Fig. 3.7(a). It should be noted that nearly all of the displacement in the pre-buckling cycles for these first four specimens was due to inelastic shear strains. This result corresponds well with the idea of normality of flow, considering the location of these specimens on the moment-shear interaction curve (Fig. 3.3).

In the longer links a large contribution to displacement is expected to come from the inelastic curvatures in the "plastic hinge" regions, making the second term on the right hand side of Eq. (3.10) important. Because of the arrangement of flange strain gages it was possible only to compute that portion of the deflection due to curvature over the five inch lengths at the beam ends. Again, this was accomplished using a numerical quadrature formula with sampling points at the gage locations. The resulting quantity is called v_{ph}, and is plotted against the total displacement in Fig. 3.7(b). For the cycles represented in this figure the plasticity in the flanges was confined almost entirely within the five inch lengths included in the integral. Therefore, deflections due to inelastic bending are well represented. Again, the normality flow assumption is qualitatively corroborated.

3.4. The Buckling Limit State

The problem of inelastic buckling under cyclically reversing loads is quite complex. One might generally expect that buckling depends on the element topology, initial imperfections, residual stresses, boundary conditions, and material constitution (through which there is a dependence upon the history of the loading). At the present time, an accurate analytical approach to the problem appears to be prohibitively complex for practical purposes if at all possible. Therefore, an attempt is made to find empirical relationships among some of the

parameters considered to be important to the problem, based on the data obtained from these tests. In this manner one does not expect to "solve" the inelastic buckling problem, but rather one endeavors to derive useful relationships for use in the design of active links.

Among all of the variables thought to influence the problem, one might hypothesize that certain ones are more important than others. Using typical elastic plate buckling solutions as a guide, it appears that the topological measure of greatest importance is the ratio of the minimum panel dimension to the thickness of the web plate, a/t_w. Additionally, it is suggested that some measure of the severity of the loading history be incorporated. Energy measures will be used to characterize the history dependence so that the derived relationships can be applied to situations different from those of the current investigation.

The three energy measures used here are denoted by E_e for elastic energy stored by a beam at yield, and E^* and E^*_Σ for the energy dissipation at a buckling state. Specifically, E^* is defined as the energy absorbed (energy dissipated plus energy stored) during the half cycle in which buckling occurs and is measured from the most recent unloaded state to the point of buckling. E^*_Σ is taken to be the total accumulated energy dissipation accrued throughout the life of the beam from the virgin state up to the point of buckling. The energies at buckling of the test specimens are presented in Table 3.1, along with the applied shear at buckling and the cycle in which buckling occurred.

The total accumulated energy dissipation at buckling, E^*_Σ, has been normalized by the elastic energy E_e and the natural logarithm of the resulting quantity has been plotted against the ratio a/t_w in Fig. 3.8(a). The remarkable correlation of the data leads one to hypothesize a log-linear relationship between the quantities. The straight line that best approximates these data in a least squared error sense is given by

$$\frac{a}{t_w} = 90 - 9 \ln \left(\frac{E^*_\Sigma}{E_e} \right) \tag{3.11}$$

This simple relationship provides a means of determining stiffener spacing based upon

Specimen	Yield Shear (k)	Buckling Shear (k)	Buckling Cycle	E_e (in-k)	E^* (in-k)	E^*_Σ (in-k)
1	121	135	2N	4.1	95	230
2	120	161	2S	4.1	260	580
3	122	184	6N	4.1	540	3300
4	126	207	9S	4.5	880	8600
5	121	172	4S	4.1	430	1860
6	128	191	5N	4.6	400	2170
7	147	206	6S	6.3	630	3850
8	189	240	5N	10.3	500	2530
9	124	172	5N	6.2	370	1900
10	118	123	2S	8.5	120	335
11	147	157	2S	9.3	150	420
12	81	96	4S	6.1	160	790
13	118	135	4S	8.5	280	1200
14	143	184	5S	9.3	390	2380
15	80	102	6S	6.1	260	1760

Table 3.1 Yield and Buckling States

knowledge of the web thickness and the expected energy dissipation requirement. Alternatively, one could determine the required web thickness based upon desired panel zone size and energy requirements. Note, however, that it is undesirable to alter the web thickness of a section through addition of welded doubler plates. Experiments have shown that composite action is rarely realized in such situations [41,43].

Since the loading program for all of the specimens in the sample was similar, Eq. (3.11) may not be adequate to cover a sufficient variety of loading histories. It is, in fact, best suited to a situation wherein a considerable amount of inelastic activity occurs prior to buckling. Most notably, Eq. (3.11) might be expected to be in error for a monotonic loading from the virgin state to buckling. For this reason a second relationship is proposed. While the data of these tests are not ideally suited to this purpose, they will be used here recognizing that the resulting formula will be conservative.

Because the test specimens showed excellent cyclic stability of their hystersis loops, it is not unreasonable to consider the energy measure E^* to be an approximate monotonic buckling energy. The natural logarithm of E^*/E_e is plotted against a/t_w in Fig. 3.8(b). Inasmuch as prior loading history probably reduces the resistance to buckling, the values presented here tend to underestimate the monotonic buckling energies. A relationship similar to Eq. (3.11) is found again by log-linear regression and is given by

$$\frac{a}{t_w} = 94 - 14 \ln \left(\frac{E^*}{E_e} \right) \tag{3.12}$$

The suggested design procedure consists of insuring that the ratio a/t_w is less than the smaller of the two values as determined by Eqs. (3.11) and (3.12), based upon the best estimate of the energy dissipation requirements. Simple manipulation of these two equations shows that when

$$\frac{E_\Sigma^*}{E_e} \geqslant \frac{2}{3} \left(\frac{E^*}{E_e} \right)^{\frac{3}{2}} \tag{3.13}$$

then the cumulative energy criterion controls and Eq. (3.11) is appropriate. Otherwise, the maximum monotonic energy criterion governs and Eq. (3.12) should be used. An accurate estimate of the energy dissipation required of an active link is best obtained from an inelastic dynamic analysis. Values of $a/t_w \leqslant 20$ indicate excessive, perhaps insatiable, energy dissipation requirements.

Under certain conditions the two energy measures can be related to member ductility demands. If it is assumed that the material is elastic-perfectly plastic and that inelastic deformations are predominantly due to shear, the problem becomes essentially one dimensional, and the following relationships apply

$$\frac{E_\Sigma^*}{E_e} = 2 \sum_i (\mu_i - 1) \tag{3.14}$$

$$\frac{E^*}{E_e} = 2\mu - 1 \tag{3.15}$$

where μ is defined as in Eq. (3.9) and the sum in Eq. (3.14) is taken over the i excursions having $\mu_i > 1$. Note that relationships involving ductility levels employed here refer exclusively to member ductilities, which may be an order of magnitude greater than any measure of structure ductility for eccentrically braced frames. Some approximate methods for estimating the relationship between member and structure ductility are given in [11].

3.5. Post Buckling Behavior

After the web of an active link buckles, the link continues to dissipate energy. However, the predominant load carrying mechanism changes and therefore so does the means of dissipating energy. The data presented in Fig. 3.4 clearly indicate that the post-buckling energy dissipation mechanism is less efficient than the pre-buckling one. In this section the post-buckling phenomenon will be treated qualitatively. To aid the discussion, reference will be made to Fig. 3.9, which shows a typical force-deformation relationship of a previously buckled active link. Figure 3.10 shows a schematic representations of the buckling fields characteristic of post-buckled links for shearing in two opposite directions.

Suppose that a buckle has fully developed as a result of loading in one direction, as shown in Fig. 3.10(a). In this configuration a tension field exists with the principal tension oriented along the buckle. A compression field oriented approximately orthogonal to the tension field also exists but the forces in it are much smaller due to the geometry of the deformed web. When the sense of the load is reversed the orientation of the tension and compression fields reverse. As the state progresses toward point **A** on Fig. 3.9, the principal tension acts to straighten the residual out-of-plane displacement left from buckling in the opposite direction while the compressive stresses act to form a new buckle. At point **A** buckling occurs and a loss of load carrying capacity results. The instability is usually not catastrophic, however, because buckling is arrested by the formation of a tension field in the opposite direction. Point **B** in

Fig. 3.9 marks the instant at which the tension field action becomes the predominant load carrying mechanism of the link. As the state approaches that shown in Fig. 3.10(b), the capacity increases, often surpassing the buckling load (V_A).

The buckled mode shape has effects on both the load carrying capacity in the post buckling range and on the eventual mode of failure. The shape that a buckled web takes appears to depend largely on the aspect ratio of the panel and the boundary conditions. The basic shape, shown in Fig. 3.10(a), consists of a diagonal bulge spanning the minimum dimension and extending some distance along the maximum dimension of the panel zone, reminiscent of the elastic buckling case. The longer the span of the buckle is, the greater is the out-of-plane displacement of the web. Upon removal of the load the buckle remains. For values of $a/b < 1.6$ the buckle angle θ is approximately given by

$$\tan\theta = \frac{b}{a}. \tag{3.16}$$

In other words, it is controlled by the panel dimension, and the buckle tends to run from corner to corner in the panel. However, for $a/b > 1.6$ there appears to be a minimum value of $\theta \approx 32°-33°$. The angle θ is influenced by the extent of flange buckling. A reversal of load causes a buckle to form which is roughly a reflection of the original one about the panel centerline as shown in Fig. 3.10(b). The relationship between the buckling modes and active link behavior will be discussed in the sequel. The peculiarities noted in the action-deformation relationships of the post-buckled links can be accounted for by looking more closely at the inelastic buckling modes of the webs of active links. The spatial distribution of the web buckle in the x,y plane, which has already been discussed, coupled with various possibilities of out-of-plane displacement of the web, lead to different post-buckling behavior.

Consider the typical buckled panel zone shown in Fig. 3.11(a), onto which the local buckle coordinates t and n have been superposed. In the t direction, which corresponds to the tension field direction, the out-of-plane displacement w goes from zero at the buckle ends to some maximum value in the center in single curvature bending (Fig. 3.11(b)). The n direction

admits two possible deformation patterns, as shown in Fig. 3.11(c). The first, symmetric about $n = 0$, has two regions of positive curvature and a single region of negative curvature (or vice-versa depending on sign convention), and admits a single maximum displacement. The second, anti-symmetric about $n = 0$, has two positive and two negative regions of curvature and admits both a maximum and a minimum displacement. In general, curvature in the central two regions has much greater magnitude than those in the outer two.

Each of the links in the test program experienced one of the buckling modes depicted in Fig. 3.12. The discussion of these buckling modes is facilitated by introducing the following definitions: A *Strong Nodal Point* is a neighborhood containing maximum curvatures in both the t and n directions which experiences a complete curvature reversal in both directions upon cycling. Similarly, a *Weak Nodal Point* is a neighborhood containing maximum curvatures in both the t and n directions which experiences a complete reversal in curvature in only one direction. A *Null Nodal Point* is similarly defined except that no curvature reversal takes place. We will find that the presence of strong nodal points have a marked effect on post-buckling link response.

The first symmetric case is shown in Fig. 3.12(a). Here the (t_1,n_1) buckle displaces in a positive direction, whereas the (t_2,n_2) buckle displaces negatively, giving rise to a single strong nodal point at the intersection of the t_1-t_2 axes. Four weak and four null nodal points exist as shown in the figure. This mode of buckling will be termed *Mode 1* buckling and was noted only in Specimen 1. The other symmetric mode, termed *Mode 2* buckling, is shown in Fig. 3.12(b). This mode admits only displacement in one direction for both the (t_1,n_1) and the (t_2,n_2) buckles, forming four strong, four weak, and one null nodal point(s). Since $|k^+_{max}| < |k^-_{max}|$, as defined in Fig. 3.11(c), the strong nodal points of Mode 2 buckling have less severe curvature reversals than the single strong nodal point of Mode 1 buckling. This difference affects the failure mode markedly and will be discussed later. Specimens 5, and 9 provided examples of Mode 2 buckling. Finally, the only anti-symmetric mode, *Mode 3* is shown in Fig. 3.12(c). This mode contains the two strong and two null nodal points shown.

Specimens 2, 8, 10, 11, and 13 exhibited this mode of buckling.

After buckling and prior to tension field formation a link has a state of lowered resistance to shear. This state appears to correspond closely with the moment of occurrence of curvature reversal in the strong nodal points (and probably also in the weak nodal points, albeit to a lesser extent). Each nodal point traverses its zero curvature point (ie. "snaps through") at a different time in the loading process. The tension field is not able to form until all nodal points have reversed their curvature. Specimen 1 showed an immediate formation of a tension field upon reaching the post-buckling minimum load because only one strong nodal point had to reverse curvature. Specimens 5 and 9, with four strong nodal points each, required a considerable deformation to form tension fields, indicating that each of the four points reversed at different times but that the effects of reversal overlapped to a large extent. Specimens 2, 8, 10, 11, and 13 showed lightly coupled or uncoupled curvature reversals which lead to two apparent minimum strength points after buckling.

Slowing of the degradation of member properties in the post-buckling regime is effectively achieved by controlling the amplitude of buckling. This control can be realized through transverse stiffening of the web region. The correlation between loss of load carrying capacity and out-of-plane displacement is shown in Fig. 3.13 for Specimens 10 and 11. As has already been noted, stiffening also delays the first occurrence of web buckling.

Interaction Between Web and Flange Buckling.- Severe flange buckling only occurred in two of the specimens: 12 and 14. However, cyclic web buckling was always accompanied by flange distress of some kind. Mode 1 and Mode 2 buckling generally caused a pinching together but no rotation of the flanges. Mode 2 buckling occurred in links with smaller a/t_w ratios where the flanges had high torsional restraint. Mode 3 buckling occurred in links with long unsupported lengths of flange and caused the flanges to rotate rather than pull together. In the two specimens in which flange buckling was important (ie. Specimens 12 and 14), web buckling was also present. In these cases, there was considerable interaction between the two

buckling fields causing lateral-torsional buckling of the link as a whole. This lateral-torsional buckling can be effectively controlled by either stiffening the flanges as was done in Specimen 15, or by providing some external torsional restraint, such as a concrete slab.

The Role of Stiffeners in Post-Buckling Behavior.- The first function the transverse stiffening elements perform is to prevent or delay the initial occurrence of web and/or flange buckling. Little data are available regarding what the stiffener stiffness should be to successfully achieve this goal for the case of inelastic web buckling. The role of the web stiffeners in the post-buckling range changes from that of enforcing a nodal line at the panel boundary to that of completing the trussing action induced by the tension field. If the active links are expected to perform into the post-buckling range, then the tension field action will be the more critical state for the stiffeners.

No rational design procedures exist for either of these limit states, and stiffener sizing for the test program was necessarily ad hoc. All of the stiffeners in the tests were of identical size and weld detail: 3/8 inch thick, fillet welded all around. Consideration of the measured strains in the stiffeners gives some indication as to their adequacy for the truss type action.

Immediately upon buckling in Specimen 2 the stiffeners registered bending skin strains in excess of yield with relatively little net axial strain. No visible distress occurred until the fifth cycle when maximum skin strains reached 6000 microstrain and net axial strains reached about 2000 microstrain. The stiffeners of Specimens 3 and 4 remained elastic throughout the tests measuring maximum axial strains of approximately 500 microstrain, well below yield. In Specimen 5 the stiffeners achieved a net axial strains of 1000 microstrain, still below yield. The stiffeners of Specimen 6 bent later in the test but strained very little axially. Specimen 7 registered net axial strains of 2500 microstrain, as did Specimen 9. Yielding of the stiffeners seemed to have minimal deleterious effect on specimen behavior in these tests.

3.6. Active Link Failure

The failure of an active link is defined as complete inability to sustain load, and is generally caused by low cycle fatigue in highly localized regions which experience extreme strain reversals due to the cyclic changing of the buckled mode shape. In all cases failure corresponded to material tearing somewhere in the link. Two distinct failure modes were noted in the tests: (1) Tearing of the web at a strong nodal point because of material fatigue from severe cyclic curvature reversals, and (2) Tearing of the web around the perimeter of the most severely buckled panel zone. Both modes of failure were catastrophic. Specific modes of failure are highly dependent upon how the link is detailed. For example, all of the single panel specimens (Specimens 1, 8, 10, 11, and 12) failed by material tearing in the middle of the panel zone, whereas Specimens 2, 4, 5, 6, 7, 9, 13, and 14, which were all multi-paneled specimens, failed by material tearing around the perimeter of the buckled panel zone(s). All cases of Mode 1 and Mode 3 buckling lead to the first type of failure. The second type of failure was characteristic of Mode 2 buckling. Specimens 3 and 15 both failed prematurely due to fracturing of the flange welds. One should note that none of the welds was tested ultrasonically.

The total energy dissipated by each specimen at failure is shown in Fig. 3.14. Also shown is the total energy dissipated at buckling, E_{Σ}^{*}. Both energy measures are normalized by the elastic energy E_e. Clearly, a considerable amount of energy is dissipated in the post-buckling range prior to failure. One can note, however, that as the panel aspect ratio a/t_w decreases the ratio of pre-buckling life to post-buckling life decreases. Since the point of failure is less predictable than the point of buckling, and since the consequences of failure are greater it is suggested that failure is a less appropriate limit state for design purposes than is buckling. It is recommended that the post-buckling energy dissipation capacity be viewed as a factor of safety against sudden catastrophic failure.

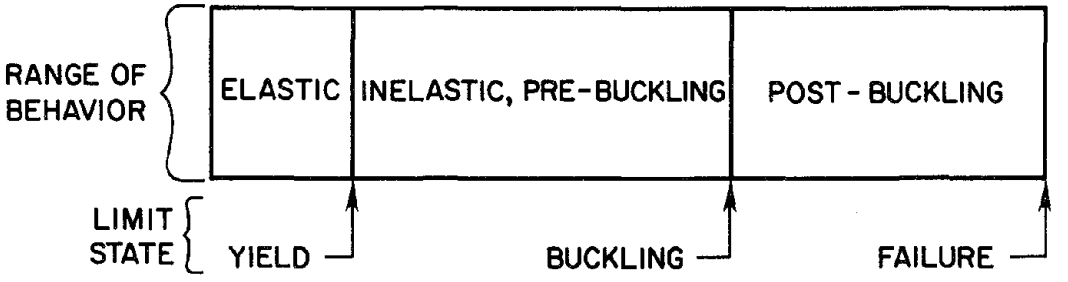

Fig. 3.1 Schematic Representation of Active Link Behavior

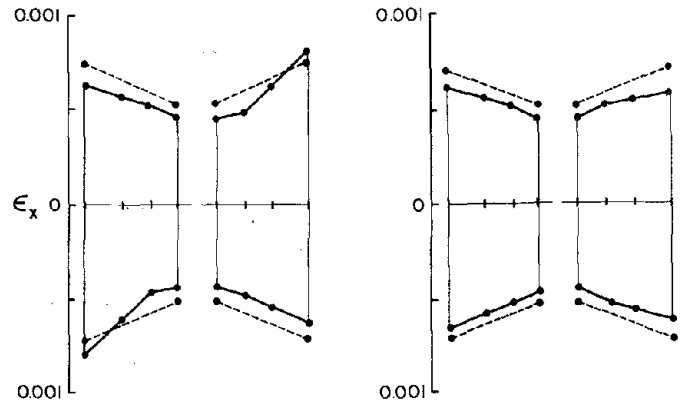

(a) Specimen 10

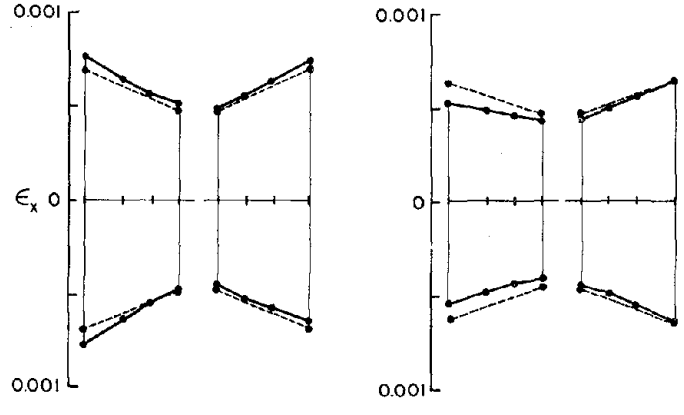

(b) Specimen 11

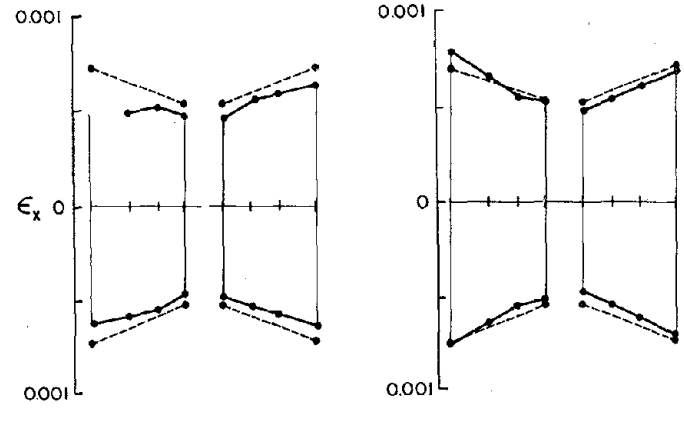

(c) Specimen 12

Fig. 3.2 Longitudinal Flange Strains for Specimens 10-15, Elastic Level Cycles (Solid line = Experimental, Dotted line = Analytical)

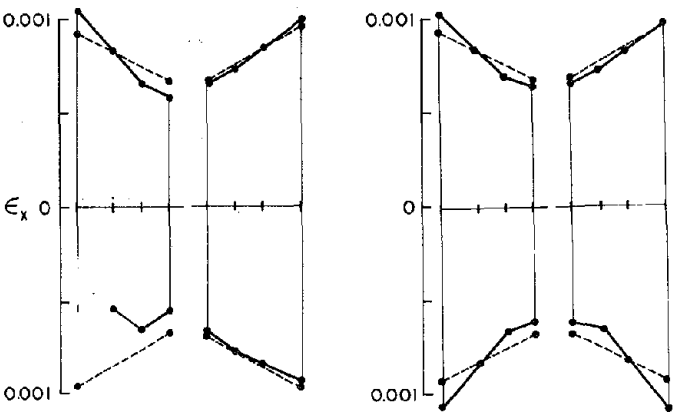

(d) Specimen 13

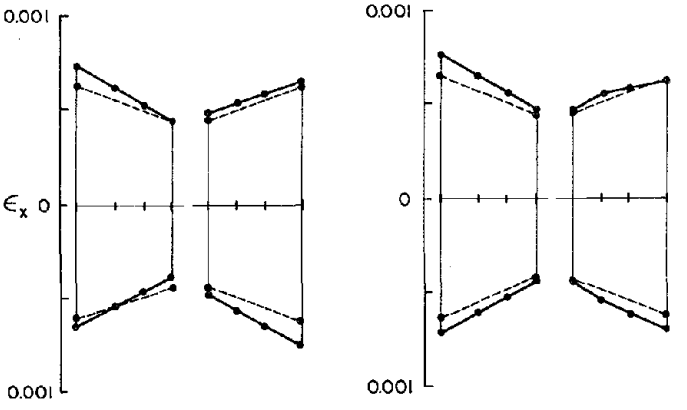

(e) Specimen 14

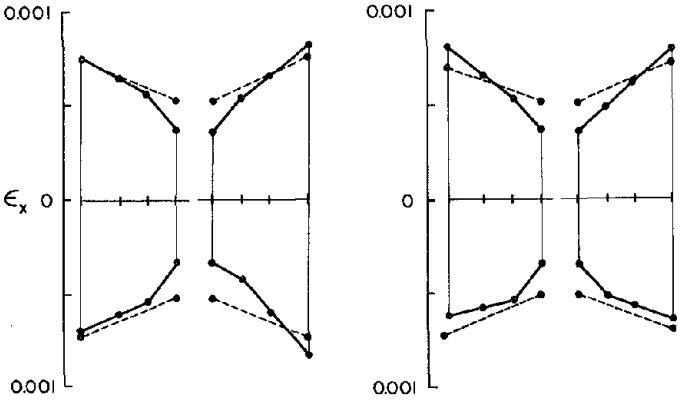

(f) Specimen 15

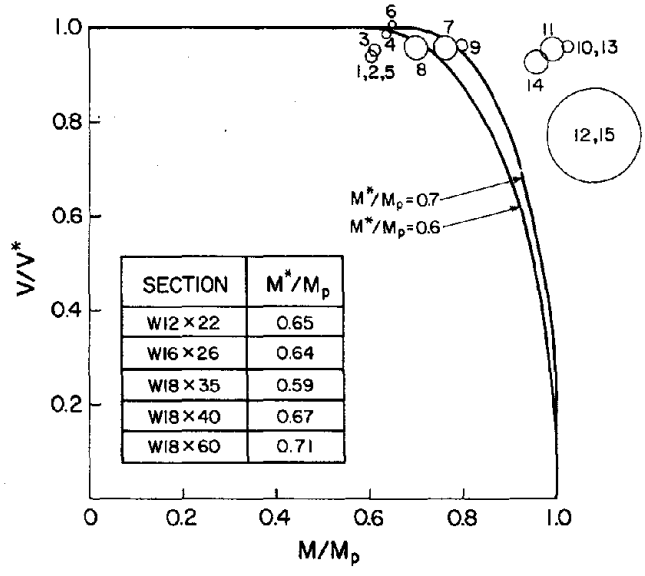

Fig. 3.3 Moment-Shear Interaction: Experimental and Analytical

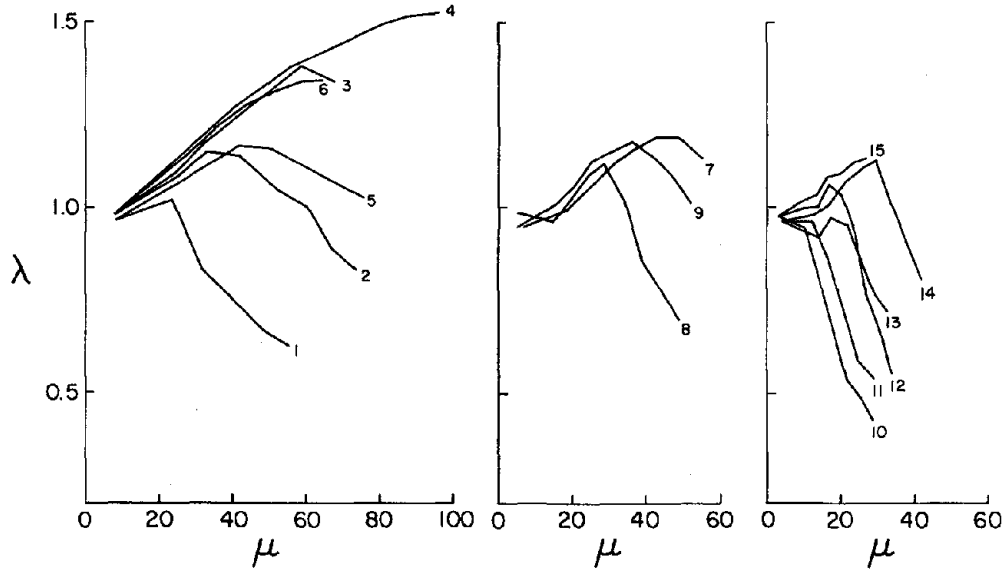

Fig. 3.4 Normalized Energy Dissipation vs. Cyclic Ductility Level
(Numbers correspond to specimen numbers)

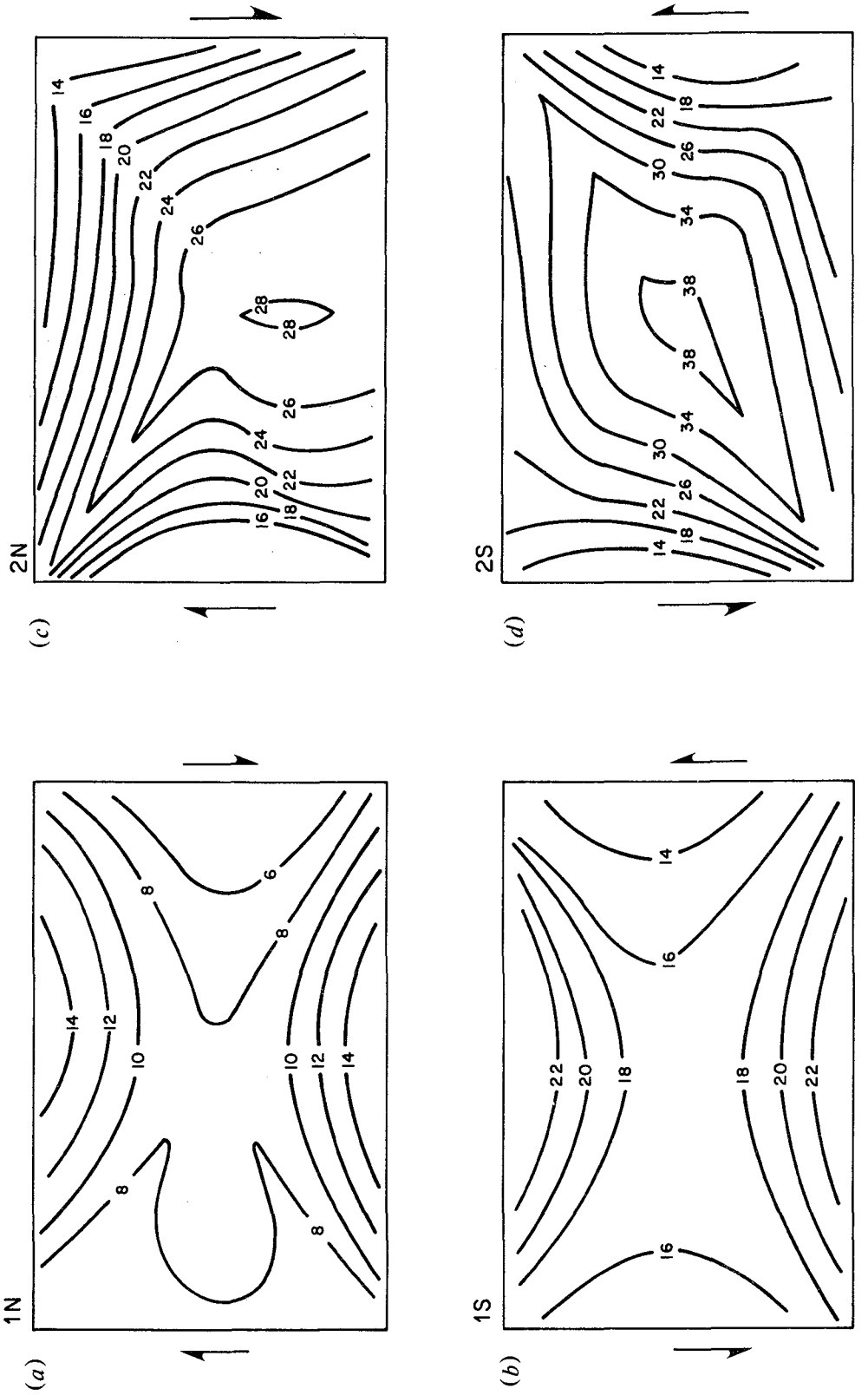

Fig. 3.5 Shear Strain Distributions for Specimen 1 for the First Two Cycles of Loading

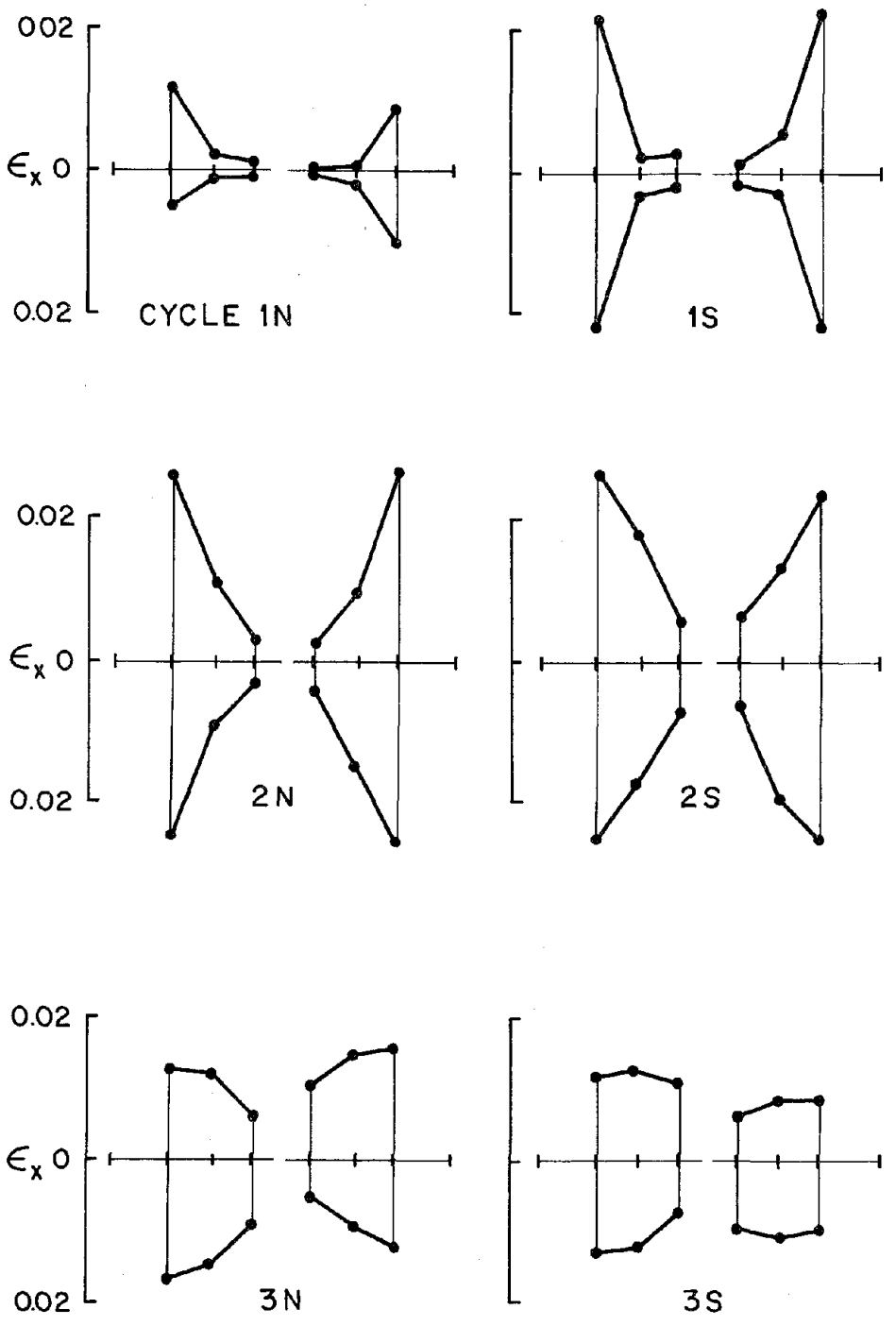

Fig. 3.6 Longitudinal Flange Strains for Specimen 10 for the First Three Cycles of Loading

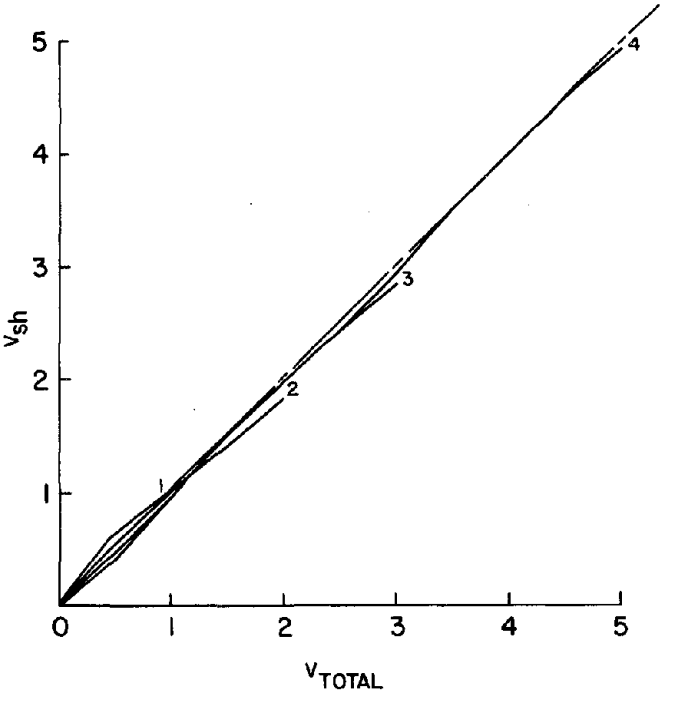

(a) Displacements Due to Shearing Strains for Specimens 1-4

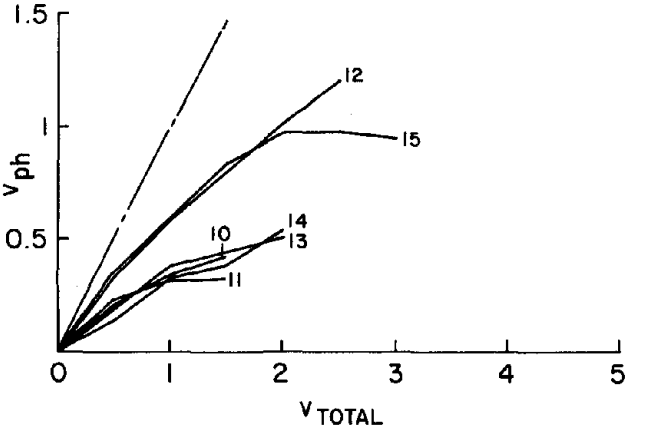

(b) Displacement Due to Curvature in End Segments for Specimens 10-15

Fig. 3.7 Components of Inelastic Pre-Buckling Displacements

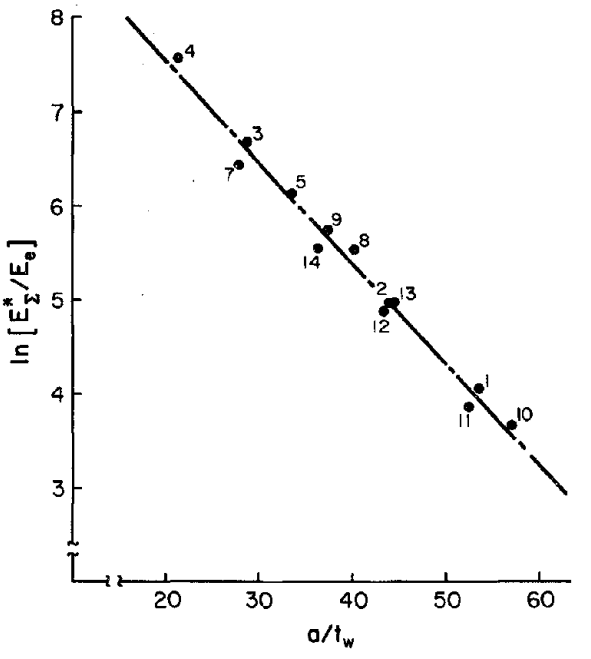

(a) Cummulative Energy Criterion

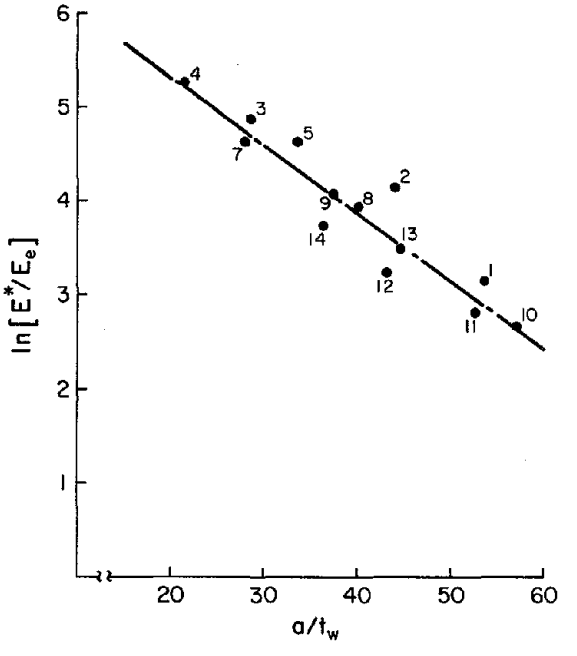

(b) Monotonic Energy Criterion

Fig. 3.8 Energy Dissipation at the Buckling Limit State

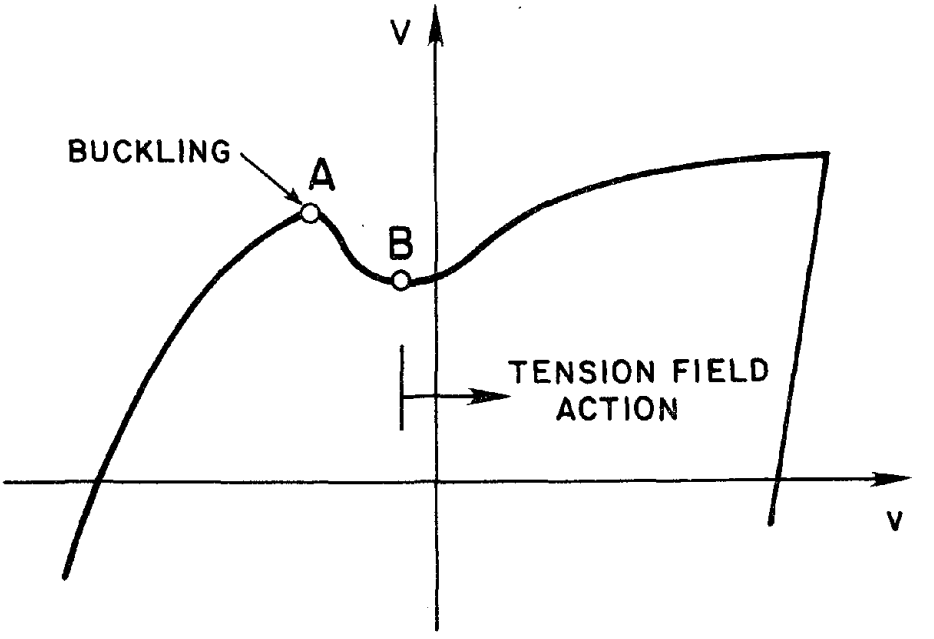

Fig. 3.9 Typical Post-Buckling Behavior of an Active Link

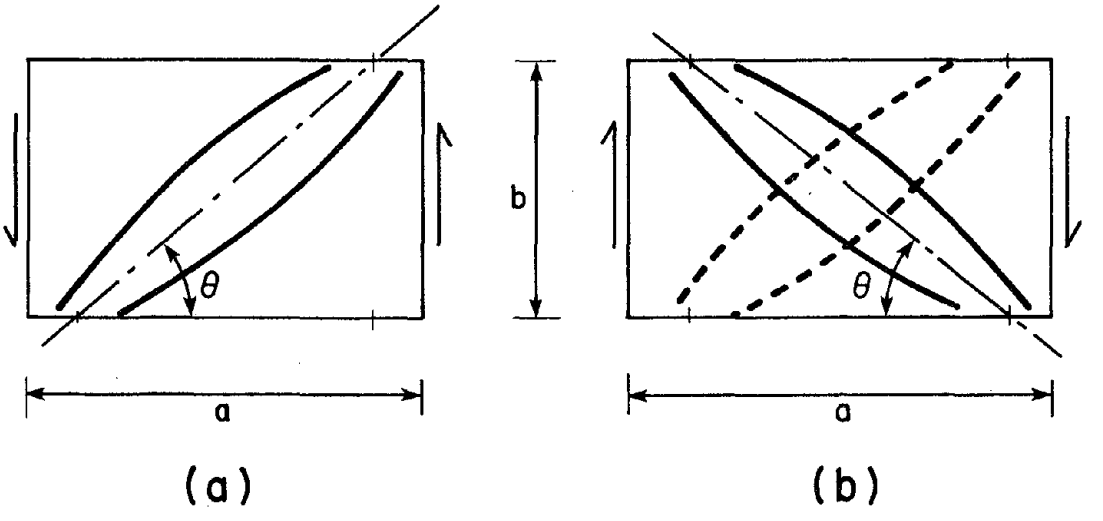

Fig. 3.10 Schematic Representation of Shear Buckling Fields

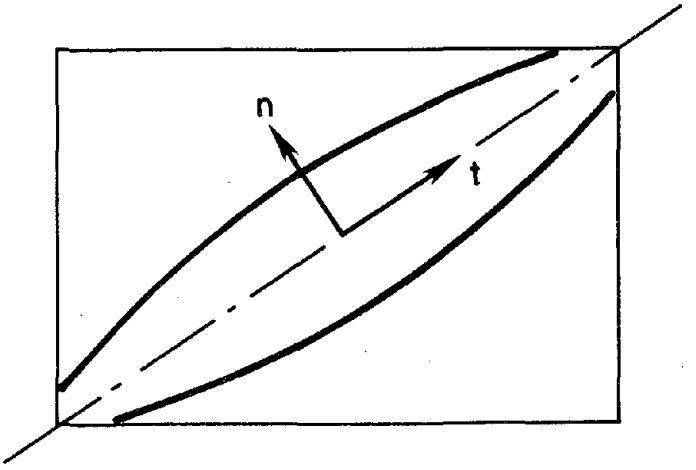

(a) Local $t - n$ Coordinates

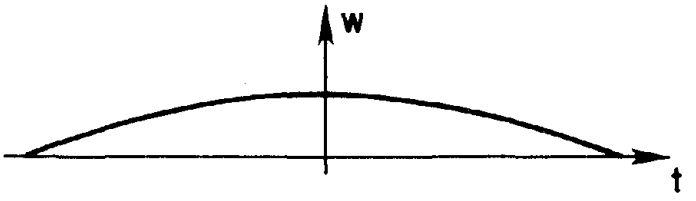

(b) Distribution Along Buckle (t direction)

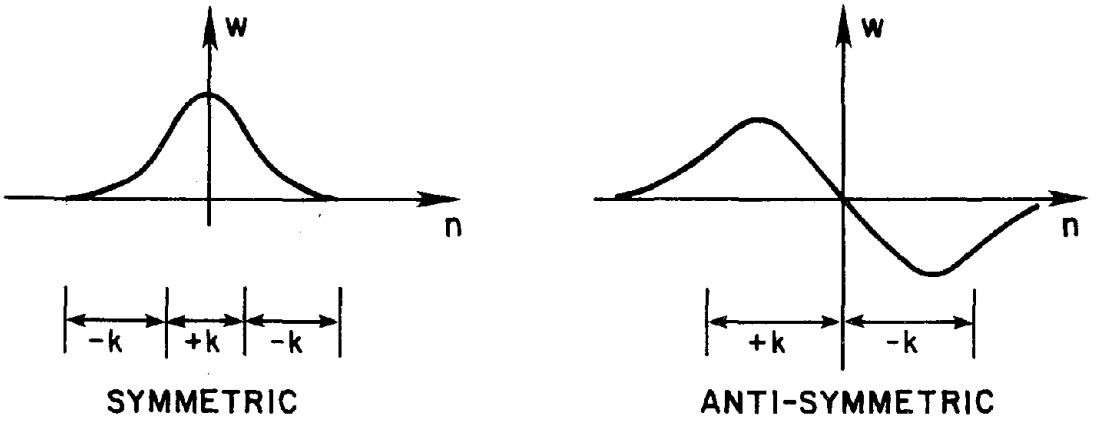

(c) Distribution Orthogonal to Buckle (n direction)

Fig. 3.11 Spatial Distribution of Out-of-Plane Displacements in a Buckled Web

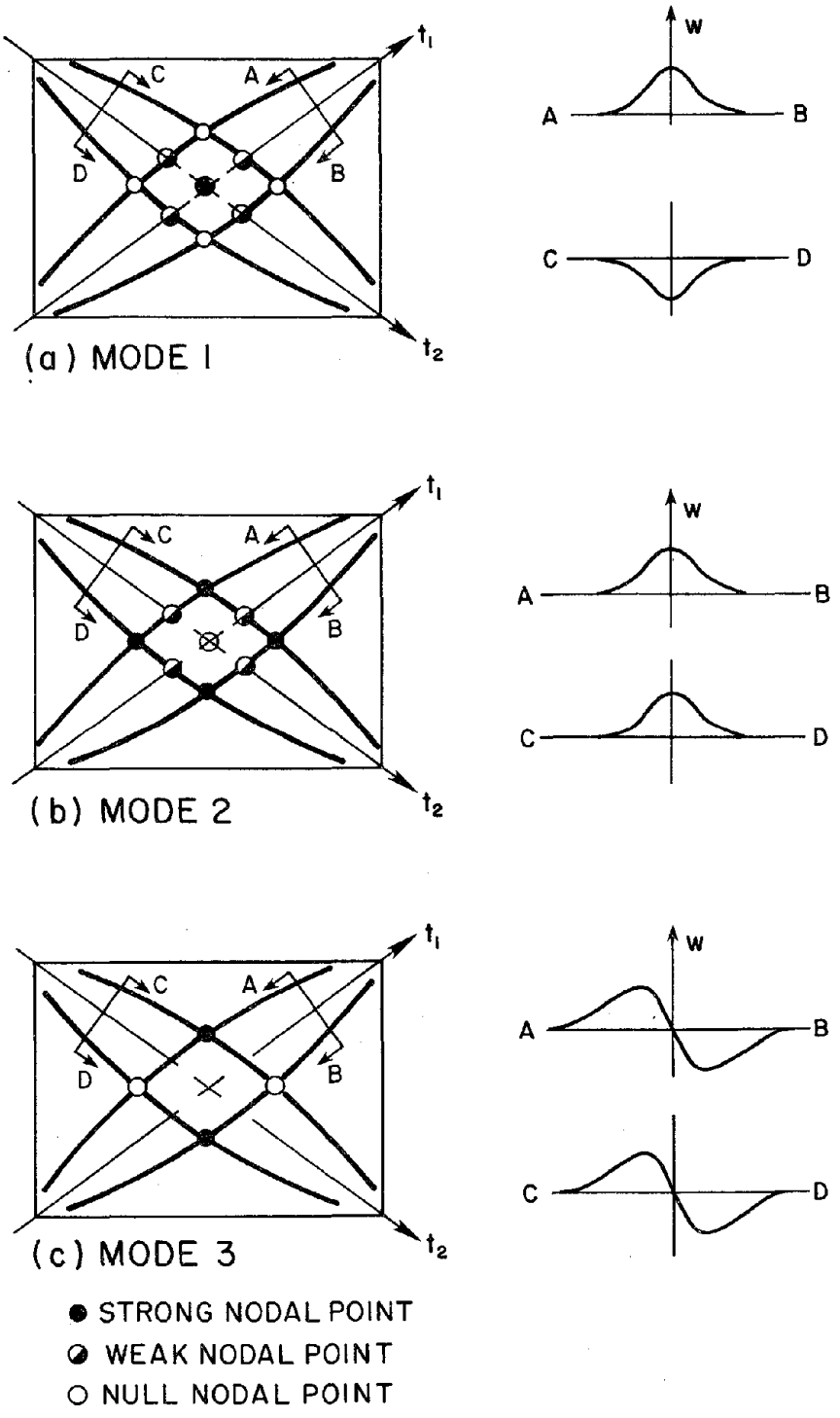

Fig. 3.12 Three Possible Modes of Inelastic Web Buckling

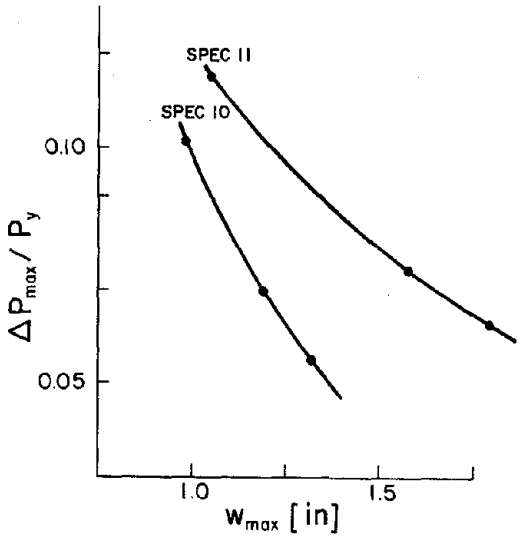

Fig. 3.13 Loss of Carrying Capacity vs. Amplitude of Out-of-Plane Web Displacements

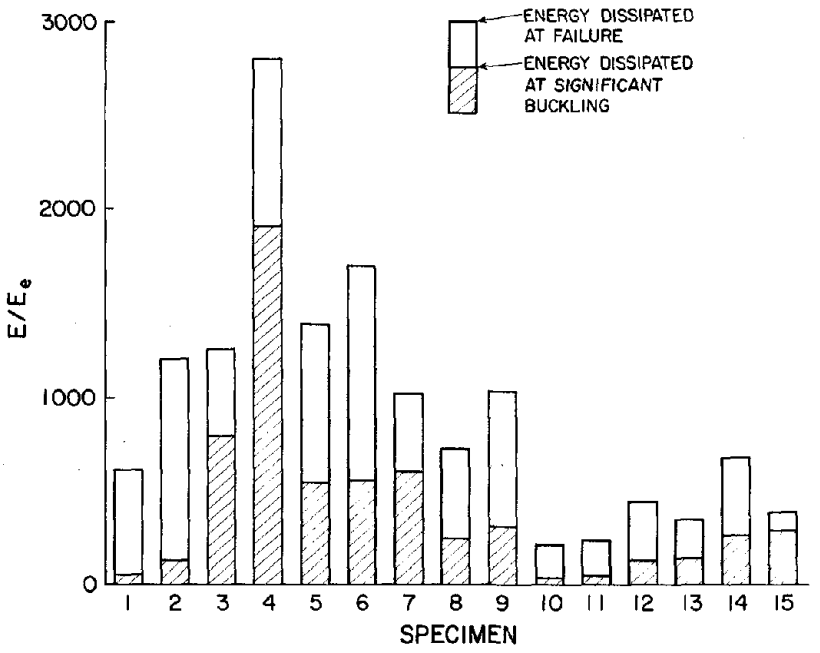

Fig. 3.14 Energy Dissipation at Buckling and Failure for the Test Specimens

Chapter 4

Introduction to the Analysis of Active Links

The inelastic response of an eccentrically braced frame is dominated by the behavior of the active link regions. Hence, accurate modeling of these elements is crucial. Many formulations employed in the analysis of structural systems neglect the effects of shear, either by neglecting elastic shearing deformations or by neglecting the effect of shear on the behavior in the inelastic range. Such models are of dubious value for the analysis of eccentrically braced frames. The following chapters consider the problem of analytically modeling the elastic and inelastic pre-buckling behavior of active links. The developed models are also applicable to the other structural components in an eccentrically braced frame, for which the effects of shear might be reasonably neglected.

Efforts have been made to analyze the global dynamic response of eccentrically braced frames, recognizing that the active link elements must be specially treated [43,49]. In these attempts, the active link has been modeled using a greatly simplified analog related to the real body. Such models offer the advantage of computational simplicity, since they represent "one dimensional" approaches to an inherently multidimensional problem. On the other hand, they can be expected to apply only in very restricted cases (generally only for shear beams, which come close to exhibiting one dimensional response).

Roeder [43] modeled the active link as a "sandwich beam" [†]. Unfortunately, the sandwich assumption is deficient in cases where interaction between axial force, shear force, and bending moment is important. This deficiency can be recognized by noting that shear and normal stresses never occur simultaneously at any point in a cross section of a sandwich beam. Therefore, the resultant shear force can never interact with the axial force and/or bending moment.

[†] A sandwich beam has a core (web) and cladding (flanges). The core is assumed to develop *only* shear stresses and the cladding *only* normal stresses.

Moment-shear-axial force interaction is often important in the behavior of active links in eccentrically braced frames.

Another important difference between the sandwich beam and the I-beam is the boundary condition on the transverse shear stress component on the inside edge of the flanges. In both cases, this shear stress component can exist only in the region where the flange connects to the web. For the sandwich the web is connected over the full length of the flange, for the I-beam the region of connection is only over the small thickness of the web. Roeder [43] attempted to address the question of the effect of warping restraint at the ends of an active link, following the derivation of Plantema [37] for the sandwich beam idealization. As a result, some inaccurate conclusions were obtained regarding the extent to which transverse shear force can be developed by the flanges. This consideration is re-examined in Appendix I utilizing the more physically reasonable thin walled beam approximation.

Yang [49] modeled the active link as an inclined truss element in an effort to represent the behavior with a one dimensional element. The shortcomings of this approach, which appear to be inspired by a pure shear assumption in the web region, are evident.

While the behavior of the simple physical models can be made to resemble experimentally observed behavior of active link by adjusting phenomenological parameters, it is felt that this type of modeling is ultimately restrictive and might lead to erroneous results when used for situations other than those for which the model was specifically tuned. The main drawbacks of the aforementioned models is that they oversimplify the problem with the result that some of the important physics of the problem is lost. As Einstien said, "Things should be as simple as possible, not simpler."

In the remaining chapters a different course is followed in the analysis of the inelastic behavior of short beams. The model presented in Chapter 5 employs the three dimensional, nonlinear equilibrium equations of continuum mechanics as its basis. These equations are supplemented with a three dimensional elasto-plastic constitutive model. The point of departure from the general three dimensional theory comes from the consideration of a specific kinematic

hypothesis which constrains the deformation map. The kinematic hypothesis employed here accounts for warping of the cross section due to transverse shear, and thereby allows a characterization of the inelastic behavior of short beams not achieved previously.

A simplified model is presented in Chapter 6 based upon stress resultants as the primitive action quantities. This development does not rely upon the introduction of physical entities called "plastic hinges" (see, for example, [3]), but upon a plasticity theory for stress resultants which has a theoretical appeal in its own right [13]. The fundamental problem in the stress resultant approach occurs due to the inclusion of transverse shear in the expression for the yield potential. One popular approach to problems of this nature is to employ a yield potential of "general" form, such as a conic with adjustable parameters. Such an approach for the problem of biaxial bending and torsion has been followed in [3]. This method avoids many of the problems associated with the stress resultant approach, but in many cases it is difficult to find a simple yield potential which can characterize the "true" yield potential over all combination of moment, shear, and axial force. Moment-shear-axial interaction for an I-beam is a case where these difficulties arise.

The purpose for presenting two approaches is one of hierarchical corroboration of results. Using the stress component model as a basis for comparison one can readily assess the performance of the stress resultant model. Inasmuch as both models are based on the same kinematic assumption, a "fair" evaluation of the results is possible. In this way one is better able to determine which effects are due to the geometry of the body and which are due to the mechanical behavior of the material.

In both models presented the constitutive behavior adopted is one of perfect elasto-plasticity using an elasto-viscoplastic model in a penalty procedure. The perfectly plastic model does capture one of the most important aspects of the inelastic behavior of eccentrically braced frames: namely, the redistribution of forces within the structure due to inelastic action. The inclusion of strain hardening effects in both of the formulations presented could be achieved by introducing "tunable" hardening parameters. Because of the uncertainties associated with tuning

these parameters, the problem of incorporating hardening effects is not pursued here and attention is focussed on providing a well-founded basis for the analysis of active links in eccentrically braced frames. It is hoped that these models can provide a useful tool in both conceiving and assessing simpler models which might be used in the analysis of large structural systems.

In Chapter 7 the two analytical models are applied to the case of interest here: the eccentrically braced frame. The first two examples have been included to illustrate some aspect of the formulations, and to compare the two approaches. The last three examples are static analyses of three frames having one bay and three stories.

Chapter 5

A Local Approach to the Analysis of Active Links

5.0. Introduction

In this chapter the problem of analyzing the inelastic bending of a beam is approached by considering it in a three dimensional setting. We begin by considering the general non-linear local equilibrium equations of a continuum. To these equations a set of constitutive relations, here taken to be those of elasto-viscoplasticity, are added. The point of departure from the three dimensional formulation of the problem comes in the consideration of kinematics.

The deformation map is restricted by postulating a kinematic hypothesis which depends passively on the cross sectional coordinates and actively on the longitudinal coordinate. This hypothesis suggests the denomination of "beam theory". Previous efforts in this direction have used the assumption that sections which are plane before deformation remain plane after deformation [35,36]. For the problem at hand, ie. the active link, this kinematic hypothesis is inadequate due to the importance of shear stresses and shear strains. The plane sections hypothesis leads, in the context of the linear theory, to a constant distribution of shear strains over the cross section of the beam. Because of this restriction, there is no possibility for yielding to propagate from the interior of the section due to shear. Furthermore, vanishing of shear stresses at the boundaries can never be realized under this restriction.

Numerical treatment of the problem is accomplished through an iterative procedure of first linearizing the equilibrium equations about an intermediate configuration and then solving the resulting linear problem for the incremental motions. The updated configuration determines the state of strain in the body, for which the corresponding state of stress can be found by solving the nonlinear constitutive equations.

Several features of the solution process are of special interest. First, since the constitutive equations depend upon time they must be integrated. Due to the nonlinearity of these relationships direct quadrature is not generally possible and hence a numerical procedure first proposed by Hughes and Taylor [16] is employed. Second, spatial aspects of the problem are treated numerically by a finite element discretization technique. Because the distribution of stress over a cross section is generally nonlinear due to the propagation of inelasticity the element stiffness matrix and out-of-balance force vector are necessarily evaluated by numerical quadrature. The global algorithm employed for the solution of the problem is the one proposed in [46].

The advantage of adopting the point of view taken here is that the constitutive behavior can be described at the local level. From the standpoint of constitution, then, the model is restricted only by our ignorance of material behavior. There is no need to assume that the force-deformation behavior of a structural element is fundamental. Even within the scope of the restricted kinematics we can accurately solve inelastic bending problems for difficult cross sectional geometries like the I-beam.

Notation.- The present development is concerned with an initially straight beam having length L and cross section Ω which has a piecewise smooth boundary $\partial\Omega$. Coordinates in the reference configuration $B \equiv (0,L)\times\Omega \subset \mathbb{R}^3$, occupied by the beam at time $t = 0$, are designated by $\{X_I\}$. The spatial coordinate system $\{x_I\}$ is taken, for our purposes to be collinear with $\{X_I\}$. The deformation map is denoted, following standard notation, by Φ and the deformation gradient by $\mathbf{F} = \dfrac{\partial\Phi}{\partial X}$. The points $X \in B$ and $x \in \Phi(B)$ will be identified by their position vectors $\mathbf{X}$ and $\mathbf{x}$ respectively.

A further assumption is made that the line of centroids of the cross sections is initially oriented along the X_1 axis. For simplicity, we will consider only cases in which the applied transverse loads pass through the shear center of the section, which for doubly symmetric sections coincides with the centroid of the section. Thus, the problem of torsion of the beam will not be treated here. A further simplification is that transverse loads are applied only in the X_2

direction. It should become clear from the presentation how to extend the formulation to the case of biaxial bending.

5.1. Equations of Equilibrium

The static balance of linear momentum is expressed by the equation [26,28]

$$\mathrm{DIV}\,\mathbf{P} + \rho_o \mathbf{B} = 0\,; \qquad \mathbf{X} \in B \tag{5.1}$$

where $\mathbf{P}$ is the first Piola-Kirchhoff stress tensor, ρ_o is the density in the reference configuration, and $\mathbf{B}$ is the body force. Balance of moment of momentum further implies the symmetry $\mathbf{P}\mathbf{F}^T = \mathbf{F}\mathbf{P}^T$.

We will denote by ∂B_u that portion of the boundary where the deformation map is prescribed and by ∂B_t that portion of the boundary where the tractions $\bar{\mathbf{t}}$ are prescribed. As usual $\partial B_t \cup \partial B_u = \partial B$ and $\partial B_t \cap \partial B_u = \varnothing$.

The local form of the equilibrium equations (5.1) can be expressed as a weak statement of equilibrium in the following way [28]

$$G(\mathbf{x},\boldsymbol{\eta}) \equiv \int_B \mathbf{P}.\mathrm{GRAD}\boldsymbol{\eta}\, dV - \int_B \rho_o \mathbf{B}.\boldsymbol{\eta}\, dV - \int_{\partial B_t} \bar{\mathbf{t}}.\boldsymbol{\eta}\, dS = 0 \tag{5.2}$$

for any kinematically admissible variation $\boldsymbol{\eta}$ which satisfies the displacement boundary conditions. The choice of the constitutive equations are addressed in the next section.

5.2. Constitutive Equations

The constitutive equations will be expressed in terms of the second Piola-Kirchhoff stress tensor $\mathbf{S} = \mathbf{F}\mathbf{P}$ and its conjugate strain measure, the Lagrangian strain $\mathbf{E} = \frac{1}{2}(\mathbf{F}^T\mathbf{F} - 1)$. Based on an essentially thermodynamic argument (see, for example, [8] †) the rate of Lagrangian

† Actually the Lagrangian strains and not their rate are decomposed in [8]. The subject of decomposition of strain rates (or deformation gradient) is not appropriately discussed here.

strain can be decomposed into an elastic and a plastic part:

$$\dot{\mathbf{E}} = \dot{\mathbf{E}}^e + \dot{\mathbf{E}}^p \tag{5.3}$$

We will assume that the elastic part of the strain rate is related to the stress rate according to the following relationship

$$\dot{\mathbf{S}} = \mathbf{D}(\mathbf{E})\,\dot{\mathbf{E}}^e \tag{5.4}$$

where $\mathbf{D}$ is a fourth order isotropic tensor.

It will prove convenient from a numerical point of view to consider the inelastic processes to be characterized by a visco-plastic material model. Thus we consider that the inelastic strains $\mathbf{E}^p$ evolve according to the rate equation

$$\dot{\mathbf{E}}^p = \frac{1}{\tau} < F(\mathbf{S}) > \frac{\partial f}{\partial \mathbf{S}} \equiv \frac{1}{\tau}\boldsymbol{\beta}(\mathbf{S}) \tag{5.5}$$

where $f(\mathbf{S})$ is the plastic flow potential and τ is the "relaxation time" of the viscoplastic process. The function $F(\mathbf{S})$ is a scalar valued potential function having the property that $F(\mathbf{S}) = 0$ can be identified with a yield locus in stress space. Noting that $<x> \equiv x\,H(x)$, $H(x)$ being the Heaviside step function, one can see that states of stress in which $F(\mathbf{S}) < 0$ are associated with vanishing plastic strain rates and hence can be called elastic. Clearly, the larger is the value of $F(\mathbf{S}) > 0$, the greater is the rate of plastic flow.

By identifying the characteristic relaxation time τ of the material to be suitably fast, rate independent plasticity can be easily modeled. This procedure is generally known as a penalty function method for modeling viscoplasticity and has been used extensively in the computational literature [25,50,51]. Ortiz [33] has shown that, in the limit as $\tau \to 0$, the viscoplastic model approaches that of rate independent plasticity.

Various forms of the plastic potential have been discussed in the literature both for the modeling of viscoplastic material behavior [34] and for use of the model in the penalty

approach to elasto-plasticity [25,52]. Attention is confined here to a von Mises type of potential given by

$$f(\mathbf{S}) = J_2 - k^2 \qquad \text{and} \qquad F(\mathbf{S}) = \frac{f(\mathbf{S})}{k^2} \tag{5.6}$$

where $J_2 = \frac{1}{2}\mathbf{S}':\mathbf{S}'$ is the second invariant of the deviator stress $\mathbf{S}' = \mathbf{S} - \frac{1}{3}\mathrm{tr}(\mathbf{S})$, and k is the yield stress of the material in pure shear.

While the developments here are restricted to the case of perfect plasticity, the formulation is flexible enough to eventually incorporate strain hardening effects. Material hardening effects can be realized by introducing additional internal variables, with their associated equations of evolution, into the constitutive model. Many hardening rules have been proposed to characterize metals. Of these, two have found a special place of importance in applications: Isotropic hardening and kinematic hardening. Examples of these two types of hardening are given below.

The case of isotropic hardening can be achieved by replacing k in Eq. (5.6) with the hardening parameter $\kappa(\mathbf{E}^p)$ which can be assumed, for example, to evolve according to the rate equation

$$\dot{\kappa} = c_I \,\mathrm{tr}(\dot{\mathbf{E}}^p \,\dot{\mathbf{E}}^p)^{\frac{1}{2}} \qquad \text{or} \qquad \dot{\kappa} = c_I \,\mathrm{tr}(\mathbf{S}\,\dot{\mathbf{E}}^p) \tag{5.7}$$

where c_I is a constant of the material which characterizes the rate of isotropic hardening. Kinematic hardening can be simply introduced by replacing $\mathbf{S}$ in the expressions for the potentials with $\mathbf{S}-\boldsymbol{\alpha}$ where $\boldsymbol{\alpha}$ can be supposed to evolve according to the rate equations respectively of Prager and Ziegler given by

$$\dot{\boldsymbol{\alpha}} = c_K \,\dot{\mathbf{E}}^p \qquad \text{or} \qquad \dot{\boldsymbol{\alpha}} = \dot{\mu}\,(\mathbf{S}-\boldsymbol{\alpha}) \tag{5.8}$$

where c_K and $\dot{\mu}$ are constants of the material characterizing the rate of kinematic hardening. Note that $\dot{\mu} > 0$.

A more complete account of hardening rules applicable to cyclic plasticity can be found in [4]. While these hardening rules appear simple from a theoretical point of view, they are difficult to implement computationally. Consideration of the effects of material hardening will be left as a topic for future research.

The constitutive model employed in this study can be summarized by its rate equation which takes the final form

$$\dot{\mathbf{E}} = \mathbf{D}^{-1}\dot{\mathbf{S}} + \frac{1}{\tau}\boldsymbol{\beta}(\mathbf{S}) \tag{5.9}$$

5.3. The Kinematic Hypothesis

For the purposes of this study, restrictions of the deformation map given by

$$\mathbf{x} = \mathbf{X} + \mathbf{u}(\mathbf{X}) \tag{5.10}$$

are considered, where the displacements $\mathbf{u}(\mathbf{X})$ are linear. Simo [45] has shown that it is sufficient to consider linear displacement measures in the equilibrium equations in a second order treatment of a problem. In this section we are concerned with describing the displacement vector $\mathbf{u}(\mathbf{X})$. We will often not distinguish between X_i and x_i in the following developments since usage will generally make the distinction clear. Where it is convenient, we will regress to the more classical notation $\{x_1, x_2, x_3\} \equiv \{x, y, z\}$.

The simplest kinematic hypothesis which is capable of characterizing the deformation of a beam corresponds to the assumption that "sections normal to the line of centroids before deformation remain plane after deformation." This hypothesis is reflected in the expressions for the displacement as

$$\begin{aligned} u_1(\mathbf{x}) &= \bar{u}(x_1) - x_2\bar{\psi}(x_1) \\ u_2(\mathbf{x}) &= \bar{v}(x_1) \end{aligned} \tag{5.11}$$

$$u_3(\mathbf{x}) = 0$$

where $\bar{u}$ and $\bar{v}$ measure the average axial and transverse displacement of the cross section and $\bar{\psi}$ measures its rotation, as shown in Fig. 5.1. While this kinematic hypothesis does account for shearing deformation it leads, in the context of the linear theory, to a constant distribution of shear strains, $\gamma_{12} = \bar{v}' - \bar{\psi}$, over the cross section and thus generally violates the shear stress boundary conditions. The hypothesis expressed by Eq. (5.11) is good for longer beams, but breaks down in cases where the influence of shear and the concomitant warping of the cross section are not negligible.

Simo [45] has shown that, by employing the exact solution to Saint Venant's problem[†], one can derive a more elaborate kinematic hypothesis which accounts for such effects as transverse warping of the cross section due to shear. Simo used this hypothesis to assess the effect of warping on the buckling of elastic beams. Here we are concerned with the effect of warping on the yielding mechanisms in the elasto-plastic bending of a beam. The hypothesis, which yields the exact solution to Saint Venant's problem in the elastic range will be taken as a basic postulate of the deformation pattern in the inelastic range. The practice of motivating the inelastic displacement field with the elastic one is commonly used in solving inelastic beams problems (see, for example, [40]). In the past, little effort has been made to account for the effects of shear in the elasto-plastic beam problem.

As shown in [45], the solution to Saint Venant's problem can be recast in terms of purely kinematic variables and results in the following expressions

$$\begin{aligned} u_1(\mathbf{x}) &= \bar{u}(x_1) - x_2\bar{\psi}(x_1) - \kappa\phi_1(x_2,x_3)\bar{\beta}(x_1) \\ u_2(\mathbf{x}) &= \bar{v}(x_1) + \nu\,[\,\phi_2(x_2,x_3)\bar{\psi}'(x_1) - x_2\bar{u}'(x_1)\,] \\ u_3(\mathbf{x}) &= \nu\,[\,\phi_3(x_2,x_3)\bar{\psi}'(x_1) - x_3\bar{u}'(x_1)\,] \end{aligned} \tag{5.12}$$

[†] Saint Venant's problem is the problem of the bending of a beam subjected only to end loads. Exact solutions can be found in the standard literature [23,47].

where the ϕ_i are given by the following expressions

$$\phi_1 = \frac{\Omega}{2(1+\nu)I_2}\left[\Psi - \frac{1}{\Omega}\int_\Omega \Psi\, d\Omega - \frac{x_2}{I_2}\int_\Omega x_2\Psi\, d\Omega\right]$$

$$\phi_2 = \frac{1}{2}\left[(x_2)^2 - (x_3)^2 - \frac{I_2 - I_3}{\Omega}\right] \tag{5.13}$$

$$\phi_3 = x_2 x_3$$

In these expressions, Ω is the cross sectional area, $I_\alpha = \int_\Omega (x_\alpha)^2\, d\Omega$ are the principal moments of inertia, ν is Poisson's ratio, and κ is a coefficient defined in terms of ϕ_1 as [45]

$$\kappa = \frac{1}{1 + \frac{1}{\Omega}\int_\Omega \frac{\partial \phi_1}{\partial x_2}\, d\Omega} \tag{5.14}$$

The function $\Psi(x_2,x_3)$ in the expression for ϕ_1 is related to Love's flexure function [23] and satisfies the following Poisson equation and boundary conditions

$$\Delta\Psi = -2x_2 \qquad x_2,x_3 \in \Omega$$

$$\left.\frac{\partial\Psi}{\partial\hat{n}}\right|_{\partial\Omega} = \frac{\nu}{2}\left[(x_2^2 - x_3^2)\, n_2 + 2x_2x_3\, n_3\right] \tag{5.15}$$

where $\hat{n} = \{n_1, n_2, n_3\}$ is the direction of the normal to the boundary of the cross section. The elastic shear stresses for this problem can also be stated in terms of Ψ as [47]

$$\tau_{12} = \frac{Q}{2(1+\nu)I_2}\left[\frac{\partial\Psi}{\partial x_2} - \frac{\nu}{2}(x_2^2 - x_3^2)\right]$$

$$\tau_{13} = \frac{Q}{2(1+\nu)I_2}\left[\frac{\partial\Psi}{\partial x_3} - \nu x_2 x_3\right] \tag{5.16}$$

The determination of the function Ψ for the case of thin walled members are treated in the following section.

5.3.1. Determination of $\Psi(x_2,x_3)$

At this point in the development, we will focus our attention on thin walled members. The thin wall assumption allows the approximate solution of Eq. (5.15) for the function $\Psi(x_2,x_3)$ from which the warping coordinate function $\phi_1(x_2,x_3)$ can be evaluated. An expansion method is employed in arriving at a solution that satisfies Eq. (5.15) up to the order of the thickness of the cross section. It is then shown that the resulting expression is equivalent to the one proposed by Cowper [2].

For the treatment of thin walled cross sections it will be convenient to introduce a curvilinear coordinate system $\{x, s, n\}$ in addition to the Cartesian system $\{x_1, x_2, x_3\} \equiv \{x, y, z\}$. The s coordinate is taken coincident with the middle line of the cross section and the n coordinate orthogonal to s and $x \equiv x_1$. These definitions are shown on a typical cross section in Fig. 5.2.

In terms of the curvilinear coordinates Eq. (5.15) can be restated as

$$\Delta \Psi(s,n) = -2\,[y_0(s) - n \sin\theta(s)\,]$$

$$\left.\frac{\partial \Psi}{\partial n}\right|_{\pm\epsilon} = \gamma_0(s) + n\,\nu y_0(s) - n^2 \frac{\nu}{2}\sin\theta(s) \tag{5.17}$$

where the function $\gamma_0(s)$ is given by

$$\gamma_0(s) = \frac{\nu}{2}\,[\,(z_0^2 - y_0^2)\sin\theta + 2y_0 z_0 \cos\theta\,] \tag{5.18}$$

and we have used the functions $y_0(s)$ and $z_0(s)$ to parametrically describe the curve defined by the middle line of the cross section. The angle $\theta(s)$ measures the inclination of the tangent to

the middle line from the x_2 axis.

The Laplacian operator Δ can be expressed in terms of the curvilinear coordinates s and n as

$$\Delta\Psi = \frac{1}{J^2}\Psi_{,ss} + \Psi_{,nn} + \frac{n\theta''}{J^3}\Psi_{,s} - \frac{\theta'}{J}\Psi_{,n} \tag{5.19}$$

where a comma followed by a subscript denotes partial differentiation, and $J = 1 - n\theta'$ is the square root of the determinant of the metric of the curvilinear system.

In the spirit of the thin wall assumption we assume that $\tau_{xn} \equiv 0$ throughout the cross section. Noting that

$$\tau_{xn} = -\tau_{12}\sin\theta + \tau_{13}\cos\theta \tag{5.20}$$

Eqs. (5.16) can be expressed as

$$\frac{\partial\Psi}{\partial n} = \gamma_0 + n\nu y_0 - n^2\frac{\nu}{2}\sin\theta \tag{5.21}$$

Differentiating (5.21) once again with respect to n and substituting the result into $(5.17)_1$, noting (5.19), yields

$$\frac{\partial^2\Psi}{\partial s^2} = -(2+\nu)y_0 + \theta'\gamma_0 + nR(s) + O(n^2) \tag{5.22}$$

where the error term $R(s)$ is given by the expression

$$R(s) = -2(1+\nu)\left[\theta''\int_{s_0}^{s} y_0(\xi)\,d\xi + 2\theta' y_0\right] - (2+\nu)\sin\theta \tag{5.23}$$

It can be seen that for locally flat cross sections $|R(s)| < 2+\nu$. $R(s)$ vanishes altogether for a thin rectangular section since $\sin\theta = 0$. Introducing the function

$$\Gamma_0(s) \equiv -\frac{\nu}{2}\left[(z_0^2 - y_0^2)\cos\theta - 2y_0 z_0\sin\theta\right] \tag{5.24}$$

Eq. (5.22) can finally be expressed as

$$\frac{\partial^2 \Psi}{\partial s^2} = \Gamma_0'(s) - 2(1+\nu)\, y_0(s) \tag{5.25}$$

Integrating (5.25) and enforcing the condition $\tau_{xs} = 0$ at the ends of the cross section we finally obtain that

$$\frac{d\Psi}{ds} = \Gamma_0(s) - 2(1+\nu) \int_{s_0}^{s} y_0(\xi)\, d\xi \tag{5.26}$$

up to order n. Equation (5.26) can be integrated once again and the result can be used in Eq. $(5.13)_1$ to evaluate ϕ_1. Note that the constant of integration obtained by integrating (5.26) disappears in the orthogonalization process implicit in $(5.13)_1$.

To see the equivalence with the expression given by Cowper [2] we note that the shear stress from elementary considerations is given by

$$\tau(s) = -\frac{V}{I\, t} \int_{s_0}^{s} y_0(\xi)\, t(\xi)\, d\xi \tag{5.27}$$

If t = const., Eq. (5.27) further simplifies and its substitution into (5.26) leads to

$$\frac{d\Psi}{ds} = \Gamma_0(s) + \frac{2(1+\nu) I}{V} \tau(s) \tag{5.28}$$

I-Beam Warping Function.- The computation of the warping function has been carried out for the case of interest here: The I-section. For notational simplicity, let the ratio of gross flange area to web area γ, and the ratio of flange width to section depth δ be denoted by

$$\gamma \equiv \frac{2bt_f}{ht} \quad \text{and} \quad \delta \equiv \frac{b}{h} \tag{5.29}$$

respectively, where b is the flange width, t_f is the flange thickness, h is the distance between the centroids of the flanges, and t is the web thickness. A rather lengthy computation gives, from Eq. (5.26), the expression for the warping function ϕ_1

$$\phi_1 = \frac{\kappa G \Omega}{120EI} \begin{cases} (2+\nu)[20y^3 - 3h^2 y C_0(\gamma,\delta,\nu)] & \text{in } \Omega_w \\ y[30(4+3\nu)z^2 - 120(1+\nu)b|z| + h^2 C_1(\gamma,\delta,\nu)] & \text{in } \Omega_f \end{cases} \tag{5.30}$$

where Ω_w and Ω_f refer to the web and flange domains respectively. In this expression $y \equiv x_2$ is the major principal axis of the cross section (and the axis along which the resultant shear acts) and $z \equiv x_3$ is the minor principal axis. The cross sectional properties Ω and I are given by

$$\Omega = ht(1+\gamma) \quad \text{and} \quad I = \frac{h^3 t}{12}(1+3\gamma) \tag{5.31}$$

An expression for the shear coefficient κ is given in [2] and is roughly equal to $\frac{1}{1+\gamma}$. G is the shear modulus, E is Young's modulus, and ν is Poisson's ratio.

The constants $C_0(\gamma,\delta,\nu)$ and $C_1(\gamma,\delta,\nu)$ appearing in Eq. (5.30) are section/material properties given by

$$C_0(\gamma,\delta,\nu) = \frac{4+20\gamma(1-2\delta^2)+\nu[2+5\gamma(2-9\delta^2)]}{2(1+3\gamma)(2+\nu)}$$

$$C_1(\gamma,\delta,\nu) = \frac{8(1+15\gamma\delta^2)+\nu(4+135\gamma\delta^2)}{2(1+3\gamma)} \tag{5.32}$$

Two limiting cases of practical interest can be obtained from the expression for the I-beam: (1) The spar-and-web section in which the flanges have area but negligible width, and (2) The thin rectangular section in which the flange area is zero.

The Spar-and-Web Section.- Letting $\delta \to 0$ with $\gamma \neq 0$ the warping function for the spar-and-web section is recovered. In this case, the two constants reduce to

$$C_0 = \frac{2+10\gamma+\nu(1+5\gamma)}{(1+3\gamma)(2+\nu)}$$

$$C_1 = \frac{2(2+\nu)}{1+3\gamma} \tag{5.33}$$

The shear coefficient notwithstanding (which can again be found in [2]), no other differences in the warping function appear.

Thin Rectangular Section.- Letting both $\delta \rightarrow 0$ and $\gamma \rightarrow 0$ the warping function for the thin rectangular section is recovered. In this case, $\Omega_f \rightarrow 0$ so that only the part of Eq. (5.30) involving Ω_w is applicable. Here $C_0 = 1$.

5.4. Solution Procedure

The motion of the system, described by the two equations (5.2) and (5.9), involves both material and geometric nonlinearities. Hence, the procedure of linearization about an intermediate configuration must be employed in the solution scheme. Specific details regarding the linearization process are treated extensively in the literature [17,28]. Here we will simply state the final results and refer the interested reader to the cited works for details.

Linearization of the weak form.- The linearization of the weak form of the equilibrium equations about an intermediate configuration, denoted by $\bar{\Phi}$, leads to the expression [28]

$$L[G]_{\bar{\Phi}} = \int_B \mathrm{GRAD}\boldsymbol{\eta}\,[\bar{\mathbf{S}} \otimes 1 + \bar{\mathbf{F}}^T \frac{\partial \mathbf{S}}{\partial \mathbf{E}}\Big|_{\bar{\Phi}} \bar{\mathbf{F}}]\,\mathrm{GRAD}(\Delta\mathbf{u})\,dV + G(\boldsymbol{\eta},\bar{\mathbf{x}}) \tag{5.34}$$

where the over bar denotes the evaluation of that quantity at the configuration $\bar{\Phi}$, and $\Delta\mathbf{u}$ is the incremental motion. The first term in Eq. (5.34) gives rise to the tangent stiffness of the system and the last term to the so called out-of-balance force at the configuration $\bar{\Phi}$ which has the expression

$$G(\boldsymbol{\eta},\bar{\mathbf{x}}) = \int_B \bar{\mathbf{F}}\bar{\mathbf{S}}\,\mathrm{GRAD}\boldsymbol{\eta}\,dV - \int_{\partial B_t} \bar{\mathbf{t}}.\boldsymbol{\eta}\,dS \tag{5.35}$$

Clearly, $G(\boldsymbol{\eta},\bar{\mathbf{x}})$ vanishes if $\bar{\Phi}$ is an equilibrium configuration.

Equation (5.34) has a form that is suitable for treatment by the Finite Element Method. We note that the deformation gradient $\bar{\mathbf{F}}$ is completely defined by the kinematic assumption (5.12). To carry out the solution a knowledge of the current state of stress $\bar{\mathbf{S}}$ and the material tangent $\left.\frac{\partial \mathbf{S}}{\partial \mathbf{E}}\right|_{\bar{\Phi}}$ is required. These items can be obtained from the constitutive equations (5.9). Inasmuch as these equations are given in rate form, they must first be integrated. This consideration is discussed in the following section.

Numerical Integration of the Constitutive Equations.- Due to the nonlinear nature of the constitutive rate equations their integration can generally not be accomplished through direct quadratures. The literature abounds with methods for the numerical integration of first order ordinary differential equations. Generally, in engineering applications one step methods are preferred because of their simplicity and computational efficiency. The implicit one step method proposed by Hughes and Taylor [16] is employed here.

Formally integrating Eq. (5.9) we obtain the expression

$$\mathbf{E}_t - \mathbf{E}_o = \mathbf{D}^{-1}[\mathbf{S}_t - \mathbf{S}_o] + \frac{1}{\tau}\int_{t_o}^{t} \boldsymbol{\beta}(\mathbf{S}_\xi)\, d\xi \tag{5.36}$$

The subscripts t_o and t indicate that the quantity is evaluated at times $t = t_o$ and $t = t_o + \Delta t$ respectively. The last term in (5.36) is then integrated numerically using the formula

$$\frac{1}{\tau}\int_{t_o}^{t} \boldsymbol{\beta}(\mathbf{S}_\xi)\, d\xi \approx \frac{\Delta t}{\tau}\boldsymbol{\beta}(\mathbf{S}_\alpha) \tag{5.37}$$

where we have employed the notation

$$\mathbf{S}_\alpha \equiv (1-\alpha)\mathbf{S}_o + \alpha \mathbf{S}_t \qquad 0 \leqslant \alpha \leqslant 1 \tag{5.38}$$

The final integrated form of the constitutive equation can be written in the form

$$\Psi_t = -(\mathbf{E}_t - \mathbf{E}_0) + \mathbf{D}^{-1}(\mathbf{S}_t - \mathbf{S}_0) + \frac{\Delta t}{\tau}\beta(\mathbf{S}_\alpha) = 0 \tag{5.39}$$

where the constitutive residual Ψ_t has been introduced. $\Psi_t = 0$ indicates exact satisfaction of the integrated form of the constitutive equations. The norm of the constitutive residual will be used as a measure of satisfaction of the constitutive equation.

Differentiating Eq. (5.39) with respect to $\mathbf{E}$, one can obtain an expression for the material tangent given by

$$\frac{\partial \mathbf{S}}{\partial \mathbf{E}} = [\mathbf{D}^{-1} + \alpha\frac{\Delta t}{\tau}\beta'(\mathbf{S}_\alpha)]^{-1} \equiv \Omega_t \tag{5.40}$$

As usual, the prime denotes differentiation with respect to the argument. The fourth order material tangent tensor has been given the name Ω_t, where the subscript t serves as a reminder that this tensor is history dependent (through the evolution of the stress state).

Choice of the Penalty.- In solving problems of elasto-plasticity using a viscoplastic material model, one hopes to approach the condition $\tau \to 0$. From a numerical standpoint, approaching this limit too closely presents the possibility of numerical ill-conditioning. For practical purposes the limit on τ is not of primary importance, but rather one is concerned with forcing the converged stress state to be in a certain proximity of the yield surface. We consider this problem briefly in this section.

Consider a loading process in which inelastic action takes place. If the constitutive rate equation (5.9) is integrated using a value of $\alpha = 1$ (backward Euler), the resulting expression has the form

$$-\mathbf{D}\Delta\mathbf{E} + (\mathbf{S} - \mathbf{S}_0) + \frac{\Delta t}{k\tau}\left(\frac{J_2}{k^2} - 1\right)\mathbf{D}\mathbf{S}' = 0 \tag{5.41}$$

where $\Delta\mathbf{E} = \mathbf{E} - \mathbf{E}_0$ and $\mathbf{S}'$ again stands for the deviator stress. The subscript t has been dropped but it should be understood. Introducing the definitions

$$\hat{\mathbf{S}} \equiv \mathbf{S}_0 + \mathbf{D}(\mathbf{E} - \mathbf{E}_0)$$

$$\mathbf{D}^0 \equiv \frac{\mathbf{D}}{||\mathbf{D}||} \tag{5.42}$$

$$\eta \equiv \frac{\tau}{\Delta t}\frac{k}{||\mathbf{D}||}$$

Eq. (5.41) takes the form

$$\mathbf{S} + \frac{1}{\eta}\left(\frac{J_2}{k^2} - 1\right)\mathbf{D}^0\mathbf{S}' - \hat{\mathbf{S}} = 0 \tag{5.43}$$

The defined stress $\hat{\mathbf{S}}$ can be interpreted as the stress state corresponding to an elastic response to the strain increment. In essence, it measures how far outside the yield surface the initial estimate of the stress point lies. It is worth noting that the norm of the elasticity matrix, $||\mathbf{D}||$, is roughly equal to Young's modulus for an isotropic material.

Our desire is to have the converged stress state close to the yield surface. This condition is achieved if the stresses satisfy the condition

$$\frac{J_2}{k^2} - 1 = \epsilon \tag{5.44}$$

where ϵ is the measure of "closeness" to the yield surface. Equation (5.44) can then be written as

$$\mathbf{S} + \frac{\epsilon}{\eta}\mathbf{D}^0\mathbf{S}' - \hat{\mathbf{S}} = 0 \tag{5.45}$$

Taking the inner product of (5.45) with $\mathbf{S}'$ and noting that $\mathrm{tr}(\mathbf{S}'\mathbf{S}) = \mathrm{tr}(\mathbf{S}'\mathbf{S}') = 2k^2$ we obtain

$$\frac{\eta}{\epsilon} = \frac{\mathrm{tr}(\mathbf{S}'\hat{\mathbf{S}}) - 2k^2}{\mathrm{tr}(\mathbf{S}'\mathbf{D}^0\mathbf{S}')} \tag{5.46}$$

Noting that

$$\mathrm{tr}(\mathbf{S}'\mathbf{D}^0\mathbf{S}') \leqslant ||\mathbf{D}^0||\mathrm{tr}(\mathbf{S}'\mathbf{S}') = 2k^2 \tag{5.47}$$

we finally arrive at the condition that if

$$\frac{\eta}{\epsilon} \leqslant \frac{\mathrm{tr}(\mathbf{S}'\hat{\mathbf{S}})}{2k^2} - 1 \tag{5.48}$$

then the converged stress point should lie within ϵ of the yield surface. This estimate provides a useful and simple means of automatically controlling the size of the penalty for the elasto-plastic problem. One can clearly see the dependence of the penalty on the influencing factors of the elastic modulus $||\mathbf{D}||$, the yield stress k, the time step Δt, and the size of the load increment as measured by $\mathrm{tr}(\mathbf{S}'\hat{\mathbf{S}})$. While the preceding development gives a sharp estimate for the value of the penalty, it should be noted that such a procedure can only be employed if the yield surface can be expressed as an inner product of the stress measures. We will find that this is rarely the case for stress resultant formulations.

Finite Element Discretization.- The terms in the kinematic hypothesis (5.12) involving $\nu\bar{\psi}'$ and $\nu\bar{u}'$ give rise to the so called "anticlastic bending" of the beam, and are not expected to be influential in the present application. In order to keep the finite element interpolation structure simple, these terms will be neglected in what follows. It is emphasised that this truncation does not reflect a limitation on the developments, merely a judicious simplification.

We will further assume that the beam is thin walled or, in other words, locally two dimensional. For the I-beam, this is a reasonable assumption. In terms of the curvilinear coordinates $\{x, s, n\}$ previously introduced, the kinematic hypothesis (5.12) takes the form

$$\begin{aligned} u_1(x,s) &= \bar{u}(x) - x_2(s)\,\bar{\psi}(x) - \kappa\phi_1(s)\,\bar{\beta}(x) \\ u_s(x,s) &= \bar{v}(x)\cos\theta(s) \end{aligned} \tag{5.49}$$

Following standard procedure we interpolate the generalized displacements $\bar{\mathbf{u}}(x) = [\bar{u}, \bar{v}, \bar{\psi}, \bar{\beta}]^T$ as

$$\bar{\mathbf{u}}(x) = \sum_{\alpha=1}^{N} h_\alpha(x)\, \mathbf{U}_\alpha \tag{5.50}$$

where $\mathbf{U} = [U, V, \Psi, B]^T$ are the nodal values of the displacements, $h_\alpha(x)$ are the interpolation functions, and N is the number of nodes in each element. Inasmuch as the admissible variations lie in the space $H^1(0,L)$, C^0 continuity of the interpolation is sufficient [48,50].

From (5.49) and (5.50) the gradient of the displacements can be computed as

$$\text{GRAD}\,\mathbf{u}(\mathbf{X}) = \sum_{\alpha=1}^{N} \mathbf{B}_\alpha(\mathbf{X})\, \mathbf{U}_\alpha \tag{5.51}$$

in which the matrix $\mathbf{B}_\alpha(\mathbf{X})$ is given by

$$\mathbf{B}_\alpha(\mathbf{X}) = \begin{bmatrix} h'_\alpha & 0 & -x_2\, h'_\alpha & -\kappa\phi_1\, h'_\alpha \\ 0 & 0 & -\cos\theta\, h_\alpha & -\kappa\phi'_1\, h_\alpha \\ 0 & h'_\alpha & 0 & 0 \\ 0 & \theta'\sin\theta\, h_\alpha & 0 & 0 \end{bmatrix} \tag{5.52}$$

Note that the rows of $\mathbf{B}_\alpha$ correspond to the components of GRAD $\mathbf{u}$ in the following manner: $\mathbf{B}(1,2,3,4) \rightarrow \text{GRAD}\mathbf{u}(11,12,21,22)$. The deformation gradient can be computed using (5.51) as

$$\mathbf{F}(\mathbf{X}) = 1 + \text{GRAD}\,\mathbf{u}(\mathbf{X}) \tag{5.53}$$

Equation (5.51) has an identical form for the increments $\Delta\mathbf{u}$ and $\Delta\mathbf{U}$.

Employing the interpolation in the weak form we are lead to the standard discrete problem for the incremental nodal displacements $\Delta\mathbf{U}$

$$\mathbf{K}_t\, \Delta\mathbf{U} = \mathbf{f}_t \tag{5.54}$$

where the tangent stiffness matrix is given by a sum over all of the elements e as

$$\mathbf{K}_t = \sum_e \int_B \mathbf{B}^T [\bar{\mathbf{S}} \otimes 1 + \bar{\mathbf{F}}^T \boldsymbol{\Omega}_t \bar{\mathbf{F}}] \mathbf{B} \, dV \tag{5.55}$$

and the right hand side or out-of-balance force has the expression

$$\mathbf{f}_t = \mathbf{F}_t - \sum_e \int_B \mathbf{B}^T [\bar{\mathbf{F}} \bar{\mathbf{S}}] \, dV \tag{5.56}$$

in which $\mathbf{F}_t$ is the vector of currently applied nodal forces. Again, the barred quantities are evaluated at the current state. Note that in (5.55) and (5.56) the terms in brackets must be appropriately transformed from tensor form to matrix form.

It is usual in Finite Element treatments of beam problems to integrate the x_2–x_3 dependence of the volume integrals in the expressions for the stiffness matrix and load vector analytically and the x_1 dependence numerically. However, since the stress $\mathbf{S}$ and the compliance $\boldsymbol{\Omega}_t$ generally vary nonlinearly over the cross section due to inelasticity, the x_2–x_3 dependence in Eqs. (5.47) and (5.48) must be evaluated numerically. Numerical integration over the cross sectional area has been employed previously [36].

In the present study, for applications to thin rectangular cross sections, Gauss-Lobotto quadrature is employed. For applications to I-beams, the cross sectional domain is subdivided into three regions: Two flanges and a web. Within each region, regular Gaussian quadrature is employed and the total integral is taken to be the sum of the integrals over the three subregions. Numerical experiments suggest that, for the I-section, three Gauss points in the web region and two Gauss points in each of the flange regions[†] is minimal. Better accuracy can be achieved by increasing the order of quadrature, but in most cases the global response is adequately captured with the minimal rule.

[†] A "flange region" is defined as half of a flange, ie. that portion of the flange between the web-flange junction and the extreme outer fiber. Symmetry of the cross sectional is then used in the computation.

To prevent shear locking effects [50], reduced integration is employed in the x_1 direction (eg. two point Gaussian quadrature for a quadratic element).

Numerical Algorithm.- The solution of the problem is carried out using the algorithm proposed in [46] which is summarized in Table 5.1. This algorithm consists of two Newton-Raphson iteration schemes, one embedded inside the other. For each time step the global equations (5.54) are solved for the incremental motion. From the updated motion, the strains are computed. The strains are then used in the local nonlinear constitutive equations (5.36) to obtain the stresses by an iterative solution procedure.

Initiate solution at time $t = t_0$
While $||\mathbf{f}_t|| > \text{tol}$
  Form $\mathbf{K}_t$, $\mathbf{f}_t$
  Solve $\mathbf{K}_t \Delta\mathbf{U} = \mathbf{f}_t$
  Update $\mathbf{U} \leftarrow \mathbf{U} + \Delta\mathbf{U}$
  Compute strains from displacements
  For each element, while $||\Psi_t|| > \text{tol}$
    Form $\mathbf{\Omega}_t$, $\mathbf{\Psi}_t$
    Update $\mathbf{S} \leftarrow \mathbf{S} - \mathbf{\Omega}_t \mathbf{\Psi}_t$

Table 5.1 Elasto-Viscoplastic Algorithm (after [46])

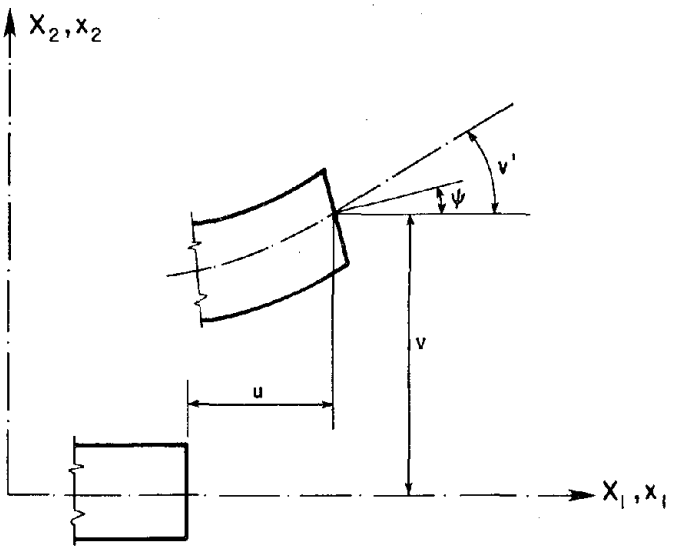

Fig. 5.1 Geometrical Representation of the Generalized Kinematic Variables for the "Plane Sections Remain Plane" Hypothesis

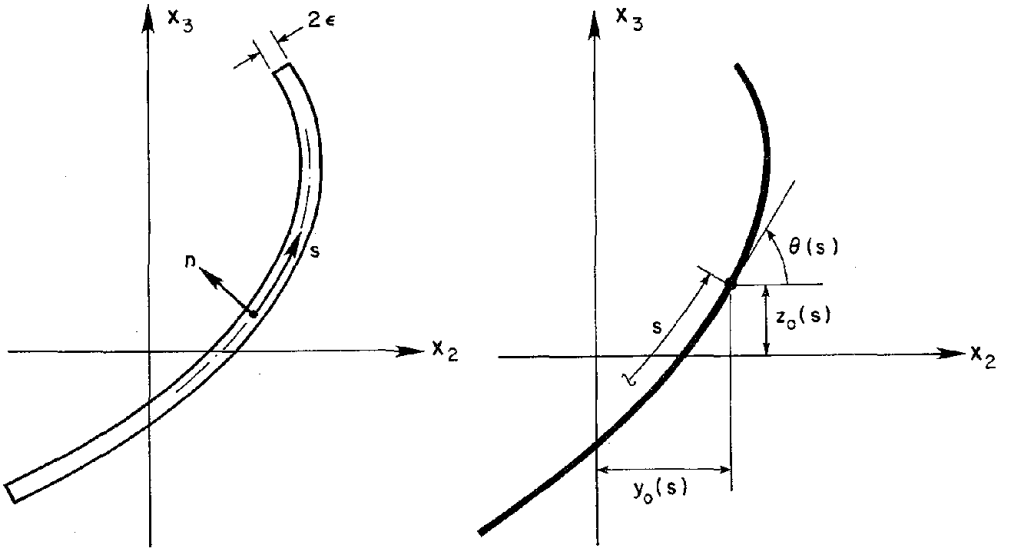

Fig. 5.2 Definition of Curvilinear Coordinates for a Typical Thin Walled Section

Chapter 6

A Stress Resultant Model for Active Links

6.0. Introduction

In the preceding chapter an analytical model was developed using the general three dimensional equilibrium and constitutive equations of an elasto-plastic continuum. Through the introduction of the kinematic hypothesis (5.12), the solution of the problem was essentially reduced to one dimension. Due to the consideration of nonlinear constitutive relations at the local level, it was found possible to discern local phenomena such as the propagation of an elastic-plastic interface through the cross section of a member. The cost of obtaining this local information is the loss of the ability to directly integrate the x_2–x_3 dependence of the weak form of equilibrium in evaluating the stiffness and load matrices. Numerical quadratures can be effectively employed in these computations but the expense of evaluating these matrices is considerably greater than the usual effort of a one dimensional theory.

Because of the additional expense involved in computing with the local model, one is lead to search for a reasonably accurate simplified model for use in the analysis of large structural systems. The suitability of the simplified model is clearly manifested in how well it is able to capture the important features of the response of a given structure. One valuable test, and one which we shall employ here, is to compare the simplified model with a more detailed approach, such as the model presented in Chapter 5.

In this chapter a simplified model based upon stress resultants is presented. Simo [45] has developed a system of second order equilibrium equations based upon the kinematic hypothesis (5.12) which accounts for the effects of warping of the cross section due to transverse shear. We shall employ these equations in the ensuing developments. It should be noted, however, that the formulation presented here can be easily extended to other beam theories [46].

The fundamental difference between the local approach of Chapter 5 and the stress resultants approach lies in the way the constitutive behavior is viewed. In the former, constitutive laws were expressed at a local level in terms of stresses and strains. These local laws do not involve the geometry of the body. The latter case is considerably different. Here, the stress resultants and their conjugate strain measures are taken to be the primitive action/deformation quantities and it is assumed that only these measures are involved in the characterization of the constitutive behavior. Clearly, the constitutive equations in terms of stress resultants should reflect the geometry of the body, especially the cross sectional geometry. This dependence upon the geometry of the body is generally assumed a priori, and is the main source of concern here because of the importance of shear.

The developments of this chapter have compelling analogs with the preceding one, and in fact, with a few reinterpretations of notation, the solution procedures are the same. The similarities will be pointed out where appropriate.

6.1. Equilibrium Equations

Utilizing the kinematic hypothesis (5.12) and employing the method of successive approximations, Simo [45] developed a second order approximation to the nonlinear equilibrium equations (5.1) in terms of stress resultants, which accounts for transverse shear and its concomitant warping of the cross section. These equations can be stated as

$$
\begin{aligned}
&[N - \psi V]' = 0 \\
&[V + \{\psi + (1-\kappa)\beta\}N]' = 0 \\
&M' + (1+u')V - \kappa\beta N = 0
\end{aligned}
\tag{6.1}
$$

In these equations N and V are defined as the resultants of normal and shearing stresses over the deformed cross section of the beam, respectively, and M is the resultant of the first moments of the normal stresses about the centroid of the cross section. The deformation measures are the same as those employed in Chapter 5, except that $\beta \equiv v' - \psi$ is taken to be dependent. Assuming β independent leads to the definition of an additional stress resultant as shown in Appendix I.

For a hyperelastic material, Simo [45] further showed that the strain measures $\boldsymbol{\lambda} \equiv [\lambda_n, \lambda_v, \lambda_\psi]^T$ conjugate to the stress resultants $\mathbf{R} \equiv [N, V, M]^T$ can be expressed as

$$\begin{aligned} \lambda_n &= u' + \frac{1}{2}(v')^2 - \frac{1}{2}\kappa\beta^2 \\ \lambda_v &= v' - (1+u')\psi \\ \lambda_\psi &= \psi' \end{aligned} \tag{6.2}$$

For the elasto-plastic problem, we make the assumption that the $\boldsymbol{\lambda}$ are still conjugate to the $\mathbf{R}$. This assumption is analogous, but not equivalent, to the assumption in the local approach that the kinematic hypothesis, which was also based upon elasticity, holds in the inelastic range.

We denote by ∂_R those directions at $x = 0$ and $x = L$ subject to applied tractions, and by $\partial_{\bar{x}}$ those directions having prescribed displacements. Furthermore, we will denote the displacements by $\mathbf{u}(x) \equiv [u, v, \psi]^T$. The weak form of the equilibrium equations (6.1) can then be expressed as [46]

$$G(\mathbf{u},\boldsymbol{\eta}) \equiv \int_0^L \mathbf{R}.D\boldsymbol{\lambda}.\boldsymbol{\eta}\, dx - \int_0^L q\eta_2\, dx - [\boldsymbol{\eta}.\hat{\mathbf{R}}]_{\partial_R} \tag{6.3}$$

for any $\boldsymbol{\eta} \in H^1(0,L)$ satisfying the displacement boundary conditions. A transversally applied load q has been included in the formulation. The expression for the variation in strains present in the first term of equation (6.3) is given by the usual definition

$$D\boldsymbol{\lambda}.\boldsymbol{\eta} \equiv \frac{d}{d\epsilon}\left[\boldsymbol{\lambda}(\mathbf{u}+\epsilon\boldsymbol{\eta})\right]_{\epsilon=0} \tag{6.4}$$

Defining the operator $\mathbf{w} \rightarrow \mathbb{B}(\mathbf{w}) \equiv [u', v', \psi', \psi]^T$ and noting (6.2), the expression (6.4) takes the explicit form

$$D\boldsymbol{\lambda}.\boldsymbol{\eta} = \Xi(\mathbf{u})\mathbb{B}(\boldsymbol{\eta}) \tag{6.5}$$

where the matrix

$$\Xi(\mathbf{u}) = \begin{bmatrix} 1 & (v'-\kappa\beta) & 0 & \kappa\beta \\ -\psi & 1 & 0 & -(1+u') \\ 0 & 0 & 1 & 0 \end{bmatrix} \tag{6.6}$$

is analogous to the deformation gradient **F** in the previous chapter.

6.2. Constitutive Equations

We assume that the strain rate[†] can be decomposed into elastic and plastic parts as

$$\dot{\boldsymbol{\lambda}} = \dot{\boldsymbol{\lambda}}^e + \dot{\boldsymbol{\lambda}}^p \tag{6.7}$$

wherein the elastic part is assumed to be related to the rate of stress resultants as

$$\dot{\boldsymbol{\lambda}}^e = \mathbf{D}^{-1}\dot{\mathbf{R}} \tag{6.8}$$

$\mathbf{D} = \text{diag}[\,E\Omega \quad \kappa G\Omega \quad EI\,]$ being the elastic compliance matrix. In a manner analogous to the local approach, we assume that the inelastic processes can be characterized by a viscoplastic model, which can be used in a penalty procedure to capture elasto-plasticity. To wit, we assume that the plastic strains evolve according to the rate equation

[†] A discussion of the proper rate for nonlinear beam theories has been given in [46].

$$\dot{\boldsymbol{\lambda}}^{p} = \frac{1}{\tau} < f(\mathbf{R}) > \frac{\partial f}{\partial \mathbf{R}} \equiv \frac{1}{\tau}\boldsymbol{\beta}(\mathbf{R}) \tag{6.9}$$

where here no distinction is made between the potential in the penalty term and the one in the term giving the direction of plastic flow. The resulting constitutive model is then given by

$$\dot{\boldsymbol{\lambda}} = \mathbf{D}^{-1}\dot{\mathbf{R}} + \frac{1}{\tau}\boldsymbol{\beta}(\mathbf{R}) \tag{6.10}$$

The constitutive equation of the viscoplastic model assumes the existence of the plastic flow potential $f(N,V,M)$, which is necessarily expressed in terms of the stress resultants. The suitability of the model for characterizing the inelastic response of a beam relies heavily on the choice of this potential. The choice of the potential is discussed in the next section.

6.2.1. The Plastic Flow Potential

It is well established that a theory of plasticity (or viscoplasticity) can be formulated in term of generalized stresses $\mathbf{Q}$ and appropriately conjugate strain measures $\mathbf{q}$ [13]. Viewed naively then, a theory employing stress resultants is on an equal footing with one in which stress components are used for the generalized stresses. In either case, the constitutive rate equation for the evolution of the plastic part of the strain relies upon the existence of a flow potential $f(\mathbf{Q})$ having the following properties:

(1) The equation $f(\mathbf{Q}) = 0$ describes a convex hypersurface in $\mathbf{Q}$–space, called the yield surface.

(2) States in which $f(\mathbf{Q}) < 0$ are elastic and hence are associated with vanishing plastic strain rates.

(3) States in which $f(\mathbf{Q}) > 0$ are not realizable in rate independent plasticity. In viscoplasticity, such states are realizable and are associated with nonvanishing plastic strain rates.

As far as the plastic flow potential is concerned, the main difference between rate independent plasticity and viscoplasticity is that in the former f must make sense only for

states satisfying $f(\mathbf{Q}) \leqslant 0$; whereas in the latter, f must be defined for all states. Further, the topology of f outside the yield surface must adequately characterize the inelastic processes for a viscoplastic material. When using a viscoplastic model to numerically represent rate independent plasticity, one need not take such great care in choosing the form of f away from the yield surface, since a *converged* stress state should lie on or inside the surface. Even in this case, however, f must still satisfy certain criteria outside of the yield surface. These requirements are described in the sequel.

For stress resultants, ie. when $\mathbf{Q} \equiv \mathbf{R}$, it is not clear that the potential $f(\mathbf{R})$ exists. Even in the case of stress components, the existence of f is a matter for experimental verification. The case of stress resultants does have the advantage that, since the resultants are integrals of the stress components, there should be a correspondence between a local $\bar{f}(\boldsymbol{\sigma})$ and $f(\mathbf{R})$, presenting the possibility of analytically determining $f(\mathbf{R})$ based upon a knowledge of $\bar{f}(\boldsymbol{\sigma})$.

The analytical approach to determining $f(\mathbf{R})$ is not without its difficulties, especially when the problem considered involves multiaxial states of stress. Drucker [5] has pointed out that determining $f(\mathbf{R})$ from a knowledge of $\bar{f}(\boldsymbol{\sigma})$ is problem dependent, depending upon both the boundary conditions of the beam and on the form of the applied loads. It is generally agreed, however, that a yield surface $f(\mathbf{R}) = 0$ derived from a local two or three dimensional analysis of a specific structure, such as a cantilever beam with end loads, can be fruitfully employed for engineering purposes as a criterion for general conditions.

Some comments on the prospect of using the local two or three dimensional approach and integrating to get a yield criterion in terms of stress resultants are worthwhile mentioning:

(1) Exact solutions to elasto-plastic beam bending problems are not currently available, even for the "simple" problem of the bending of a cantilever. Hence, one must resort to the bounding theorems of plasticity to obtain an approximate solution.

(2) Tight upper and lower bounds are difficult to achieve even in the simplest cases. Lower bound solutions are generally easier to obtain than upper bound solutions (and have the advantage of being "safe"). A good lower bound to the problem of a cantilever of

rectangular section under end shear was obtained by Drucker [5] assuming that the transverse normal stresses vanish everywhere. This solution was extended by Neal [29] to the case including axial thrust. Lower bound solutions for the I-beam were presented by Neal for both the case $N=0$ [30] and the case $N\neq 0$ [31]. Neal [30] has also improved the upper bound solution of Leth [22] for the case $N=0$, and has pointed out that an upper bound for $N\neq 0$ is difficult to obtain because the problem is three dimensional. The upper bound solutions for the I-beam are reasonable only for high shear (ie. short cantilevers).

(3) Most derived expressions for a yield surface $f(\mathbf{R}) = 0$ (either approximate or rigorous bounds) are expressible only in parametric form. Such implicit formulas usually cannot be extended for use as potentials, and hence cannot be employed in the viscoplastic formulation presented here. It is clearly desirable to have an explicit formula for $f(\mathbf{R})$.

(4) Solutions based upon local yield criteria generally require a specific form for the applied stresses, leading to some ambiguity with respect to the uniqueness of the result. Inasmuch as St. Venant's principle does not hold, these differences are irreconcilable.

(5) For certain cross sectional geometries, most notably the I-section, $f = 0$ is not everywhere convex. Figure 6.1 shows upper and lower bounds on the $v-m$ interaction curve for an I-beam (after Neal [30]), between which no convex curve can possibly pass. Since plasticity theories generally depend upon convexity of the yield surface, some objection to the stress resultant approach might be raised. It should be noted, however, that the regions of non-convexity generally are confined to combinations of (n,v,m) not possibly achieved by beams in practical problems (ie. beams so short that a stress resultant approach would hardly seem applicable).

In many cases it is possible to obtain an approximation to the yield surface using a physically motivated model which does not meet all of the requirements of the bounding theorems of plasticity. Often, it can be shown that these approximations correspond well with, for example, a lower bound solution over all or at least part of the yield surface. This approach will be

adopted here to treat the elasto-plastic I-beam problem. The question then arises: Is the yield surface $f(\mathbf{R}) = 0$ a level set of a suitable potential $f(\mathbf{R})$? If not, how can the problem be resolved?

In order to answer the first question it is necessary to define what is meant by a "suitable potential". For a potential to be suitable for use in a viscoplastic penalty approach to rate independent plasticity we propose the following requirements:

(1) The equation $f(\mathbf{R}) = 0$ must describe a closed, convex locus in $\mathbf{R}$–space.

(2) The inside of the yield surface must be characterized by the condition $f(\mathbf{R}) < 0$.

(3) Outside the yield surface, the potential must be everywhere positive, ie. $f(\mathbf{R}) > 0$. Furthermore, it seems reasonable that $f(\mathbf{R})$ should be coercive, that is

$$f(\mathbf{R}) \to \infty \quad \text{as} \quad ||\mathbf{R}|| \to \infty \tag{6.11}$$

where $||\mathbf{R}||$ can be taken to mean the Euclidean norm of the stress resultants $\mathbf{R}$.

Remark.- The expression for the hypersurface $f(\mathbf{R}) = 0$ is not necessarily a level set of a *suitable* potential $f(\mathbf{R})$. In essence, this means that it is not sufficient to merely remove the equal sign and the zero from the expression of the yield locus to arrive at a suitable expression for the potential. This point will be illustrated with the example of a beam with rectangular cross section.

Example.- Noting the similarity between the relationship between m and v found from a local criterion[†] with $n = 0$ and $m(1+n^2)$ and $v^2(1+n^2)$ found from a similar approach with $n \neq 0$, Neal extended Drucker's approximate expression for the moment-shear interaction of a rectangular beam without axial force, given by

$$|m| + v^4 - 1 = 0 \tag{6.12}$$

[†] By local criterion we mean a criterion which is obtained by considering only a single cross section rather than an entire beam. See, for example, the approach in Hodge [13,14].

to

$$|m| + n^2 + \frac{v^4}{1-n^2} - 1 = 0 \tag{6.13}$$

which gives rise to the naive potential

$$\bar{f}(n,v,m) \equiv |m| + n^2 + \frac{v^4}{1-n^2} - 1 \tag{6.14}$$

In these expressions, normalized values of the stress resultants have been used. The normalized quantities are defined as $n = N/N_0$, $v = V/V_0$ and $m = M/M_0$, where the quantities having a subscript zero denote fully plastic values of a stress resultant in the absence of the other two, and depend upon the cross section considered. The specific expressions for N_0, V_0, and M_0 in this example are not of interest, and hence will not be given.

To see that $\bar{f}$ fails the condition of positivity, consider a state of stress given by $m = 0$, $v = 1$, and $n^2 = 1 + \epsilon$, which clearly lies outside the yield surface for values of $\epsilon > 0$. Substitution of these values into Eq. (6.14) leads to

$$\bar{f}(\sqrt{1+\epsilon},1,0) = \epsilon - \frac{1}{\epsilon} \tag{6.15}$$

which is less than zero for values of $0 \leqslant \epsilon \leqslant 1$, and hence fails the requirement of positivity outside the yield surface.

The potential $\bar{f}$ is obviously not the only one giving rise to the surface (6.13). One might hope that, through some manipulation, a suitable potential might be obtained. A manipulation of Eq. (6.13) leads to a potential satisfying the positivity condition which is given by

$$\bar{\bar{f}} \equiv \frac{|m| + 2n^2 + v^4}{1 + n^2(|m| + n^2)} - 1 \tag{6.16}$$

which has the property $\bar{\bar{f}} = 0$ is equivalent to (6.13). Considering stress states in which $m = v = 0$, $n \neq 0$, it can be seen that this potential is not coercive, ie.

$$\lim_{n\to\infty} \bar{\bar{f}}(n,0,0) = \lim_{n\to\infty} \frac{2n^2}{1+n^4} = \lim_{n\to\infty} \frac{1}{n^2} = 0 \tag{6.17}$$

where the second equality comes from successive application of L'Hospital's rule [44].

It is conjectured that the hypersurface (6.13) cannot be extended to a suitable potential. An alternative approximation to the yield surface having projections on $(n,v,0)$, $(n,0,m)$, and $(0,v,m)$ identical to (6.13) was given in [46] which satisfies the proposed requirements. The corresponding potential is given by

$$f \equiv |m| + n^2(1+v^2) + v^4 - 1 \tag{6.18}$$

The two surfaces $f = 0$ and $\bar{f} = 0$ are plotted along with Neal's [29] rigorous lower bound in Fig. 6.2.

In the next section we discuss an approach for determining a yield potential for the I-beam which is suitable for computational purposes. It is again found that the obtained yield surface cannot be extended to a potential which is suitable for use in the viscoplastic algorithm. An approximate potential is developed for this purpose.

I-Beam Yield Potential.- In developing an $n-v-m$ interaction surface for an I-beam we employ an idealization of the stress state which was first proposed by Horne [15]. In contrast with usual approaches to I-beam interaction (even the simple case of $n-m$ interaction), we view the cross section as being *thin walled.* An immediate consequence of the thin wall assumption is that the flanges carry no transverse shear. The validity of this assumption can be seen by again considering the upper and lower bound solutions of Neal [30] shown in Fig. 6.1. Increases in resultant shear carrying capacity above that achievable by the web alone can be seen to be negligible except for extremely short beams. The thin wall assumption is also in accord with the developments of Chapter 5.

It is necessary in this idealization to reinterpret what is meant by having the neutral axis in the flange. Instead of having the neutral axis location described by some distance of

penetration through the thickness of the flange, it will be viewed as a distance measured along its width. The interaction relationship obtained in this way is given explicitly in terms of the stress resultants n, v, and m and a single topological parameter which characterizes the cross section. The procedure followed in developing the interaction surface can be summarized as:

(1) Assume a simplified state of stress throughout a cross section in which the flanges have normal stresses equal to $\pm\sigma_0$, and the web has normal stress equal to $\pm\sigma$ and a shear stress equal to τ, where σ_0 is the yield stress in pure tension and σ and τ are as yet undetermined. Note that we are not forcing the assumed stress state to satisfy the two dimensional equations of equilibrium. For this reason the result is not a true lower bound solution.

(2) Assume a location of the neutral axis, either in the web or a flange, described by the parameter ξ.

(3) Impose the von Mises yield condition $\sigma^2+3\tau^2=\sigma_0^2$ throughout the web region. Note that, by assumption, this condition is trivially satisfied in the flanges.

(4) Compute the values of the stress resultants by direct integration of the stress components over the cross section.

The resulting yield surface will be characterized (in a quadrant of $n-v-m$ space) by three different functions each having its own unique domain of definition.

For convenience, the dimensionless ratio γ relating the gross flange area to the gross web area is defined as

$$\gamma \equiv \frac{2bt_f}{ht} \tag{6.19}$$

where b is the flange width, t_f is the flange thickness, h is the distance between the centroids of the flanges, and t is the web thickness. In terms of this ratio, the fully plastic values of the stress resultants are given by

$$N_0 = (1+\gamma)\, ht\, \sigma_0$$

$$V_0 = ht\,\tau_0 \tag{6.20}$$

$$M_0 = (1+2\gamma)\,\frac{h^2 t}{4}\,\sigma_0$$

where τ_0 is the yield stress of the material in pure shear. As usual, we will employ the normalized stress resultants $n = N/N_0$, $v = V/V_0$, and $m = M/M_0$. For purposes of notational convenience we make the following definitions:

$$m_* \equiv (1+2\gamma)|m| - 2\gamma$$

$$\beta \equiv 1+\gamma. \tag{6.21}$$

Neutral Axis in Web.- Assuming that the normal stress changes sign at a distance $\xi h/2$ from the centroid of the section we obtain the following expressions for the normalized stress resultants:

$$\beta n = \xi\frac{\sigma}{\sigma_0}; \qquad v = \frac{\tau}{\tau_0}; \qquad m_* = (1-\xi^2)\frac{\sigma}{\sigma_0} \tag{6.22}$$

Applying the von Mises yield criterion to σ and τ we arrive at the result

$$\sqrt{1-v^2}\,m_* + v^2 + \beta^2 n^2 = 1 \tag{6.23}$$

Equation (6.23) is applicable for the values $0 \leqslant \beta|n| \leqslant 1$, $0 \leqslant v \leqslant 1$, and $0 \leqslant m_* \leqslant 1$.

Neutral Axial in Flange.- Assuming that the normal stress changes sign in the flange at a distance $\xi b/2$ from the flange-web junction, we obtain the following expression for the normalized stress resultants

$$\beta n = \gamma\xi + \frac{\sigma}{\sigma_0}; \qquad v = \frac{\tau}{\tau_0}; \qquad m_* = -2\gamma\xi \tag{6.24}$$

Again applying the von Mises criterion, we obtain

$$\frac{1}{4}[m_* + 2\beta|n|]^2 + v^2 = 1 \tag{6.25}$$

from which we note that, for constant values of shear, the relationship between moment and axial force is linear. Equation (6.25) is valid for the values $1 \leqslant \beta|n| \leqslant \beta$, $0 \leqslant v \leqslant 1$, and $-2\gamma \leqslant m_* \leqslant 0$.

Web Fully Plastic, Flanges Not Fully Developed.- The case in which the shear stress in the web region is equal to τ_0 and the flanges have normal stress less than or equal to σ_0 leads to the interaction relationship

$$v^2 = 1 \tag{6.26}$$

which holds for values of n and m satisfying the inequality

$$m_* + 2\beta|n| \leqslant 0 \tag{6.27}$$

One quadrant of the complete interaction surface is shown in Fig. 6.3. Regions I, II, and III correspond to Eqs. (6.23), (6.25), and (6.26) respectively. Line **A** in the figure is given by the equality in Eq. (6.27). Line **B** is given by

$$v^2 + \beta^2 n^2 = 1; \qquad m_* = 0 \tag{6.28}$$

A check of the normal derivatives across lines **A** and **B** shows that the yield surface is continuous and smooth (except for a corner at $m = 0$).

Some comments regarding the obtained yield surface are in order:

(1) The projection $v = 0$ of the surface onto the $n-m$ plane gives an $n-m$ interaction curve which is exact within the thin wall approximation.

(2) The projection $n = 0$ onto the $v-m$ plane corresponds to the approximate $v-m$ interaction curve proposed by Neal [30]. This approximation was shown by Neal to correspond well with a rigorous lower bound solution. Recall that this curve, in a slightly different

form, was used in Chapter 3 to make a comparison between analytical and experimental results.

(3) The yield surface is everywhere convex.

(4) The yield surface is *not* suitable for extension to a potential. The problem arises in region I. It can be seen from Eq. (6.23) that, due to the presence of the term $\sqrt{1-v^2}$, stress states having $v \geqslant 1$ lead to imaginary values of the yield potential. Manipulation of the expression (6.23) was not found to completely resolve this situation.

Because the yield surface cannot be extended to a suitable potential, it cannot be used in the computational scheme proposed here. Therefore, we propose that the following potential be employed

$$f(\mathbf{R}) \equiv \begin{cases} m^2+\beta^2 n^2+v^2+\beta m_* |n| - 1 & \text{in I} \\ \frac{1}{4} m^2+\beta^2 n^2+v^2+\beta m_* |n| - 1 & \text{in II} \\ v^2 - 1 & \text{in III} \end{cases} \tag{6.29}$$

The surface $f = 0$ is compared with the "true" yield surface, given by Eqs. (6.23), (6.25), and (6.26) in Fig. 6.4 for a value of $\gamma = 0.5$.. Good correspondence between the two surfaces can be noted.

The approximate potential f has corners at $m = 0$ and and $n = 0$. The treatment of corners numerically can be satisfactorily achieved by the following procedure:

(1) Extend the two functions to have domains of definition beyond the corner.

(2) For each stress state in question, check whether none, one, or both of the potentials are positive.

(3) If both are positive, assume a plastic strain rate equation as a linear combination of the two potentials:

$$\dot{\boldsymbol{\lambda}}^p = \frac{1}{2\tau} \left[<f_1> \frac{\partial f_1}{\partial \mathbf{R}} + <f_2> \frac{\partial f_2}{\partial \mathbf{R}} \right] \tag{6.30}$$

Otherwise proceed as usual.

6.3. Solution Procedure

The solution procedure for the stress resultant formulation is completely analogous to the local approach. Again, the problem involves both geometric and constitutive nonlinearities, suggesting the procedure of linearization about an intermediate configuration. As the development closely follows [46] the results are given with only a few intermediate details.

Linearization of the Weak Form.- Employing standard procedures, the weak form of the equilibrium equations can be linearized about an intermediate configuration $\bar{\mathbf{u}}$, with incremental motion $\Delta\mathbf{u}$. The linear part of $G(\mathbf{u},\eta)$ can then be expressed as

$$L[G]_{\bar{\mathbf{u}}} \equiv \int_0^L \mathbb{B}^T(\eta)\,[\,\mathbf{A}_G + \Xi^T(\bar{\mathbf{u}})\,\frac{\partial \mathbf{R}}{\partial \lambda}\Big|_{\bar{\mathbf{u}}}\,\Xi(\bar{\mathbf{u}})\,]\,\mathbb{B}(\Delta\mathbf{u})\,dx \;+\; G(\bar{\mathbf{u}},\eta) \tag{6.31}$$

where, for the formulation considered here, the matrix $\mathbf{A}_G$ has the form

$$\mathbf{A}_G = \begin{bmatrix} 0 & 0 & 0 & -V \\ 0 & (1-\kappa)N & 0 & \kappa N \\ 0 & 0 & 0 & 0 \\ -V & \kappa N & 0 & \kappa N \end{bmatrix} \tag{6.32}$$

and gives rise to the geometric part of the stiffness matrix. The so-called residual $G(\bar{\mathbf{u}},\eta)$ is given by Eqs. (6.3) and (6.5) as

$$G(\bar{\mathbf{u}},\eta) = \int_0^L \mathbb{B}^T(\eta)\Xi^T(\bar{\mathbf{u}})\bar{\mathbf{R}}\,dx - \int_0^L q.\eta_2\,dx - [\eta.\hat{\mathbf{R}}]_{\partial R} \tag{6.33}$$

Numerical Integration of the Constitutive Equations.- Proceeding in a manner completely analogous to that presented in the previous chapter for the local approach, the rate constitutive equations (6.10) are integrated numerically. Again introducing the constitutive

residual Ψ_t, whose norm is a measure of satisfaction of the integrated constitutive equation, we arrive at the result that

$$\Psi_t \equiv -(\lambda_t - \lambda_0) + \mathbf{D}^{-1}(\mathbf{R}_t - \mathbf{R}_0) + \frac{\Delta t}{\tau}\beta(\mathbf{R}_\alpha) = 0 \tag{6.34}$$

where we have again set

$$\mathbf{R}_\alpha = (1-\alpha)\mathbf{R}_0 + \alpha\mathbf{R}_t \qquad 0 \leqslant \alpha \leqslant 1 \tag{6.35}$$

The subscripts 0 and t indicate that the quantity is evaluated at time $t = t_0$ and $t = t_0 + \Delta t$ respectively. Differentiating Eq. (6.34) with respect to λ, one can obtain an expression for the material tangent given by

$$\frac{\partial \mathbf{R}}{\partial \lambda} = [\,\mathbf{D}^{-1} + \alpha\frac{\Delta t}{\tau}\beta'(\mathbf{R}_\alpha)\,]^{-1} \equiv \Omega_t \tag{6.36}$$

Finite Element Discretization.- Following the standard Finite Element discretization procedure, the displacements $\mathbf{u}(x) = [\,u, v, \psi\,]^T$ are interpolated as [†]

$$\mathbf{u}(x) = \sum_{\alpha=1}^{N} h_\alpha(x)\mathbf{U}_\alpha \tag{6.37}$$

where N is the number of nodes per element, $h_\alpha(x)$ are the C^0 interpolation functions, and $\mathbf{U}_\alpha = [\,U, V, \Psi\,]^T$ are the nodal displacement values.

From the interpolation (6.37) the operator $\mathbb{B}(\mathbf{u})$ can be evaluated as

$$\mathbb{B}(\mathbf{u}) = \sum_{\alpha=1}^{N} \mathbf{B}_\alpha(x)\mathbf{U}_\alpha \tag{6.38}$$

where $\mathbf{B}_\alpha(x)$ is given by

[†] Recall that, in this formulation, the displacement variable β is dependent.

$$\mathbf{B}_\alpha(x) = \begin{bmatrix} h'_\alpha & 0 & 0 \\ 0 & h'_\alpha & 0 \\ 0 & 0 & h'_\alpha \\ 0 & 0 & h_\alpha \end{bmatrix} \tag{6.39}$$

Substituting Eq. (6.38) into the weak form (6.31), one is lead to the standard discrete problem for the incremental motion $\Delta\mathbf{U}$

$$\mathbf{K}_t \, \Delta\mathbf{U} = \mathbf{f}_t \tag{6.40}$$

where the tangent stiffness matrix is given by a sum over all of the elements as

$$\mathbf{K}_t = \sum_e \int_0^L \mathbf{B}^T [\mathbf{A}_{G_t} + \boldsymbol{\Xi}_t^T \boldsymbol{\Omega}_t \boldsymbol{\Xi}_t] \mathbf{B} \, dx \tag{6.41}$$

and the right-hand-side by

$$\mathbf{f}_t = \mathbf{F}_t - \sum_e \int_0^L \mathbf{B}^T \boldsymbol{\Xi}_t^T \mathbf{R}_t \, dx \tag{6.42}$$

the term $\mathbf{F}_t$ again denoting the current applied nodal forces. In these expressions $\mathbf{A}_G$, $\boldsymbol{\Xi}$, $\boldsymbol{\Omega}$ and $\mathbf{R}$ all depend upon the current state. Hence an iterative solution procedure is warranted.

With some minor reinterpretation of notation, the algorithm for solving the stress resultant problem is identical to that of the local approach. Therefore, Table 5.1 is again appropriate.

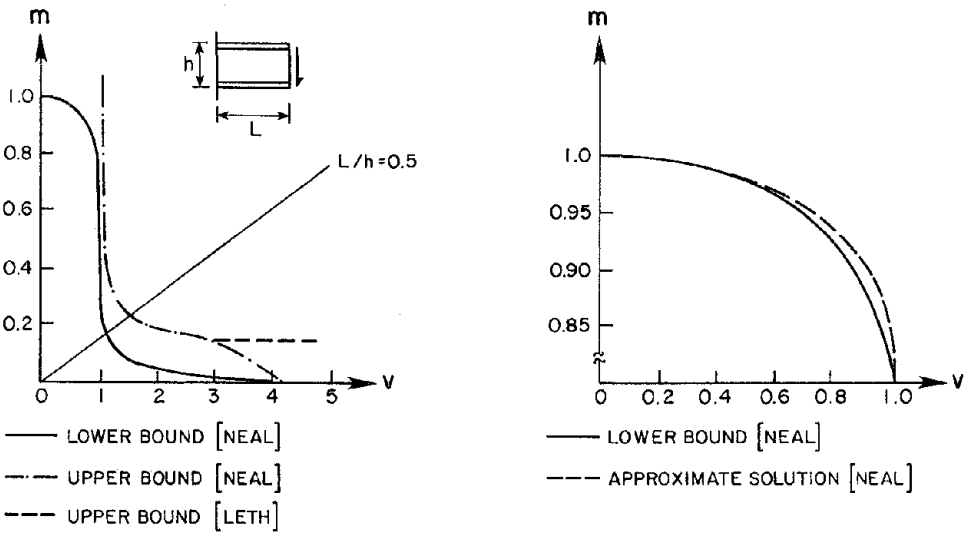

Fig. 6.1 Upper and Lower Bounds on the Carrying Capacity of a Cantilever Beam, W8×40 Section (after Neal [30])

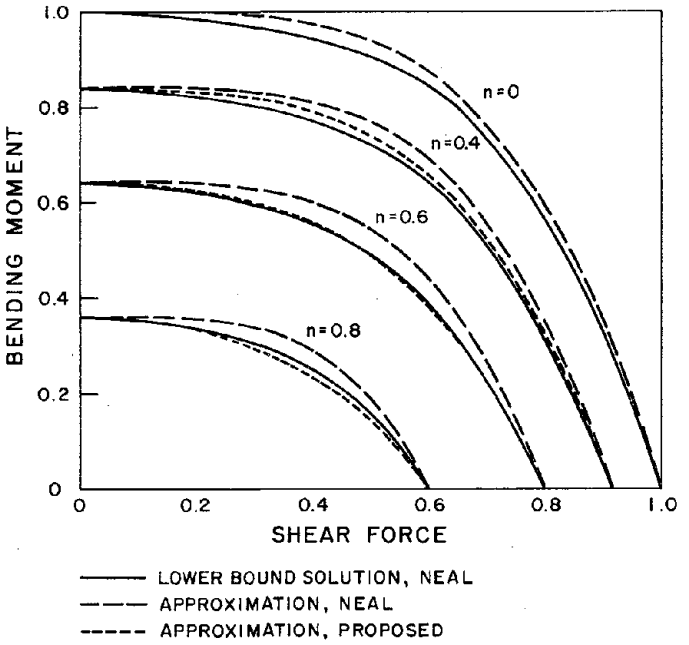

Fig. 6.2 Moment-Shear-Axial Interaction for Rectangular Section

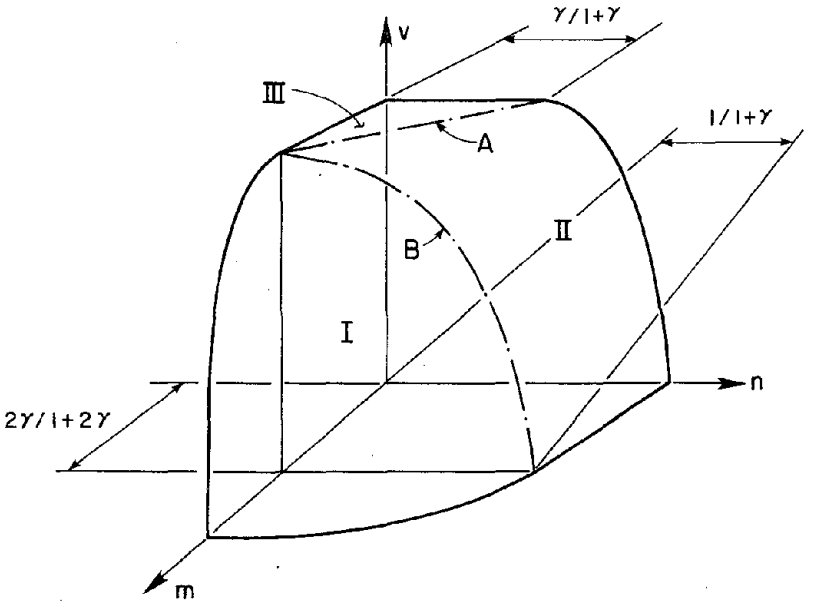

Fig. 6.3 Moment-Shear-Axial Interaction for I-Section, Schematic

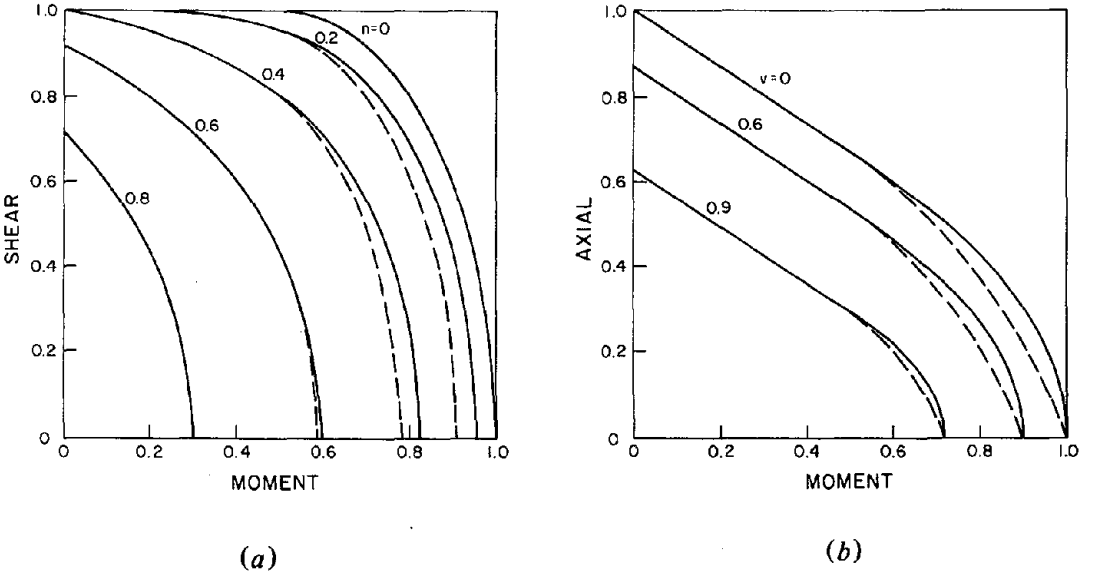

Fig. 6.4 Moment-Shear-Axial Interaction for I-Section, $\gamma = 0.5$
Solid Line = True Yield Locus
Dashed Line = Yield Locus for Approximate Potential

Chapter 7

Applications of Analysis to Eccentrically Braced Frames

7.0. Introduction

The preceding two chapters were devoted to developing two analytical approaches to the problem of inelastic bending, shearing, and stretching of short beams. The local approach presented in Chapter 5 involved the introduction of a kinematic hypothesis which constrained the otherwise three dimensional formulation. The stress resultant approach presented in Chapter 6 was a one dimensional formulation. The development of the local approach involved fewer assumptions than the stress resultant approach and hence can be expected to yield more accurate results. The local approach is employed in this chapter not only as a primary computational tool but also as a means of assessing the acceptability of the stress resultant model.

The purpose of this chapter is to apply the developed computational tools to the case of interest here: Active links in eccentrically braced frames. To this end, five numerical examples are presented. The first example is an isolated active link, subjected to loading conditions similar to those used in the experimental program described in Chapter 1. Both analytical models are employed and commented upon in this example. Next a detailed study is made of a one story, one bay eccentrically braced frame in order to compare the performance of the two models when employed in a more complicated structural assemblage. The last three examples are devoted to a study of three frames, having one bay and three stories, which employ different bracing arrangements. These analyses are carried out using only the stress resultant model.

The numerical computations performed for the examples presented in this chapter were carried out using the general purpose Finite Element program FEAP which is described in Chapter 24 of [50]. The computations were performed in double precision arithmetic on a VAX 11/780 computer.

7.1. A Link from the Experimental Program

The first example models analytically the typical pre-buckling behavior of Specimens 1 through 5 of the experimental program described previously. The purpose of presenting this example is to show the features of the local model which allow it to capture certain aspects of active link behavior. An extensive comparison between analysis and experiments is not attempted here.

The beam under consideration had length $L = 28$ inches and was fixed at one end and restrained against rotation at the other. The cross sectional dimensions of the beam are given in Table 7.1, in which h is the distance between the centroids of the flanges, b is the flange width, t is the web thickness, and t_f is the flange thickness. These dimensions closely approximate those of the W18×40 section used in the experiments. The idealized material properties are also given in the table. Here E is Young's modulus, G is the shear modulus, σ_0 is the yield stress in pure tension, and τ is the penalty parameter.

Section Dimensions			Material Properties		
h	(in)	18.00	E	(ksi)	30000
b	(in)	6.00	G	(ksi)	15000
t	(in)	0.33	σ_0	(ksi)	36
t_f	(in)	0.50	τ	(sec)	1

Table 7.1 Section and Material Properties for Isolated Link

The beam was discretized into four quadratic elements having equal length. Three Gauss points in the web and two in each half flange (symmetry of the cross section is noted) were employed to carry out the numerical integration over the cross section. The time integration of the constitutive equations was carried out using a value of $\alpha = 1$. The integrated constitutive equations were satisfied to within $||\Psi|| < 10^{-12}$ at each load increment.

The response of the beam to a cyclically applied shear force is shown in Fig. 7.1. The beam sustained an ultimate load of 124 k, compared to an average of 121 k for the first five specimens of the test program. Upon load reversal, the beam had a more rounded force-displacement curve due to the residual stresses resulting from the inelastic deformation.

Figure 7.2 shows the extent of plastification, determined by yielding at the integration points (the dots in the figure), at various levels of loading. The numbers 1, 2, 3, and 4 correspond to states at the numbered points on the force-deflection curve, Fig. 7.1. The inelastic zone at load point 1 consisted of a band across the center of the web and occurred due to the presence of large shear stresses at the middle fibers of the beam. This type of yield pattern, an experimentally observed phenomenon, cannot be realized with the "plane sections remain plane" kinematic hypothesis. Subsequent yielding (load points 2 and 3) developed more rapidly at the ends of the beam than in the middle due to the influence of the bending moment. The yield pattern at load point 4 showed that the center of the beam experienced a slight unloading at full plastic flow, caused by a redistribution of the shearing stresses over the cross section. The flanges, which remained elastic throughout the loading process, are not shown in the figure.

The local model is also able to give information on the distribution of the stress components over the cross section of the member. The shear and normal stress distributions at the end of the beam are shown for three load points in Fig. 7.3. The letters A, B, and C correspond to load points on the force-displacement diagram, Fig. 7.1. At point **A** the beam was completely elastic and the stress distribution was exactly the same as that of elementary beam theory[†]. In this formulation, however, in contrast to the elementary theory, the shear stress component S_{12} is not computed as the equilibrating reaction to the normal stress S_{11}, but is given directly from the strain E_{12} through a constitutive equation. At point **B** considerable plastic flow had taken place. At that point, the shear stress components were nearly constant

[†] In this example, no boundary condition was specified on the variable β. This condition corresponds to neglecting warping restraint. Warping restraint does affect the distribution of the stress components.

and the normal stress components were relatively small in the web region. This result lends credence to the assumption of the stress distribution employed in Chapter 6 to determine the expression for the yield potential in stress resultant space. Point **C** represents an elastic unloading from point **B**. Note that the shear stress at the extreme outer fibers of the cross section always vanished in this example. This will not be true in general for this model. Warping restraint and propagation of plasticity in the flange regions may lead to stress distributions which violate the shear stress boundary condition.

The stress resultant model exhibited the simple bilinear elastic-perfectly plastic response and thus is not shown in the figure. The elastic stiffnesses of the two models were identical and the collapse loads were nearly the same. Since the stress point was on the flat portion of the interaction diagram, the collapse load for the stress resultant model was simply $P_u = V_0$, where V_0 is given by Eq. (6.20). Using the properties given in Table 7.1, we have that $P_u = V_0 = 124.7$ k, compared with $P_u = 124.0$ k obtained from the local approach.

7.2. A Simple Eccentrically Braced Frame

The second example concerns a simple one story, one bay eccentrically braced frame with a single diagonal brace and a single active link. The purpose of this example is to critically compare the two developed mathematical models in a more complex structural system. Except for the section used for the brace, the proportions of this frame are identical to those in a typical story of the multistory frames considered in the last three examples. Hence, the present example can be viewed as a direct assessment of the accuracy of the stress resultant approach in the subsequent examples.

The bay width, story height, and eccentricity were taken to be $L = 216$ inches, $h = 108$ inches and $e = 36$ inches, respectively (See Fig. 7.4 for a sketch of the structure). The section dimensions of each of the members are given in Table 7.2 below. Material properties for all of the members were the same: $E = 29000$ ksi, $G = 14500$ ksi, and $\sigma_0 = 36$ ksi.

		Beam	Brace	Columns
h	(in)	13.28	7.69	13.22
b	(in)	8.06	7.69	8.03
t	(in)	0.37	0.32	0.34
t_f	(in)	0.66	0.32	0.59

Table 7.2 Section Dimensions for the Simple Frame

The columns, the brace, and the segment of the beam to the left of the brace were discretized using three quadratic elements each. The active link was discretized using two quadratic elements. Integration over the cross section, for the local model, was carried out with three Gauss points in the web and two in each of the half flanges. The constitutive equations of both models were integrated using a value of $\alpha = 1$ and the integrated equations were satisfied to within $||\Psi|| < 10^{-10}$.

The penalty was taken to be $\tau = 1$ for the local model and $\tau = 10^{-5}$ for the stress resultant model. Recall from Chapter 5 that the choice of the penalty depends upon the desired proximity of the converged stress points to the yield surface. The required magnitude of the penalty depends upon different quantities for the two models (eg. E and k for the local model, EI and M_0, etc. for the stress resultant model). The value $\tau = 10^{-5}$ used for the stress resultant model kept the stress points within 10^{-5} of the yield surface. The value of $\tau = 1$ used for the local model kept the stress points within 10^{-4} of the yield surface. Both tolerances were measured by the respective yield potentials of the models.

The response of the frame to the applied lateral load[†] is shown in Fig. 7.4. The numbered load points correspond to the stress resultant model while lettered load points correspond to the local model. Correspondence between the solutions found using the two models was quite good for this example. The local model exhibited initial yielding at a lower load than the stress

[†] Displacement control was used in solving this example.

resultant model but achieved a slightly higher collapse load. The stress resultant model showed a slight degradation in load carrying capacity after load point 6, whereas the local model showed no such loss of capacity. This difference in behavior is due to the way in which the inelasticity is manifested in each case, and is discussed below.

The sequence of plastification is shown for the stress resultant model in Fig. 7.5, in which the numbers correspond to load points on the force-deflection curve (Fig. 7.4). At load point 1 no plastic regions had formed. Load points 2, 3, and 4 show that, in order for plastification of the active link to occur, the top end of the brace needed to yield first but subsequently unloaded. At load point 5 the right column reached capacity at its base. The structure had formed a collapse mechanism by load point 6, consisting of plastic zones at the bottom of both columns and the brace and a plastic zone in the active link. The loss of capacity occurred due to the so-called $P-\Delta$ effect on an otherwise perfectly plastic structure.

Even though the active link yielded in shear at the integration point at the right end (ie. the stress point was on the flat portion of the interaction surface), the link never yielded at the other three integration points. This phenomenon can be explained by noting that due to the nonlinearity of the equilibrium equations (6.1), the shear force is not necessarily constant for the case of end loading as it is in the linear theory. In most cases, however, the formation of a shear mechanism in the active link will involve plastification at all of the integration points.

The propagation of inelasticity is more complex for the local model. The extent of plastification for this model is shown for four load points in Fig. 7.6, where again the corresponding load points are labeled on the force-deflection curve (Fig. 7.4). At load point **A** a plastic zone had begun to form in the web region of the active link, accompanied by a small amount of plastification due to bending and axial thrust at the top of the brace and the right column. At load point **B** the web of the active link was fully yielded in shear with some plastic action in the lower flange at the right end. The plastification at the top of the brace and right column had progressed into the web and a small plastic zone had formed at the base of the right column. Load point **C** showed that plastic zones had formed in the left column and the

bottom of the brace in addition to the zones previously formed. However, at this point, which corresponds to load point 6 of the stress resultant model, the plastic zones were not completely developed, and hence no loss of capacity occurred. By load point **D** a collapse mechanism had nearly been achieved. The similarities between the two models as regards the propagation of plasticity through the structure should be noted.

It is particularly important to verify that the two models redistribute the internal forces in the same manner upon yielding. The elastic distributions of moments were identical for the two models. The distribution of bending moments at load point **D** for both cases are shown in Fig. 7.7. The results are seen to be in good correspondence, verifying the proper behavior of the stress resultant model.

Based upon the results of this example it appears that the stress resultant model is capable of accurately capturing the response of a structure employing active links. In the following examples a verification with the local model are not made.

7.3. A Study of Three Eccentrically Braced Frames

The remaining three examples presented in this chapter are concerned with three story, one bay eccentrically braced frames employing different bracing arrangements. The first system analyzed (Frame I) employed the so-called split-K bracing arrangement with the two braces in each bay emanating from each of the lower corners and forming an active link in the middle of the beam above. A variant of this system has been explored experimentally by Manheim [27]. The other two systems employed a single diagonal brace. In Frame II the brace emanated from the lower left corner and formed an active link at the upper right corner between the brace and the column. The topology of Frame III was similar to that of Frame II except that the diagonal braces were also offset from the column at the lower left corners. The system characterized by Frame III has been explored experimentally by Roeder and Popov [42]. The three frames presented in this study were designed by Kasai [20] employing his newly developed plastic design method.

Each of the frames had a bay width of 216 inches and three equal stories, each having a height of 108 inches. All of the link beams had 36 inch lengths. The members sizes employed were the same for each of the frames in the study. The member properties are summarized in Table 7.3.

		Beams	Braces	Columns
$E\Omega$	(k)	452400	271440	408900
$G\Omega$	(k)	226200	135720	204450
EI	(k–in^2)	15370000	2636100	14065000
κ		0.33	0.50	0.32
N_0	(k)	561	336	508
V_0	(k)	107	100	93
M_0	(k-in)	3070	1000	2822
γ		2.0	1.0	2.1

Table 7.3 Member Properties for the Three Story Frames

The columns, the brace, the beam segment to the left of the brace, and the links in each story were discretized using two quadratic elements each. The constitutive equations were integrated in all cases with a value of $\alpha = 1$, and employed a penalty of $\tau = 10^{-2}$. This value of the penalty kept the stress points within 0.01 of the yield surface, as measured by the yield potential. The integrated constitutive equations were satisfied to within $||\Psi|| < 10^{-10}$ at each load increment.

In all cases, the lateral load was a single concentrated force applied at the top of the structure. Except for the absence of dead loading, this type of loading might be representative of the conditions found in the lower three stories of a braced bay of a multistory building under earthquake type excitation [42]. Hence, these examples provide a reasonable representation of the behavior of real eccentrically braced frames.

Frame I.- The response of the first structure to an applied lateral load at the top is shown

in Fig. 7.8, in which the applied force is plotted versus the displacement of the structure at the point of loading. First yielding of the structure occurred sometime between load points **A** and **B**, after which the structure experienced a great reduction in lateral stiffness. At a displacement of 4.0 inches, the sense of the loading was reversed. Increased rounding of the force-deflection curve, due to residual internal forces, can be seen. Loading was continued to a displacement of 4.0 inches in the opposite direction. A slight drop in load carrying capacity was noted at load points **D** and **H**, due to $P-\Delta$ effects.

The propagation of inelasticity is shown schematically in Fig. 7.9. At load point **B**, the active links in the top two beams had yielded in shear. The bottom active link yielded prior to load point **C**. Just prior to load point **D**, the structure formed a collapse mechanism. The sequence of plastification in the opposite direction was exactly the same, except that the sense of deformation in each of the members was reversed. Thus, load point **F** corresponds with load point **B**, load point **G** with **C**, and load point **H** with **D**.

The bending moment fields at the elastic load level **A** and at the fully plastic load level **D** are shown in Fig. 7.10. In the elastic regime (prior to load point **A**), the columns had very small bending moments while the active links sustained large moments and moment gradients. By load point **D** the columns had attained much larger bending moments, due to redistribution of forces in the structure. Further, the columns in essentially all three of the stories were in single curvature bending. The explanation of this type of behavior is quite simple. After all three of the active links had yielded, the additional resistance of the structure to the applied loading came from a cantilever type bending of the three story column. Thus the incremental bending moment field was linear over the three stories, vanishing at the top of the structure and reaching a maximum at the base. The lateral tip loading is the worst possible case in this regard. It is also interesting to note that the bending moment was of constant sign in the beam segment between the active link and the column. This observation may be important for cases considering uniformly applied dead loading on these beams. Apart from the change in the sense of bending, the distribution of moments at load point **H** were quite similar to that shown

for **D**, differences being on the average less than one percent of the fully plastic moment and at most less than two percent.

Frame II.- The response of the second frame to the applied loading is shown in Fig. 7.11. The global force-deflection characteristics were similar to the previous case. Frame II was substantially more flexible than Frame I.

The states of plastification for load points **A** through **H** are shown in Fig. 7.12. Load point **A** the structure was elastic. At point **B**, the bottom two active links and the right column base had yielded. The top active link had yielded by load point **C**. A collapse mechanism formed just prior to **D**. Upon reversal, the sequence was similar except that early yielding in the middle active link occurred at load point **E**.

The bending moment fields at load points **A** and **D** are shown in Fig. 7.13. The major difference between the elastic distribution for this frame and that of the previous one was the presence of substantial bending moments in the right columns of Frame II. The fully plastic distribution (load point **D**) was remarkably similar to the elastic distribution. Note that the columns on the right remained in double curvature bending at all stages of loading. This type of behavior can be largely attributed to the early plastification of the structure at the right column base. The presence of this plastic zone prevented the three story cantilever type bending moment field from developing after the active links had all yielded. Again, the difference between the bending moment field at load points **D** and **H** were small, the maximum being seven percent of the fully plastic moment and the average being two percent of the fully plastic moment.

Frame III.- The response of the last frame to a monotonic loading is shown in Fig. 7.14. The stiffness of this structure was only slightly less than its counterpart having a concentric joint at the lower left corner of each bay (Frame II). Again, a dramatic loss of stiffness took place shortly after initial yielding of the structure.

The propagation of inelasticity throughout the structure is shown in Fig 7.15, and can be seen to be quite different from the previous frame. The structure was elastic at load point **A**. At load point 1, the top two (right) active links had yielded in shear. This pattern should be contrasted to the previous frame in which the bottom two active links and the right column base plastified first. At load point 2, these differences had been recovered (compare load point **C** in Fig. 7.12). Inelastic zones formed both at the left column base and in the bottom (left) link by load point 3. Load points 4 and 5 show that some unloading occurred in the top (right) active link prior to formation of a collapse mechanism.

The bending moment fields at load points **A** and **B** are shown in Fig. 7.16. In contrast with the previous frame, the left columns sustain considerable bending moment even at elastic load levels. Additionally, the presence of links at the bottom left of each bay forced the bending moment to change sign in the beam at midspan as well as within each link. The fully plastic bending moment field (point **D**) was again remarkably like the elastic field.

Comparisons Among the Three Frames.- The properties of the three frames presented in the preceding examples were quite similar. It is, therefore, possible to make some meaningful comparisons between them. These comparisons cover three basic aspects of structural behavior that are of particular importance in seismic applications: Stiffness, ultimate capacity, and inelastic member deformation requirements.

To facilitate the comparisons some definitions are made. Inasmuch as all of the frames were excited by a single load at the top of the structure, it is reasonable to define a measure of structural stiffness as

$$\bar{K} = \frac{H_A}{\Delta_A} \tag{7.1}$$

where H_A is the applied lateral load and Δ_A the corresponding lateral displacement measured at the point of loading. The subscript A indicates that the two values are taken at some elastic

state, which, for definiteness can been taken to be load point A. Note that this definition makes sense only for the present case and would probably not be a reliable measure of structural stiffness for generalized loading conditions.

To make comparisons between the frames, ductility measures are employed. Here structural ductility is defined as

$$\mu_s = \frac{\bar{K}}{H_u}\Delta \tag{7.2}$$

where $\bar{K}$ is as given above, H_u is the ultimate frame load, and Δ is the displacement at the top of the structure. Since the deformation in the active link regions was realized predominantly through shear deformation, member ductility is reasonably defined as

$$\mu_m = \frac{\kappa G \Omega}{V_u}\lambda_v \tag{7.3}$$

where $\kappa G \Omega$ is the elastic cross sectional shear stiffness, V_u is the ultimate shear capacity, possibly reflecting interaction effects, and λ_v is the strain measure conjugate to the shear stress resultant defined by Eq. (6.2).

The stiffness and ultimate frame capacity obtained from the analyses are recorded in Table 7.4. The stiffnesses of Frames II and III were nearly equal, indicating that offsetting the brace from the beam column joint in the lower left corner of each bay had little effect on the elastic stiffness. This result is somewhat surprising when one considers that the bending moment field was dramatically changed by this adjustment. The split-K bracing arrangement was approximately 45% stiffer than the two frames having single diagonal braces. The ultimate capacity of the first two structures was nearly the same, but the collapse load of the third structure was seven percent less than the first two.

As was pointed out in Chapter 3, the proper detailing of an active link depends upon the inelastic deformations it will be required to sustain. Energy dissipation measures were employed in deriving appropriate design recommendations in that chapter. When load carrying

		Frame I	Frame II	Frame III
$\bar{K}$	(k/in)	250	172	165
H_u	(k)	228	230	215

Table 7.4 Stiffnesses and Ultimate Capacities of the Three Story Frames

capacity does not degrade, member ductility measures can also be employed. The active link ductilities obtained from the present analyses, corresponding to a selected structure ductility of $\mu_s = 3.0$, are presented in Table 7.5 [†]. Note that the first story is at the bottom and that the third story is at the top. The split-K framing system (Frame I) gave rise to the smallest member ductility demands at the reported level of structure deformation. The modified single diagonal bracing arrangement (Frame III) gave rise to the largest demands. In Frames I and III the active link ductilities increased with story height, whereas Frame II had its maximum value at the middle story. Based upon the results of the experimental program, it appears that the ductility magnitudes computed here could be sustained by a properly detailed active link.

	Frame I	Frame II	Frame III
Story 1	11.5	25.5	18.5
Story 2	28.5	39.6	31.5
Story 3	37.5	36.6	51.8

Table 7.5 Link Ductilities Corresponding to $\mu_s = 3$

One might conclude from the preceding study that any of the three bracing arrangements would be acceptable for use in seismic design. The member ductility demands in each of the three frames were comparable, Frames I and II showing a slight superiority over Frame III in

[†] The value $\mu_s = 3$ is chosen only as a reference value. It does *not* represent the maximum ductility capability of the frame.

this regard. The split-K framing system had a higher stiffness than the other two but had a less favorable redistribution of bending moments upon plastification. None of the frames in this study experienced buckling. However, the way in which moments redistribute may be an important consideration when dead loading is included or in general for tall, slender structures. In such cases the final plastic moment distribution may be of great importance to the stability of the structure. It is emphasized that this was not the case here. Hence, the split-K system (Frame I) appears to have an advantage for the situation studied. For narrow bays, one might expect the single diagonal bracing arrangement to be stiffer, and perhaps more desirable.

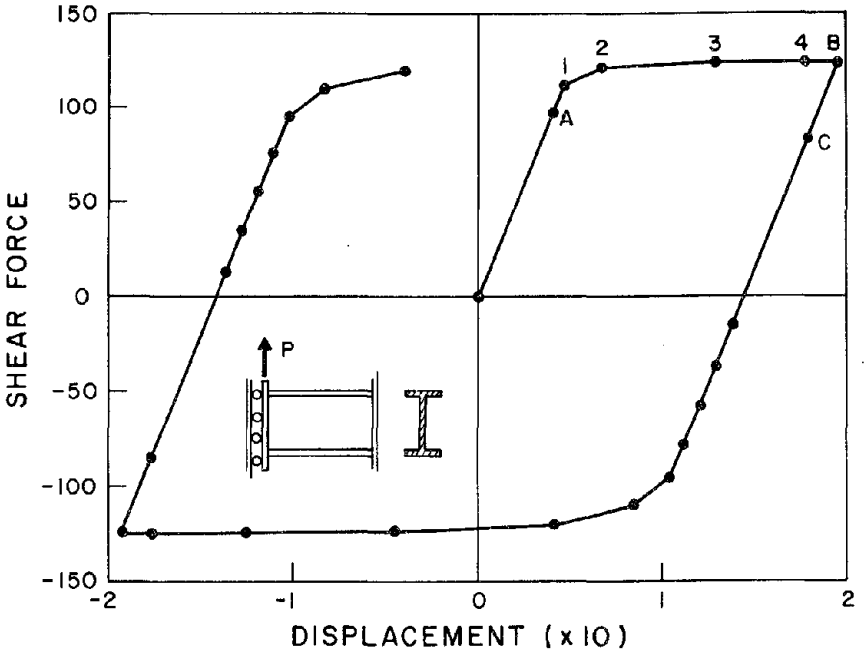

Fig. 7.1 Shear-Displacement Response for Single Link Example

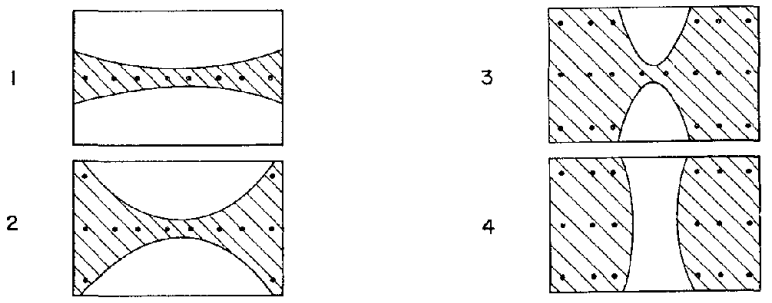

Fig. 7.2 Propagation of Inelasticity in Web Region for Single Link Example

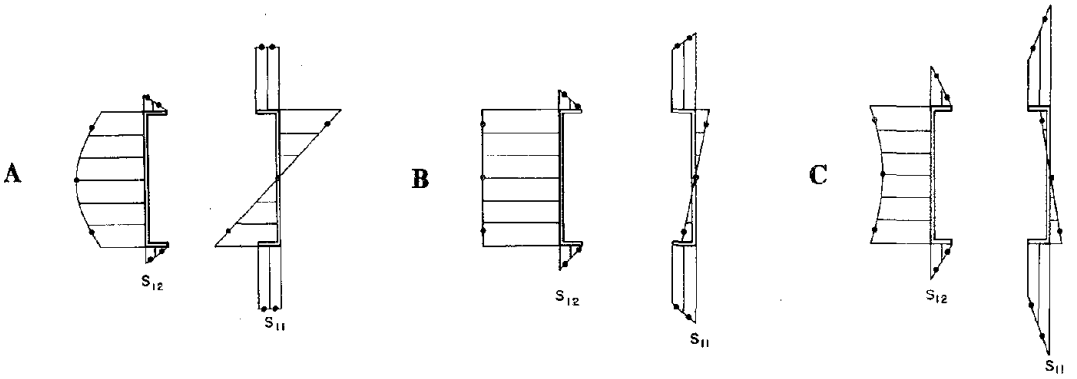

Fig. 7.3 Stress Distributions at Load Points A, B, and C for Single Link Example

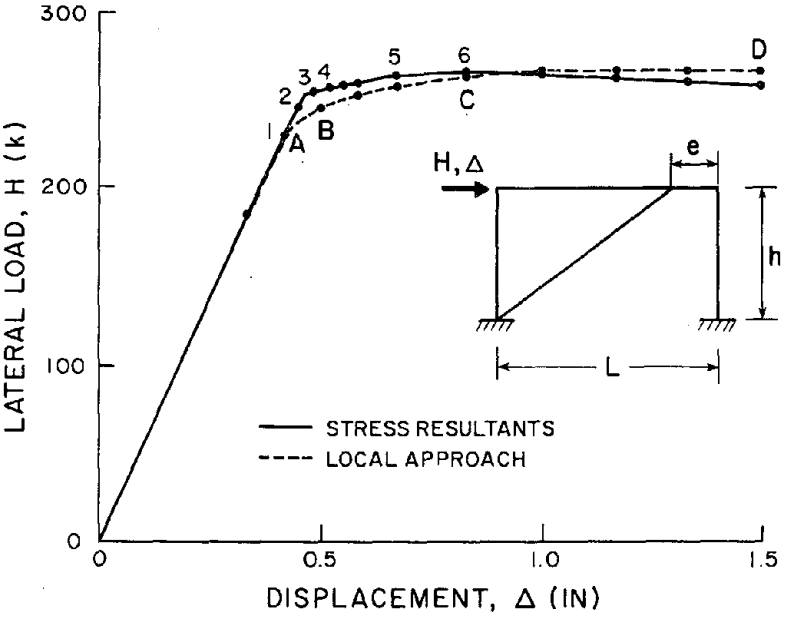

Fig. 7.4 Load-Deflection Curve for Simple Eccentrically Braced Frame Example

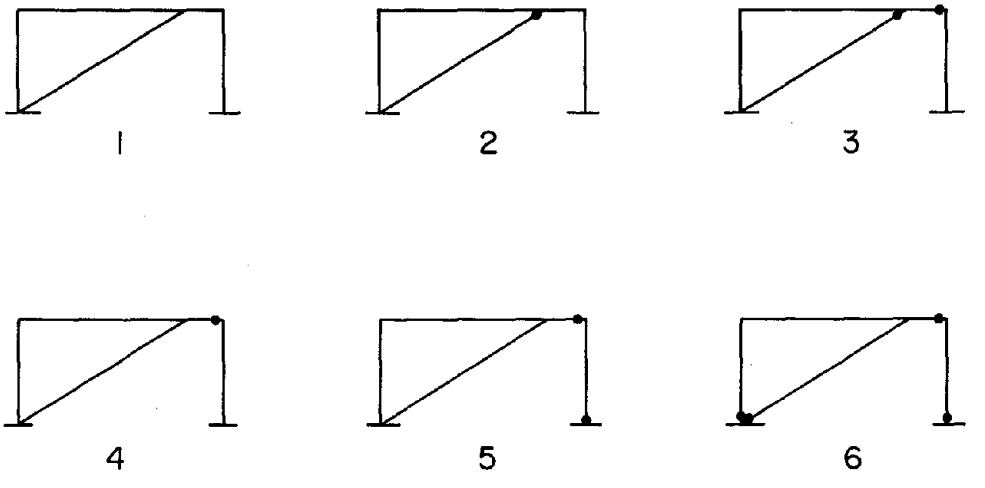

Fig. 7.5 Propagation of Inelasticity for Stress Resultant Model, Simple EBF Example

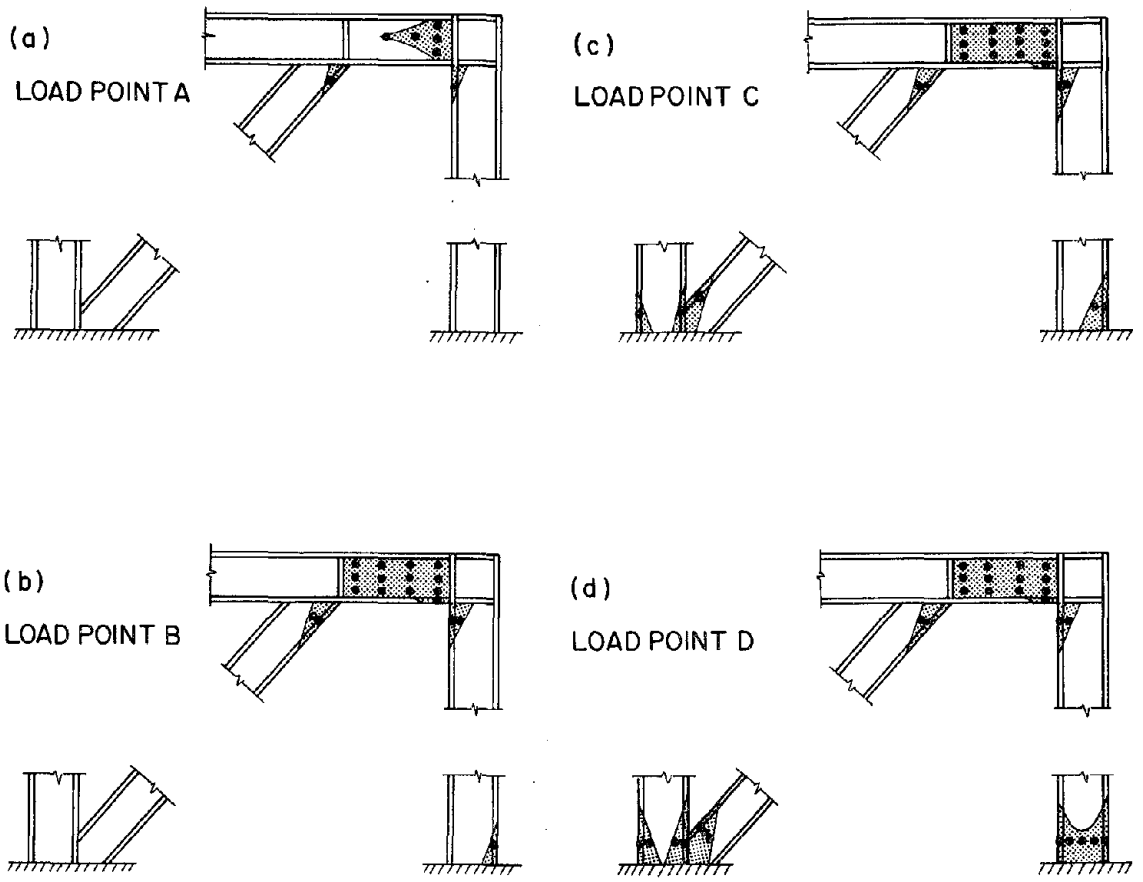

Fig. 7.6 Propagation of Inelasticity for Local Model, Simple EBF Example

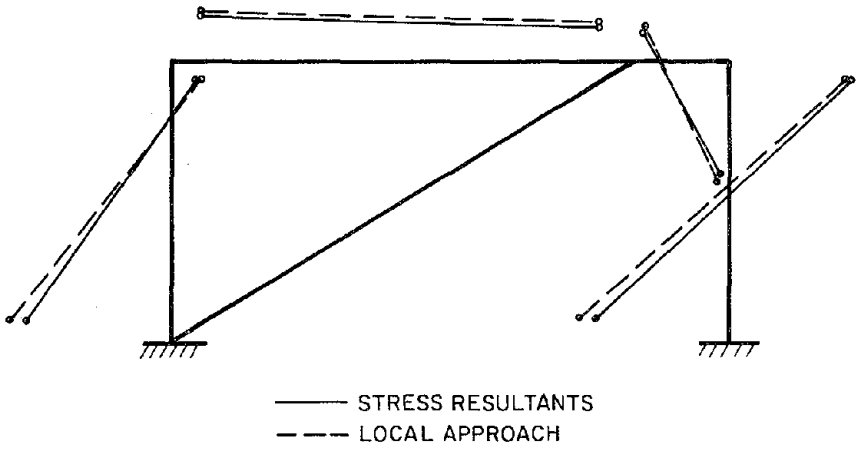

Fig. 7.7 Comparison the of Bending Moment Fields, Obtained with the Two Models, at Load Point D, Simple EBF Example

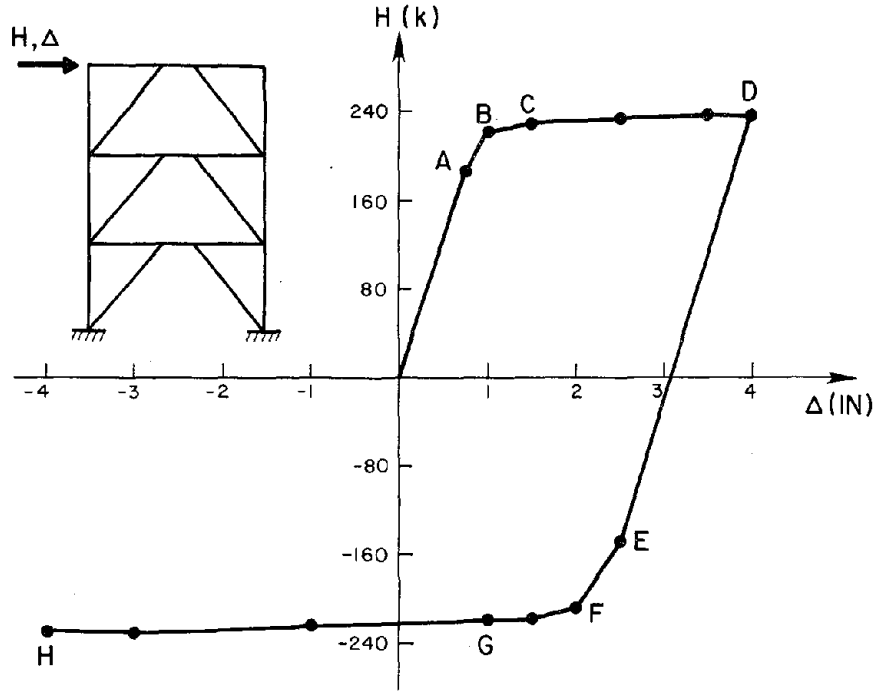

Fig. 7.8 Load-Displacement Relation for Frame I

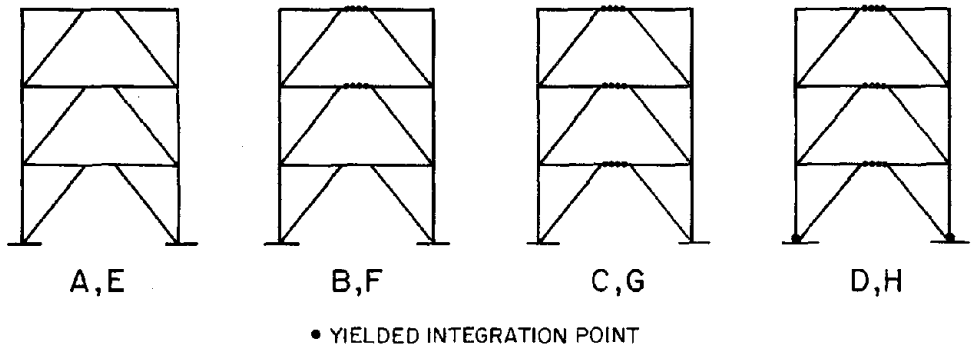

Fig. 7.9 Propagation of Inelasticity for Frame I

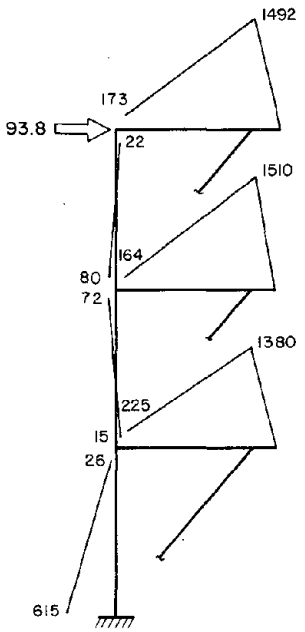

LOAD POINT A

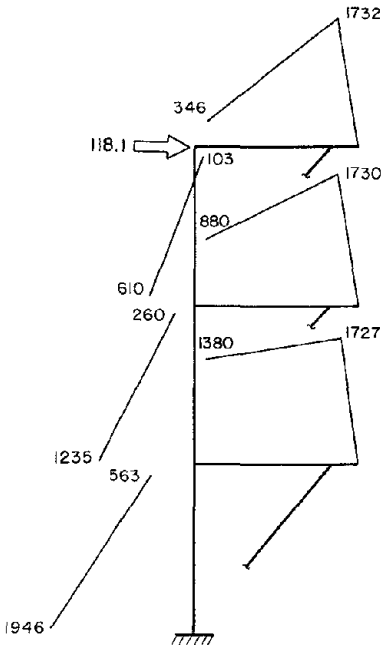

LOAD POINT E

Fig. 7.10 Bending Moment Fields at Load Points A and E for Frame I

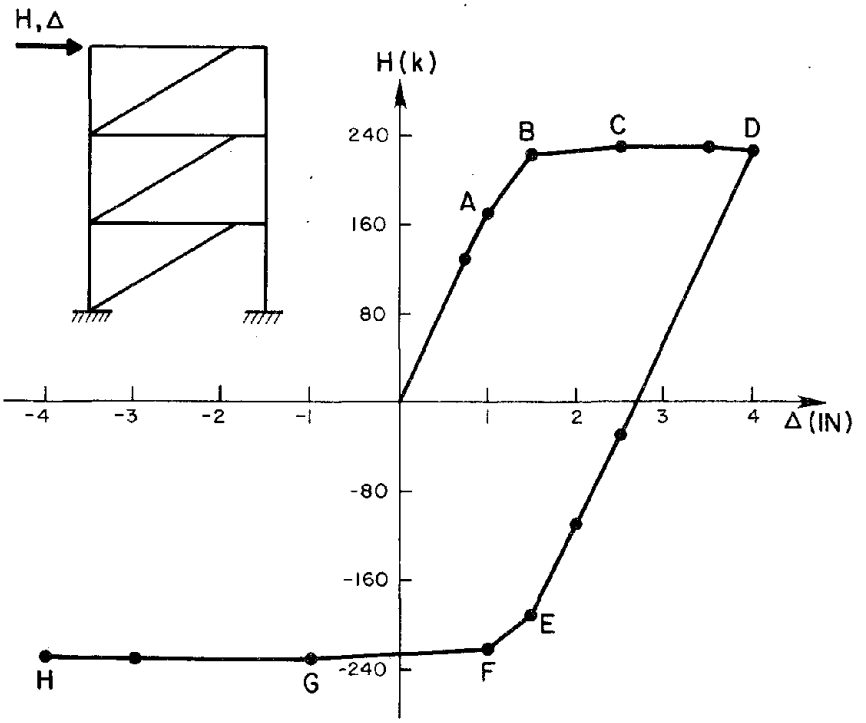

Fig. 7.11 Load-Displacement Relation for Frame II

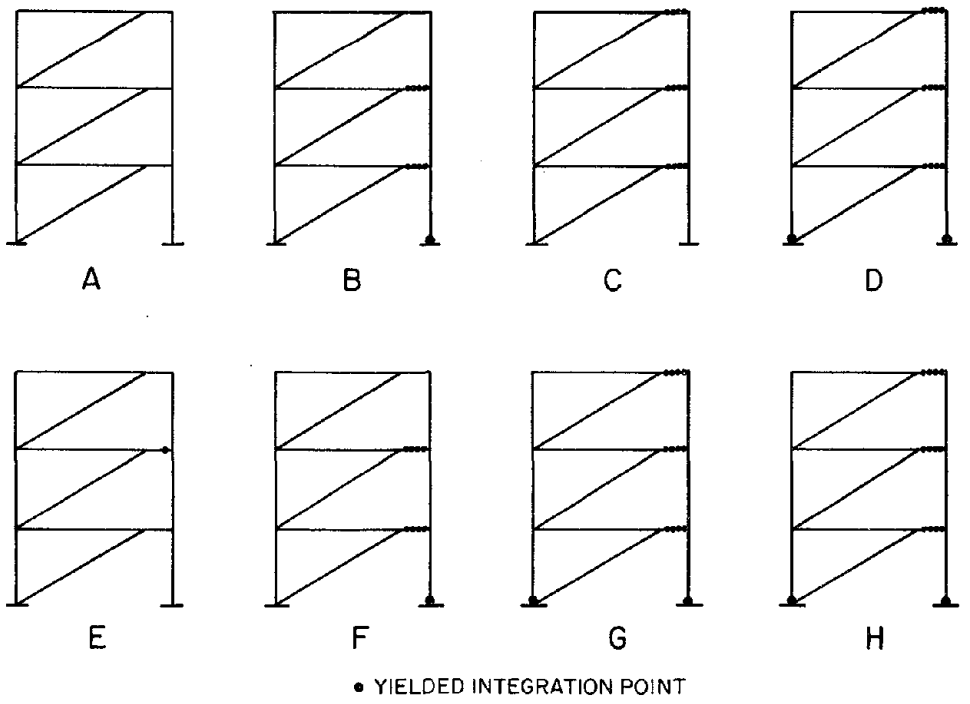

Fig. 7.12 Propagation of Inelasticity for Frame II

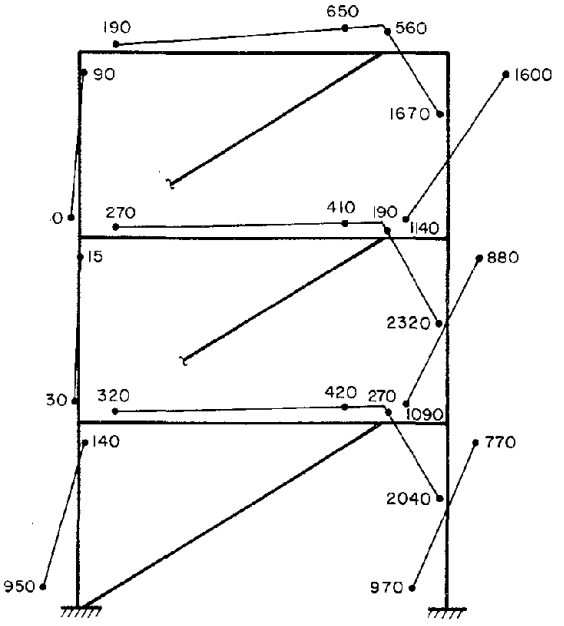

LOAD POINT A

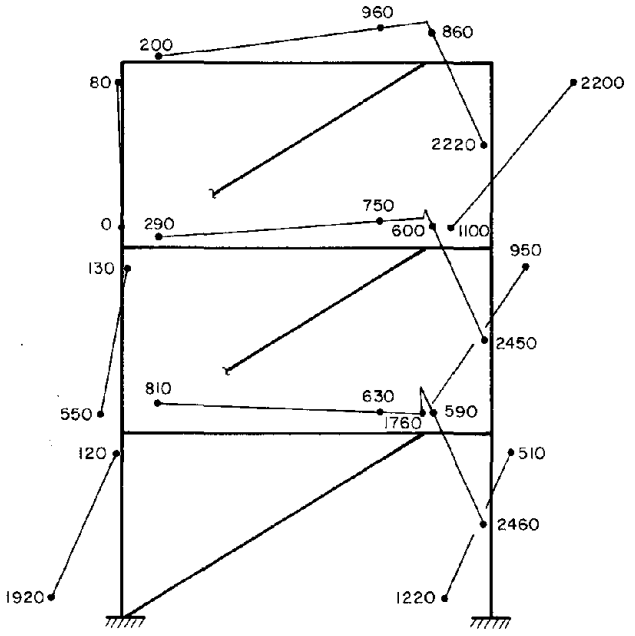

LOAD POINT D

Fig. 7.13 Bending Moment Fields at Load Points A and D for Frame II

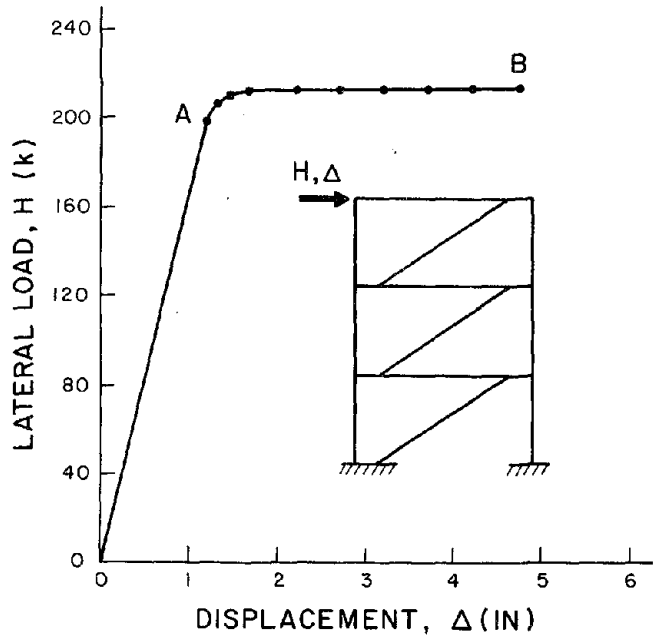

Fig. 7.14 Load-Displacement Relation for Frame III

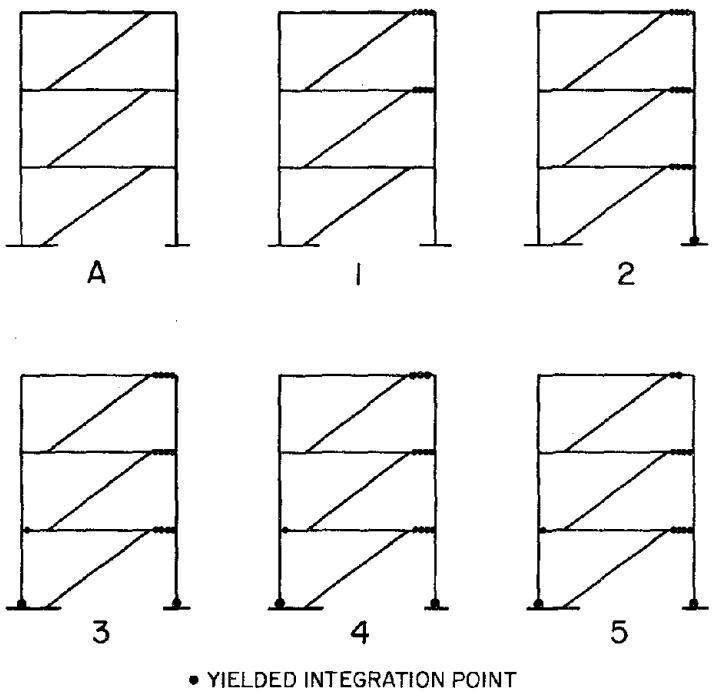

Fig. 7.15 Propagation of Inelasticity for Frame III

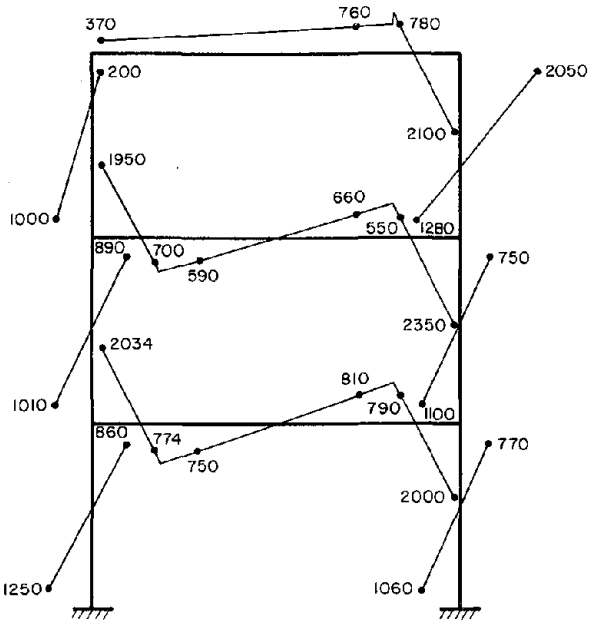

LOAD POINT A

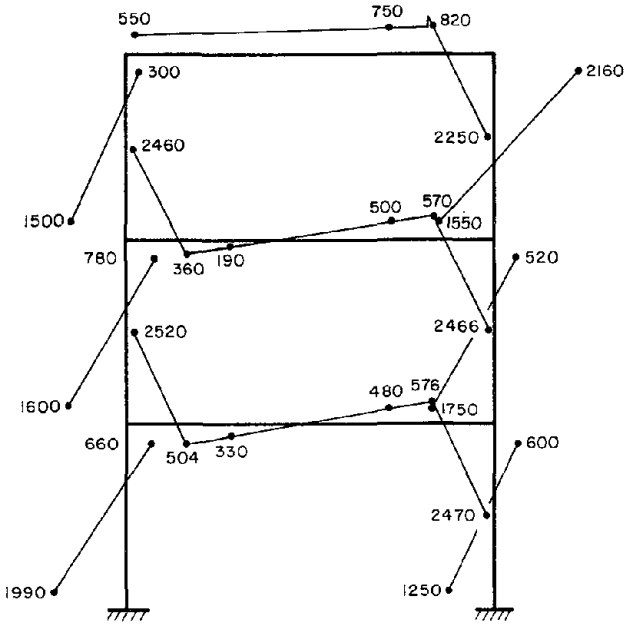

LOAD POINT B

Fig. 7.16 Bending Moment Fields at Load Points A and B for Frame III

REFERENCES

[1] Basler, K., "Strength of Plate Girders under Combined Shear and Bending", *Journal of the Structural Division,* ASCE, Vol. 87(ST7), 1961.

[2] Cowper, G. R., "The Shear Coefficient in Timoshenko's Beam Theory," *Journal of Applied Mechanics,* Vol. 33(6), 1966.

[3] Chen, P. F.-S., "Generalized Plastic Hinge Concepts for 3D Beam-Column Elements", Thesis presented to the University of California, Berkeley, in partial fulfillment of the degree of Doctor of Philosophy, 1981.

[4] Dafalias, Y. F., and Popov, E. P., "Plastic Internal Variables Formalism of Cyclic Plasticity", *Journal of Applied Mechanics,* Vol. 98(4), 1976.

[5] Drucker, D. C., "The Effect of Shear on the Plastic Bending of Beams", *Journal of Applied Mechanics,* Vol. 23(4), 1956.

[6] Evans, H. R., Porter, D. M., and Rockey, K. C., "The Collapse Behavior of Plate Girders Subjected to Shear and Bending", *IABSE Proceedings,* P-18/78, 1978.

[7] Fung, Y. C., **Foundations of Solid Mechanics,** Prentice-Hall, Inc., Englewood Cliffs, New Jersey, 1965.

[8] Green, A. E., and Naghdi, P. M., "Some Remarks on Elastic-Plastic Deformation at Finite Strain," *International Journal of Engineering Science,* Vol. 9, 1971.

[9] Green, A. P., "Theory of the Plastic Yielding Due to Bending of Cantilevers and Fixed-Ended Beams", *Journal of Mechanics and Physics of Solids,* Vol. 3(1), 1954.

[10] Herrmann, H., and Luther, J., "Die Klöppel-Yamadaschen Fliessgelenkbedingungen für I-Querschnitte und ihre numerische Aufbereitung", *Der Stahlbau,* Vol. 51(3), 1982.

[11] Hjelmstad, K. D., and Popov, E. P., Some Characteristics of Eccentrically Braced Frames", *Journal of Structural Engineering,* ASCE, to appear.

[12] Hjelmstad, K. D., and Popov, E. P., "Cyclic Behavior and Design of Link Beams", *Journal of Structural Engineering,* ASCE, to appear.

[13] Hodge, P. G:, **Plastic Analysis of Structures,** McGraw-Hill Book Company, New York, 1959.

[14] Hodge, P. G., "Interaction Curves for Shear and Bending of Plastic Beams", *Journal of Applied Mechanics,* Vol. 24(3), 1957.

[15] Horne, M. R., "Full Plastic Moments of Sections Subjected to Shear Force and Axial Load", *British Welding Journal,* Vol. 5, 1958.

[16] Hughes, T. J. R., and Taylor, R. L., "Unconditionally Stable Algorithms for Quasi-Static Elasto/Viscoplastic Finite Element Analysis", *Computers and Structures,* Vol. 8(2), 1978.

[17] Hughes, T. J. R., and Pister, K. S., "Consistent Linearization in Mechanics of Solids and Structures", *Computers and Structures,* Vol. 8, 1978.

[18] Kachanov, L. M., **Fundamentals of the Theory of Plasticity,** Mir Publishers, Moscow, 1974.

[19] Kantorovich, L. V., and Krylov, V. I., **Approximate Methods of Higher Analysis,** Wiley-Interscience, New York, 1962.

[20] Kasai, K., private communication.

[21] Klöppel, K., and Yamada, M., "Fliesspolyeder des Rechteck- und I-Querschnittes unter der Wirkung von Biegemoment, Normalkraft und Querkraft", *Der Stahlbau,* Vol. 27(11), 1958.

[22] Leth, C.-F., "Effect of Shear Stresses on the Carrying Capacity of I-Beams", *Technical Report No. A-11-107,* Brown University, 1954.

[23] Love, A. E. H., **A Treatise on the Mathematical Theory of Elasticity,** Dover Publications, New York, 1944.

[24] Lubliner, J., "A Simple Theory of Plasticity", *International Journal of Solids and Structures,* Vol. 10, 1974.

[25] Lukkunaprasit, P., and Kelly, J. M., "Dynamic Plastic Analysis Using Stress Resultant Finite Element Formulation", *International Journal of Solids and Structures,* Vol. 15, 1979.

[26] Malvern, L. E., **Introduction to the Mechanics of a Continous Medium,** Prentice-Hall, Inc., Englewood Cliffs, New Jersey, 1969.

[27] Manheim, D. N., "On the Design of Eccentrically Braced Frames", Thesis presented to the University of California, Berkeley, in partial fulfillment of the degree of Doctor of Engineering, 1982.

[28] Marsden, J. E., and Hughes, T. J. R., **Mathematical Foundations of Elasticity,** Prentice-Hall, Inc., Englewood Cliffs, New Jersey, 1983.

[29] Neal, B. G., "The Effect of Shear and Normal Forces on the Fully Plastic Moment of a Beam of Rectangular Cross Section", *Journal of Applied Mechanics,* Vol. 28(2), 1961.

[30] Neal, B. G., "Effect of Shear Force on the Fully Plastic Moment of an I-Beam", *Journal of Mechanical Engineering Science,* Vol. 3(3), 1961.

[31] Neal, B. G., "Effect of Shear and Normal Forces on the Fully Plastic Moment of an I-Beam", *Journal of Mechanical Engineering Science,* Vol. 3(3), 1961.

[32] Oden, J. T., **Mechanics of Elastic Structures,** McGraw-Hill Book Company, New York, 1967.

[33] Ortiz, M., "Topics in Constitutive Theory for Inelastic Solids", Thesis presented to the University of California, Berkeley, in partial fulfillment of the degree of Doctor of Philosophy, 1981.

[34] Perzyna, P., "Fundamental Problems in Viscoplasticity," in *Advances in Applied Mechanics,* Vol. 9, Academic Press, New York, 1966.

[35] Pinsky, P. M., Taylor, R. L., and Pister, K. S., "Finite Deformation of Elastic Beams" in *Proceedings* IUTAM Symposium on Variational Methods in the Mechanics of Solids, (S. Nemat-Nasser and K. Washizu, Eds.), Northwestern University, 1978.

[36] Pinsky, P. M., and Taylor, R. L., "A Finite Deformation Formulation for Elasto/Viscoplastic Beam Structures" in **Computational Methods in Nonlinear Mechanics,** (J. T. Oden, Ed.), North Holland Publishing Co., 1980.

[37] Plantema, F. J., **Sandwich Construction: The Bending and Buckling of Sandwich Beams, Plates, and Shells,** John Wiley and Sons, Inc., New York, 1966.

[38] Popov, E. P., and Manheim, D. N., "Eccentric Bracing of Steel Frames in Seismic Design", *Transactions,* 6th International Confrerence on Structural Mechanics in Reactor Technology, Paris, France, Vol. K(b), K13/8, 1981.

[39] Popov, E. P., and Roeder, C. W., "Design of an Eccentrically Braced Frame", *AISC Engineering Journal,* Third Quarter, 1978.

[40] Prager, W., and Hodge, P. G., **Theory of Perfectly Plastic Solids,** John Wiley and Sons, Inc, New York, 1951.

[41] Roeder, C. W., and Popov, E. P., "Cyclic Shear Yielding of Wide Flange Beams", *Journal of the Engineering Mechanics Division,* ASCE, Vol. 104(EM4), 1978.

[42] Roeder, C. W., and Popov, E. P., "Eccentrically Braced Steel Frames for Earthquakes", *Journal of the Structural Division,* ASCE, Vol. 104(ST3), 1978.

[43] Roeder, C. W., and Popov, E. P., "Inelastic Behavior of Eccentrically Braced Steel Frames Under Cyclic Loading", *EERC Report No. 77-18,* University of California, Berkeley, 1977.

[44] Rudin, W., **Principles of Mathematical Analysis,** McGraw-Hill Book Company, New York, 1976.

[45] Simo, J. C., "A Consistent Formulation of Nonlinear Theories of Elastic Beams and Plates," *Report No. UCB/SESM-82/06,* University of California, Berkeley, 1982.

[46] Simo, J. C., Hjelmstad, K. D., and Taylor, R. L., "Finite Element Formulations for Problems of Finite Deformation of Elasto- Viscoplastic Beams," *Report No. UCB/SESM-83/01,* University of California, Berkeley, 1983.

[47] Sokolnikoff, I. S., **Mathematical Theory of Elasticity,** McGraw-Hill Book Company, New York, 1956.

[48] Strang, G. and Fix, G. J., **An Analysis of the Finite Element Method,** Prentice-Hall, Inc., Englewood Cliffs, New Jersey, 1973.

[49] Yang, M. S., "Shaking Table Studies of an Eccentrically X-Braced Frame", Thesis presented to the University of California, Berkeley, in partial fulfillment of the degree of Doctor of Philosophy, 1982.

[50] Zienkiewicz, O. C., **The Finite Element Method,** McGraw-Hill Book Company (UK) Limited, London, 3rd Edition, 1977.

[51] Zienkiewicz, O. C., and Cormeau, I. C., "Vicso-plasticity, Plasticity, and Creep in Elastic Solids -- A Unified Numerical Solution Approach", *International Journal for Numerical Methods in Engineering,* Vol. 8, 1974.

Appendix I

The Effect of Warping Restraint on the Transverse Bending of Thin Walled Beams

I.0. Introduction

For extremely short beams is it well known that plane sections do not remain plane when bent by transversely applied forces. In general, at a boundary which is fixed against displacement and rotation it is impossible to realize freedom to warp simultaneously. Thus, in these situations one has a condition of warping restraint. In this appendix the effect of warping restraint is considered within the context of the linear theory. While the analysis is carried out for thin walled beams, it should be clear how to extend it to sections of any shape. We assume that the axial axis of the beam is aligned with the x_1 coordinate axis, and that the loads are contained in the x_1–x_2 plane.

I.1. Kinematic Hypothesis

In addition to the Cartesian coordinate system $\{x_1,x_2,x_3\}$ we introduce the curvilinear system $\{x,s,n\}$, where the s coordinate coincides with the middle line of the cross section and the n coordinate is orthogonal to it, and $x \equiv x_1$, as shown in Fig. 5.2. In a manner similar to Chapter 5, we shall assume that the deformation of the beam is described by the following displacement field:

$$u_1(x,s) = u(x) - x_2(s)\,\psi(x) - \phi(s)\,\beta(x)$$

$$u_s(x,s) = v(x)\cos\theta(s) \tag{I.1}$$

where $\theta(s)$ measures the angle between the tangent to the cross section and the x_2 axis as shown in Fig. 5.2. Note that

$$\frac{dx_2}{ds} = \cos\theta(s) \qquad \frac{dx_3}{ds} = \sin\theta(s) \tag{I.2}$$

Owing to the thin wall nature of the cross section we can reasonably assume that the shear stress component σ_{1n} vanishes identically throughout the cross section. Hence we have the condition

$$\sigma_{1s} = \sigma_{12}\cos\theta(s) + \sigma_{13}\sin\theta(s)$$

$$0 = \sigma_{12}\sin\theta(s) - \sigma_{13}\cos\theta(s) \tag{I.3}$$

Clearly, from these equations the component σ_{12} can be expressed as

$$\sigma_{12} = \sigma_{1s}\cos\theta(s) \tag{I.4}$$

The non vanishing strain components are readily calculated from (I.1) as

$$\epsilon_{11} = u'(x) - x_2(s)\,\psi'(x) - \phi(s)\,\beta'(x)$$

$$\gamma_{1s} = [\,v'(x) - \psi(x)\,]\cos\theta(s) - \phi'(s)\,\beta(x) \tag{I.5}$$

where a prime denotes differentiation with respect to the argument.

I.2. Equilibrium Equations

Inasmuch as the strains are derived directly from an assumed displacement field they must be compatible. Therefore, the principle of virtual work can be employed to deduce the equations of equilibrium, as well as the appropriate conjugate stress and strain resultants. Assuming that $\sigma_{ss} = \sigma_{sn} = \sigma_{nn} \equiv 0$, the equation of virtual work can be written as

$$\int_0^L \int_\Omega (\sigma_{11}\bar{\epsilon}_{11} + \sigma_{1s}\bar{\gamma}_{1s})\, d\Omega\, dx = \int_0^L (q\bar{v} + p\bar{u})\, dx \tag{I.6}$$

where $q(x)$ and $p(x)$ are the applied transverse and axial loads, and an overbar has been used to denote a "virtual" quantity. Substitution of Eqs. (I.5) into (I.6) and defining the following stress resultants

$$N = \int_\Omega \sigma_{11}\, d\Omega \qquad V = \int_\Omega \sigma_{12}\, d\Omega \qquad H = \int_\Omega \phi'(s)\sigma_{1s}\, d\Omega$$

$$M = -\int_\Omega x_2(s)\sigma_{11}\, d\Omega \qquad W = -\int_\Omega \phi(s)\sigma_{11}\, d\Omega \tag{I.7}$$

we arrive at the statement of virtual work in terms of the defined stress resultants

$$\int_0^L (N\bar{u}' + M\bar{\psi}' + W\bar{\beta}' + V(\bar{v}' - \bar{\psi}) - H\bar{\beta} - q\bar{v} - p\bar{u})\, dx = 0 \tag{I.8}$$

from which one can readily deduce which strain measures are conjugate to which stress measures. Integration by parts leads us to the Euler equations and boundary conditions

$$\begin{aligned} N'(x) + p(x) &= 0 & N(L)\bar{u}(L) - N(0)\bar{u}(0) &= 0 \\ V'(x) + q(x) &= 0 & V(L)\bar{v}(L) - V(0)\bar{v}(0) &= 0 \\ M'(x) + V(x) &= 0 & M(L)\bar{\psi}(L) - M(0)\bar{\psi}(0) &= 0 \\ W'(x) + H(x) &= 0 & W(L)\bar{\beta}(L) - W(0)\bar{\beta}(0) &= 0. \end{aligned} \tag{I.9}$$

Note that the boundary conditions do not involve the stress resultant H.

I.3. Constitutive Equations

Integration of the elastic constitutive equations $E\epsilon_{11} = \sigma_{11}$ and $G\gamma_{1s} = \sigma_{1s}$ over the cross section of the beam leads to the following constitutive equations in terms of stress resultants and strain resultants

$$N = E\Omega u' \qquad M = EI\psi' \qquad W = E\Gamma\beta'$$

$$V = G\Omega_0(\nu'-\psi) - G\Omega_1\beta \qquad H = G\Omega_1(\nu'-\psi) - G\Omega_2\beta \tag{I.10}$$

where the cross sectional properties I, Γ, Ω, Ω_0, Ω_1, and Ω_2 are defined as

$$I = \int_\Omega (x_2)^2\, d\Omega \qquad \Gamma = \int_\Omega \phi^2\, d\Omega \qquad \Omega = \int_\Omega d\Omega$$

$$\Omega_0 = \int_\Omega \cos^2\theta\, d\Omega \qquad \Omega_1 = \int_\Omega \phi'\cos\theta\, d\Omega \qquad \Omega_2 = \int_\Omega (\phi')^2 d\Omega. \tag{I.11}$$

I.4. Equations of Motion

Since the axial equation is uncoupled from the transverse equations it can be integrated independently. Hence no further reference will be made to the axial force N. Substituting Eqs. (I.10) into Eqs. (I.9) we arrive at a system of three second order ordinary differential equations:

$$\begin{aligned} &EI\psi'' + G\Omega_0(\nu'-\psi) - G\Omega_1\beta = 0 \\ &E\Gamma\beta'' + G\Omega_1(\nu'-\psi) - G\Omega_2\beta = 0 \\ &-G\Omega_0(\nu'-\psi)' + G\Omega_1\beta' = q \end{aligned} \tag{I.12}$$

Note that Eqs. (I.12) imply that the cross section of the beam does not vary along the x_1 direction. Extension of these developments to the case of non-cylindrical beams is not difficult. Equations (I.12) can be reduced to the following more convenient form:

$$\begin{aligned} &EI\psi''' = q(x) \\ &\beta'' - \lambda^2\beta = \frac{\Omega_1}{\Omega_0}\frac{I}{\Gamma}\psi'' \\ &\nu' = \psi + \frac{\Omega_1}{\Omega_0}\beta - \frac{EI}{G\Omega_0}\psi'' \end{aligned} \tag{I.13}$$

The parameter λ has been introduced for notational simplicity, and has the expression

$$\lambda^2 = \frac{G\Omega_0}{E\Gamma}\left(\frac{\Omega_0\Omega_2 - \Omega_1\Omega_1}{\Omega_0\Omega_0}\right) \tag{I.14}$$

Also for notational simplicity, we define the cross sectional parameters α_{ij} to be the following

$$\alpha_{ij} \equiv \frac{\Omega_i\,\Omega_j}{\Omega_0\,\Omega_2 - \Omega_1\,\Omega_1} \tag{I.15}$$

where the range of the subscripts i and j is 1,2.

I.5. Homogeneous Solution

For the case in which $q(x) = 0$, Eqs. (I.13) can be evaluated successively by direct quadrature to yield the following results:

$$\psi(x) = a_1 + a_2 x + \frac{a_3}{2}x^2$$

$$\beta(x) = -a_3\frac{EI}{G\Omega_0}\alpha_{01} + a_4 e^{\lambda x} + a_5 e^{-\lambda x} \tag{I.16}$$

$$v(x) = a_6 + [a_1 - a_3\frac{EI}{G\Omega_0}\alpha_{02}]\,x + \frac{a_2}{2}x^2 + \frac{a_3}{6}x^3 + \frac{\Omega_1}{\lambda\Omega_0}[a_4 e^{\lambda x} - a_5 e^{-\lambda x}]$$

where the six unknown constants $a_1, \ldots, a_6$ can be determined from the boundary conditions in particular cases. We now present two examples to illustrate the consequences of introducing the warping variable.

Example 1.- The first case under consideration is that of a cantilever beam subjected to a tip load with the warping *unrestrained* at the fixed end. While this boundary condition may be difficult to realize in a physical situation, the example provides a valuable reference point for the assessment of the effect of warping restraint. The appropriate boundary conditions for this case are

$$v(0) = \psi(0) = \beta'(0) = 0$$

$$\psi'(L) = \beta'(L) = 0 \tag{I.17}$$

$$G\Omega_0[v'(x) - \psi(x)] - G\Omega_1\beta(x) = Q$$

where Q is the applied shear at the tip of the beam. Substitution of these boundary conditions into Eqs. (I.16) lead, after some computation to the results

$$\psi(x) = \frac{Q}{2EI}[2xL - x^2]$$

$$\beta(x) = \frac{Q}{G\Omega_0}\alpha_{01} \tag{I.18}$$

$$v(x) = \frac{Q}{6EI}[3x^2L - x^3] + \frac{Q}{G\Omega_0}\alpha_{02}x$$

Some important results can be seen from this example:

(i) The warping variable β is constant over the length of the beam and proportional to the shear force. Furthermore, the quantity $v' - \psi$ is proportional to β. This result is in accord with the exact solution to Saint Venant's problem [23,45].

(ii) The rotation of the cross section ψ, due to bending, is wholly unaffected by the warping and reproduces exactly the same values as the elementary solution.

(iii) The term in the expression for the transverse displacement v that is due to bending is unaffected by the introduction of the warping degree of freedom. However, the term arising due to transverse shear is modified from the elementary case by a factor of α_{02}. This correction may be identified with the so called *shear coefficient* in Timoshenko's beam theory, and appears naturally as a consequence of the introduction of the warping variable.

Example 2.- The second case considered is that of a cantilever beam with end load and with warping *restrained* at the fixed end. The appropriate boundary conditions for this case are

$$v(0) = \psi(0) = \beta(0) = 0$$

$$\psi'(L) = \beta'(L) = 0 \tag{I.19}$$

$$G\Omega_0[v'(x) - \psi(x)] - G\Omega_1\beta(x) = Q$$

The solution for these boundary conditions can, again, be found from Eqs. (I.15) and has the expressions

$$\psi(x) = \frac{Q}{2EI}[2xL - x^2]$$

$$\beta(x) = \frac{Q}{G\Omega_0}[1 - \delta(x)]\alpha_{01} \tag{I.20}$$

$$v(x) = \frac{Q}{6EI}[3x^2L - x^3] + \frac{Q}{G\Omega_0}[\alpha_{02} - \alpha_{11}\gamma(x)]x$$

where the two functions $\delta(x)$ and $\gamma(x)$[†] have the expressions

$$\delta(x) = \frac{e^{\lambda x} + e^{\lambda(2L-x)}}{1 + e^{2\lambda L}}$$

$$\gamma(x) = \frac{e^{2\lambda L} - 1 + e^{\lambda x} - e^{\lambda(2L-x)}}{\lambda x\,(1 + e^{2\lambda L})} \tag{I.21}$$

The influence of the warping restraint is manifested in the functions $\delta(x)$ and $\gamma(x)$, which depend upon the cross sectional properties through the parameter λ. The two functions are plotted in Fig. I.1 for several values of λL.

To get a feeling for the appropriate magnitude of the parameter λL it is instructive to consider the thin rectangular cross section of depth h and unit thickness. Up to a multiplicative constant, the warping coordinate function $\phi(s)$ is given by (see Eq. 5.30)

[†] The function $\gamma(x)$ should not be confused with the shear strain.

$$\phi(s) = 20\frac{s^3}{h^2} - 3s \tag{I.22}$$

Using this expression in Eqs. (I.11) the cross sectional properties are given by

$$\Omega = h\ ; \qquad \Omega_0 = h\ ; \qquad \Omega_1 = 2h\ ; \qquad \Omega_2 = 24h$$

$$I = \frac{h^3}{12}\ ; \qquad \Gamma = \frac{h^3}{7} \tag{I.23}$$

The "shear coefficient" α_{02} and the parameter λ are then given by Eqs. (I.14) and (I.15), respectively, as

$$\alpha_{02} = \frac{6}{5}\ ; \qquad \lambda = \sqrt{\frac{140G}{E}}\,\frac{1}{h} \tag{I.24}$$

where G and E are the elastic moduli. For an homogeneous, isotropic material having, say $E = 2G$, the parameter λL is

$$\lambda L = 8.4\frac{L}{h} \tag{I.25}$$

Beams having lengths greater than their depth have values of $\lambda L > 10$, for which the effects of warping restraint damp out quite rapidly. For long beams, the effect is negligible.

Although the cross sectional constants are not the same, the form of the solution is precisely the same as that presented by Plantema [37] for the sandwich beam following a completely different approach. The sandwich beam equations can be formulated in precisely the same manner as presented here. The warping coordinate function $\phi(s)$ for this case is a continuous piecewise linear function having a discontinuities of slope at the face-core junctions.

I.6. Inelastic Bending

It is of some interest to consider the effects of warping and warping restraint on the propagation of inelasticity over the cross section of a beam. The problem is nonlinear, and hence we will employ the Finite Element solution procedure presented in Chapter 5. The effects of warping and warping restraint will be illustrated through a numerical example.

Consider the two cantilever beams of rectangular cross section shown in Fig. I.2. The first has length $L = 10$, the second has length $L = 15$, and both have depth $h = 10$. In both cases the transverse load Q is applied at a distance $x = 10$ from the fixed support.

Warping is not restrained at the fixed end of the first (shorter) beam, that is, $\beta(0)$ is not specified as a boundary condition[†]. This case corresponds with Example 1 given previously.

In the second (longer) beam, warping is restrained both at the fixed end and at the point of loading. At the fixed end, restraint is realized by specifying $\beta(0) = 0$, whereas at the point of loading the warping is restrained by the region of beam having vanishing resultant shear.

The load-displacement relationships for the two cases are shown in Fig. I.3. The global elastic stiffnesses (measured as $K = \Delta/Q$, where Δ is the displacement under the load) are nearly identical for the two cases. The beam having restrained warping has an earlier initial yielding than the one in which warping is not restrained. However, the beam without warping restraint collapses at a smaller load than the one with restraint. In fact, the resisted load of the restrained beam at an imposed displacement of $\Delta = 1.1 \times 10^{-3}$ is 11 percent greater than the unrestrained beam.

The importance of including the warping degree-of-freedom for problems involving inelasticity can be seen by considering the evolution of the warping variable $\beta(x)$ as the inelasticity progresses. Again, we consider the two examples at hand.

[†] Vanishing of the bimoment W is the actual boundary condition. This is a natural boundary condition and is not enforced in the Finite Element solution procedure which employs the weak form of the differential equation.

Figure I.4 shows the distribution of β along the length of the beam for the unrestrained case. The load points designated by **A**, **B**, **C**, and **D** are defined on the load-displacement curve, Fig. I.3. At load point **A** the beam is elastic and β is constant, in accordance with the results of Example 1. As inelasticity progresses, β deviates dramatically from the constant distribution near the fixed end. The disturbances increase as inelasticity progresses but damp out rapidly along the length of the beam.

Figure I.5 shows the distribution of $\beta(x)$ at various stages of loading for the restrained beam. At the elastic load level **A** the distribution is no longer constant due to the warping restraint. It can be seen that the restraint imposed by the beam segment with vanishing shear is considerable, but not complete. Apparently, the length of the "tail" required to impose the restraint condition is small. The manifestations of progressive inelasticity are roughly the same as in the previous case except that the value of β at $x=0$ is constrained to be zero. This example is closely related to the active links studied in the experimental program.

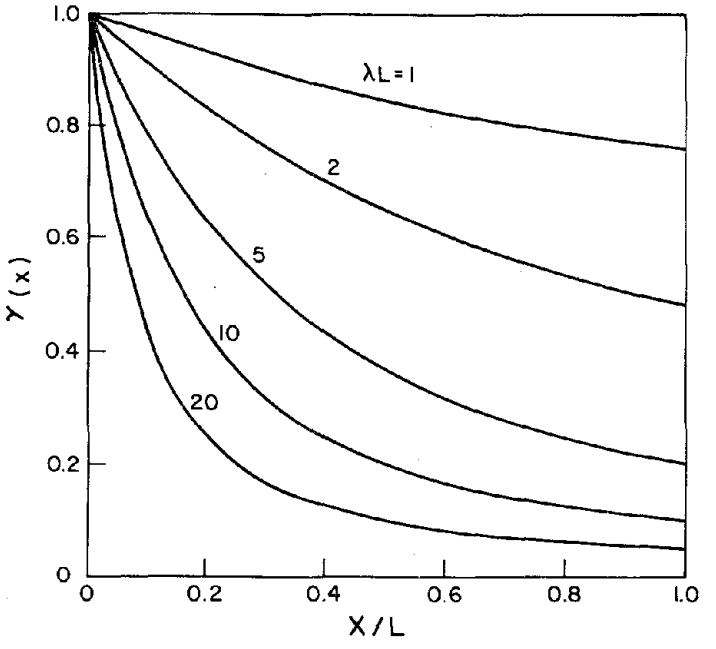

(*a*)

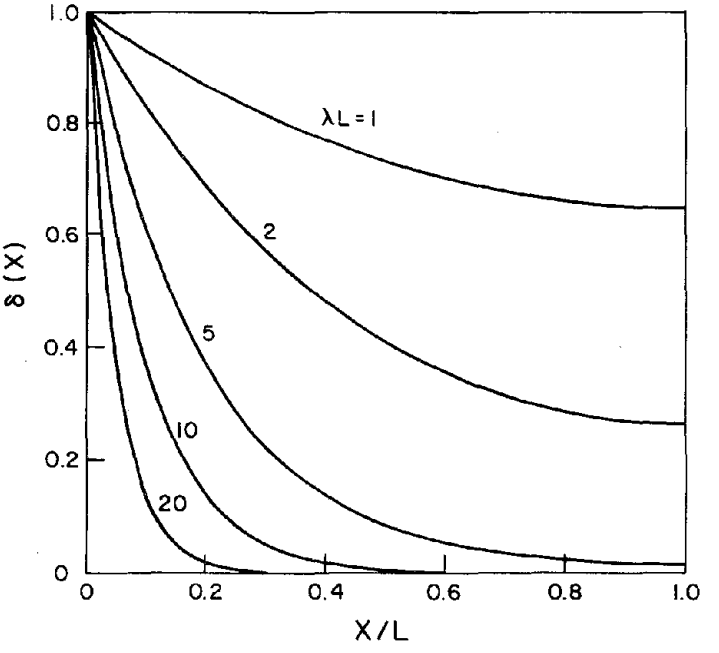

(*b*)

Fig. I.1 Variation of Warping Parameters $\gamma(x)$ and $\delta(x)$

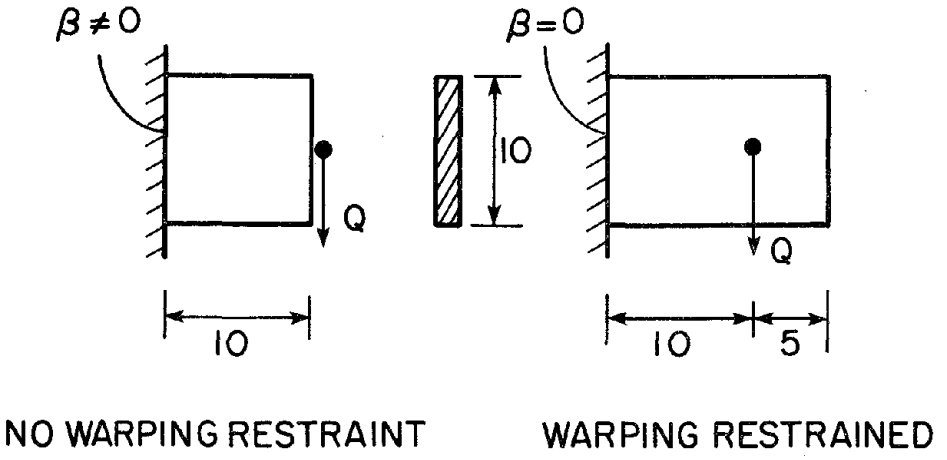

Fig. I.2 Two Cantilever Beams Having Different Warping Boundary Conditions

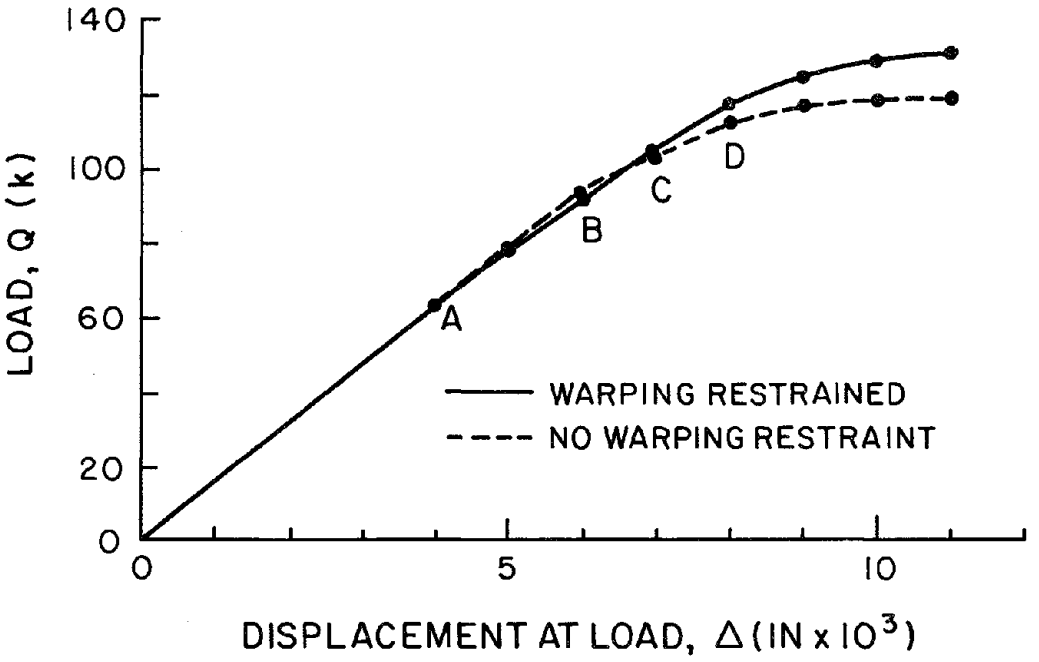

Fig. I.3 Load-Displacement Relation for the Two Cantilevers

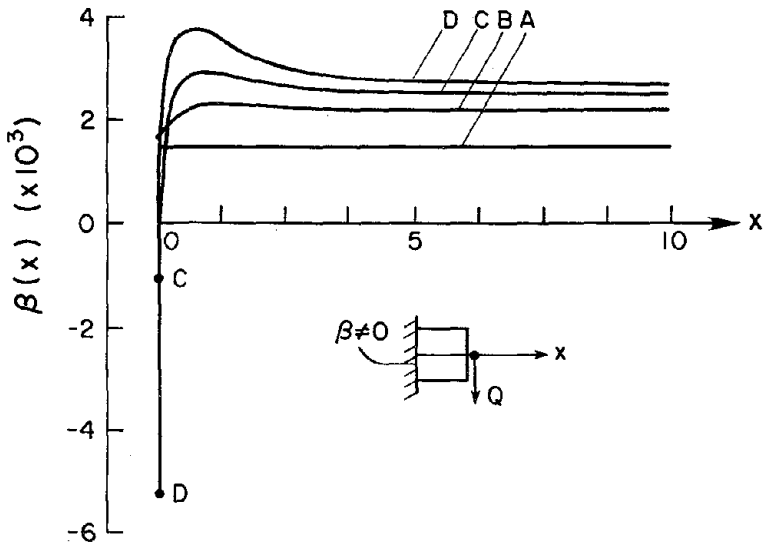

Fig. I.4 Variation of $\beta(x)$ for Cantilever with no Warping Restraint

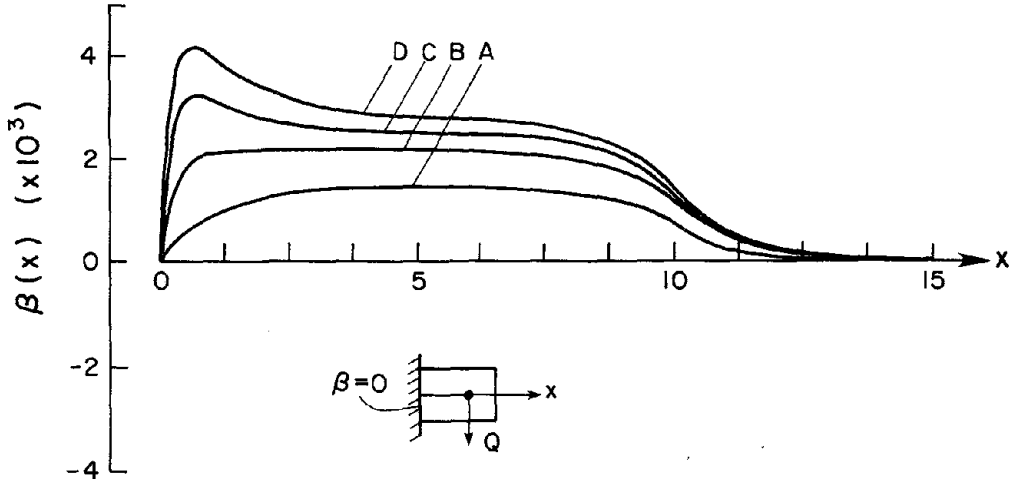

Fig. I.5 Variation of $\beta(x)$ for Cantilever with Warping Restraint

EARTHQUAKE ENGINEERING RESEARCH CENTER REPORTS

NOTE: Numbers in parentheses are Accession Numbers assigned by the National Technical Information Service; these are followed by a price code. Copies of the reports may be ordered from the National Technical Information Service, 5285 Port Royal Road, Springfield, Virginia, 22161. Accession Numbers should be quoted on orders for reports (PB --- ---) and remittance must accompany each order. Reports without this information were not available at time of printing. The complete list of EERC reports (from EERC 67-1) is available upon request from the Earthquake Engineering Research Center, University of California, Berkeley, 47th Street and Hoffman Boulevard, Richmond, California 94804.

UCB/EERC-77/01 "PLUSH - A Computer Program for Probabilistic Finite Element Analysis of Seismic Soil-Structure Interaction," by M.P. Romo Organista, J. Lysmer and H.B. Seed - 1977 (PB81 177 651)A05

UCB/EERC-77/02 "Soil-Structure Interaction Effects at the Humboldt Bay Power Plant in the Ferndale Earthquake of June 7, 1975," by J.E. Valera, H.B. Seed, C.F. Tsai and J. Lysmer - 1977 (PB 265 795)A04

UCB/EERC-77/03 "Influence of Sample Disturbance on Sand Response to Cyclic Loading," by K. Mori, H.B. Seed and C.K. Chan - 1977 (PB 267 352)A04

UCB/EERC-77/04 "Seismological Studies of Strong Motion Records," by J. Shoja-Taheri - 1977 (PB 269 655)A10

UCB/EERC-77/05 Unassigned

UCB/EERC-77/06 "Developing Methodologies for Evaluating the Earthquake Safety of Existing Buildings," by No. 1 - B. Bresler; No. 2 - B. Bresler, T. Okada and D. Zisling; No. 3 - T. Okada and B. Bresler; No. 4 - V.V. Bertero and B. Bresler - 1977 (PB 267 354)A08

UCB/EERC-77/07 "A Literature Survey - Transverse Strength of Masonry Walls," by Y. Omote, R.L. Mayes, S.W. Chen and R.W. Clough - 1977 (PB 277 933)A07

UCB/EERC-77/08 "DRAIN-TABS: A Computer Program for Inelastic Earthquake Response of Three Dimensional Buildings," by R. Guendelman-Israel and G.H. Powell - 1977 (PB 270 693)A07

UCB/EERC-77/09 "SUBWALL: A Special Purpose Finite Element Computer Program for Practical Elastic Analysis and Design of Structural Walls with Substructure Option," by D.Q. Le, H. Peterson and E.P. Popov - 1977 (PB 270 567)A05

UCB/EERC-77/10 "Experimental Evaluation of Seismic Design Methods for Broad Cylindrical Tanks," by D.P. Clough (PB 272 280)A13

UCB/EERC-77/11 "Earthquake Engineering Research at Berkeley - 1976," - 1977 (PB 273 507)A09

UCB/EERC-77/12 "Automated Design of Earthquake Resistant Multistory Steel Building Frames," by N.D. Walker, Jr. - 1977 (PB 276 526)A09

UCB/EERC-77/13 "Concrete Confined by Rectangular Hoops Subjected to Axial Loads," by J. Vallenas, V.V. Bertero and E.P. Popov - 1977 (PB 275 165)A06

UCB/EERC-77/14 "Seismic Strain Induced in the Ground During Earthquakes," by Y. Sugimura - 1977 (PB 284 201)A04

UCB/EERC-77/15 Unassigned

UCB/EERC-77/16 "Computer Aided Optimum Design of Ductile Reinforced Concrete Moment Resisting Frames," by S.W. Zagajeski and V.V. Bertero - 1977 (PB 280 137)A07

UCB/EERC-77/17 "Earthquake Simulation Testing of a Stepping Frame with Energy-Absorbing Devices," by J.M. Kelly and D.F. Tsztoo - 1977 (PB 273 506)A04

UCB/EERC-77/18 "Inelastic Behavior of Eccentrically Braced Steel Frames under Cyclic Loadings," by C.W. Roeder and E.P. Popov - 1977 (PB 275 526)A15

UCB/EERC-77/19 "A Simplified Procedure for Estimating Earthquake-Induced Deformations in Dams and Embankments," by F.I. Makdisi and H.B. Seed - 1977 (PB 276 820)A04

UCB/EERC-77/20 "The Performance of Earth Dams during Earthquakes," by H.B. Seed, F.I. Makdisi and P. de Alba - 1977 (PB 276 821)A04

UCB/EERC-77/21 "Dynamic Plastic Analysis Using Stress Resultant Finite Element Formulation," by P. Lukkunapvasit and J.M. Kelly - 1977 (PB 275 453)A04

UCB/EERC-77/22 "Preliminary Experimental Study of Seismic Uplift of a Steel Frame," by R.W. Clough and A.A. Huckelbridge 1977 (PB 278 769)A08

UCB/EERC-77/23 "Earthquake Simulator Tests of a Nine-Story Steel Frame with Columns Allowed to Uplift," by A.A. Huckelbridge - 1977 (PB 277 944)A09

UCB/EERC-77/24 "Nonlinear Soil-Structure Interaction of Skew Highway Bridges," by M.-C. Chen and J. Penzien - 1977 (PB 276 176)A07

UCB/EERC-77/25 "Seismic Analysis of an Offshore Structure Supported on Pile Foundations," by D.D.-N. Liou and J. Penzien 1977 (PB 283 180)A06

UCB/EERC-77/26 "Dynamic Stiffness Matrices for Homogeneous Viscoelastic Half-Planes," by G. Dasgupta and A.K. Chopra - 1977 (PB 279 654)A06

UCB/EERC-77/27 "A Practical Soft Story Earthquake Isolation System," by J.M. Kelly, J.M. Eidinger and C.J. Derham - 1977 (PB 276 814)A07

UCB/EERC-77/28 "Seismic Safety of Existing Buildings and Incentives for Hazard Mitigation in San Francisco: An Exploratory Study," by A.J. Meltsner - 1977 (PB 281 970)A05

UCB/EERC-77/29 "Dynamic Analysis of Electrohydraulic Shaking Tables," by D. Rea, S. Abedi-Hayati and Y. Takahashi 1977 (PB 282 569)A04

UCB/EERC-77/30 "An Approach for Improving Seismic - Resistant Behavior of Reinforced Concrete Interior Joints," by B. Galunic, V.V. Bertero and E.P. Popov - 1977 (PB 290 870)A06

UCB/EERC-78/01 "The Development of Energy-Absorbing Devices for Aseismic Base Isolation Systems," by J.M. Kelly and D.F. Tsztoo - 1978 (PB 284 978)A04

UCB/EERC-78/02 "Effect of Tensile Prestrain on the Cyclic Response of Structural Steel Connections, by J.G. Bouwkamp and A. Mukhopadhyay - 1978

UCB/EERC-78/03 "Experimental Results of an Earthquake Isolation System using Natural Rubber Bearings," by J.M. Eidinger and J.M. Kelly - 1978 (PB 281 686)A04

UCB/EERC-78/04 "Seismic Behavior of Tall Liquid Storage Tanks," by A. Niwa - 1978 (PB 284 017)A14

UCB/EERC-78/05 "Hysteretic Behavior of Reinforced Concrete Columns Subjected to High Axial and Cyclic Shear Forces," by S.W. Zagajeski, V.V. Bertero and J.G. Bouwkamp - 1978 (PB 283 858)A13

UCB/EERC-78/06 "Three Dimensional Inelastic Frame Elements for the ANSR-I Program," by A. Riahi, D.G. Row and G.H. Powell - 1978 (PB 295 755)A04

UCB/EERC-78/07 "Studies of Structural Response to Earthquake Ground Motion," by O.A. Lopez and A.K. Chopra - 1978 (PB 282 790)A05

UCB/EERC-78/08 "A Laboratory Study of the Fluid-Structure Interaction of Submerged Tanks and Caissons in Earthquakes," by R.C. Byrd - 1978 (PB 284 957)A08

UCB/EERC-78/09 Unassigned

UCB/EERC-78/10 "Seismic Performance of Nonstructural and Secondary Structural Elements," by I. Sakamoto - 1978 (PB81 154 593)A05

UCB/EERC-78/11 "Mathematical Modelling of Hysteresis Loops for Reinforced Concrete Columns," by S. Nakata, T. Sproul and J. Penzien - 1978 (PB 298 274)A05

UCB/EERC-78/12 "Damageability in Existing Buildings," by T. Blejwas and B. Bresler - 1978 (PB 80 166 978)A05

UCB/EERC-78/13 "Dynamic Behavior of a Pedestal Base Multistory Building," by R.M. Stephen, E.L. Wilson, J.G. Bouwkamp and M. Button - 1978 (PB 286 650)A08

UCB/EERC-78/14 "Seismic Response of Bridges - Case Studies," by R.A. Imbsen, V. Nutt and J. Penzien - 1978 (PB 286 503)A10

UCB/EERC-78/15 "A Substructure Technique for Nonlinear Static and Dynamic Analysis," by D.G. Row and G.H. Powell - 1978 (PB 288 077)A10

UCB/EERC-78/16 "Seismic Risk Studies for San Francisco and for the Greater San Francisco Bay Area," by C.S. Oliveira - 1978 (PB 81 120 115)A07

UCB/EERC-78/17 "Strength of Timber Roof Connections Subjected to Cyclic Loads," by P. Gülkan, R.L. Mayes and R.W. Clough - 1978 (HUD-000 1491)A07

UCB/EERC-78/18 "Response of K-Braced Steel Frame Models to Lateral Loads," by J.G. Bouwkamp, R.M. Stephen and E.P. Popov - 1978

UCB/EERC-78/19 "Rational Design Methods for Light Equipment in Structures Subjected to Ground Motion," by J.L. Sackman and J.M. Kelly - 1978 (PB 292 357)A04

UCB/EERC-78/20 "Testing of a Wind Restraint for Aseismic Base Isolation," by J.M. Kelly and D.E. Chitty - 1978 (PB 292 833)A03

UCB/EERC-78/21 "APOLLO - A Computer Program for the Analysis of Pore Pressure Generation and Dissipation in Horizontal Sand Layers During Cyclic or Earthquake Loading," by P.P. Martin and H.B. Seed - 1978 (PB 292 835)A04

UCB/EERC-78/22 "Optimal Design of an Earthquake Isolation System," by M.A. Bhatti, K.S. Pister and E. Polak - 1978 (PB 294 735)A06

UCB/EERC-78/23 "MASH - A Computer Program for the Non-Linear Analysis of Vertically Propagating Shear Waves in Horizontally Layered Deposits," by P.P. Martin and H.B. Seed - 1978 (PB 293 101)A05

UCB/EERC-78/24 "Investigation of the Elastic Characteristics of a Three Story Steel Frame Using System Identification," by I. Kaya and H.D. McNiven - 1978 (PB 296 225)A06

UCB/EERC-78/25 "Investigation of the Nonlinear Characteristics of a Three-Story Steel Frame Using System Identification," by I. Kaya and H.D. McNiven - 1978 (PB 301 363)A05

UCB/EERC-78/26 "Studies of Strong Ground Motion in Taiwan," by Y.M. Hsiung, B.A. Bolt and J. Penzien - 1978 (PB 298 436)A06

UCB/EERC-78/27 "Cyclic Loading Tests of Masonry Single Piers: Volume 1 - Height to Width Ratio of 2," by P.A. Hidalgo, R.L. Mayes, H.D. McNiven and R.W. Clough - 1978 (PB 296 211)A07

UCB/EERC-78/28 "Cyclic Loading Tests of Masonry Single Piers: Volume 2 - Height to Width Ratio of 1," by S.-W.J. Chen, P.A. Hidalgo, R.L. Mayes, R.W. Clough and H.D. McNiven - 1978 (PB 296 212)A09

UCB/EERC-78/29 "Analytical Procedures in Soil Dynamics," by J. Lysmer - 1978 (PB 298 445)A06

UCB/EERC-79/01 "Hysteretic Behavior of Lightweight Reinforced Concrete Beam-Column Subassemblages," by B. Forzani, E.P. Popov and V.V. Bertero - April 1979(PB 298 267)A06

UCB/EERC-79/02 "The Development of a Mathematical Model to Predict the Flexural Response of Reinforced Concrete Beams to Cyclic Loads, Using System Identification," by J. Stanton & H. McNiven - Jan. 1979(PB 295 875)A10

UCB/EERC-79/03 "Linear and Nonlinear Earthquake Response of Simple Torsionally Coupled Systems," by C.L. Kan and A.K. Chopra - Feb. 1979(PB 298 262)A06

UCB/EERC-79/04 "A Mathematical Model of Masonry for Predicting its Linear Seismic Response Characteristics," by Y. Mengi and H.D. McNiven - Feb. 1979(PB 298 266)A06

UCB/EERC-79/05 "Mechanical Behavior of Lightweight Concrete Confined by Different Types of Lateral Reinforcement," by M.A. Manrique, V.V. Bertero and E.P. Popov - May 1979(PB 301 114)A06

UCB/EERC-79/06 "Static Tilt Tests of a Tall Cylindrical Liquid Storage Tank," by R.W. Clough and A. Niwa - Feb. 1979 (PB 301 167)A06

UCB/EERC-79/07 "The Design of Steel Energy Absorbing Restrainers and Their Incorporation into Nuclear Power Plants for Enhanced Safety: Volume 1 - Summary Report," by P.N. Spencer, V.F. Zackay, and E.R. Parker - Feb. 1979(UCB/EERC-79/07)A09

UCB/EERC-79/08 "The Design of Steel Energy Absorbing Restrainers and Their Incorporation into Nuclear Power Plants for Enhanced Safety: Volume 2 - The Development of Analyses for Reactor System Piping,""Simple Systems" by M.C. Lee, J. Penzien, A.K. Chopra and K, Suzuki "Complex Systems" by G.H. Powell, E.L. Wilson, R.W. Clough and D.G. Row - Feb. 1979(UCB/EERC-79/08)A10

UCB/EERC-79/09 "The Design of Steel Energy Absorbing Restrainers and Their Incorporation into Nuclear Power Plants for Enhanced Safety: Volume 3 - Evaluation of Commercial Steels," by W.S. Owen, R.M.N. Pelloux, R.O. Ritchie, M. Faral, T. Ohhashi, J. Toplosky, S.J. Hartman, V.F. Zackay and E.R. Parker - Feb. 1979(UCB/EERC-79/09)A04

UCB/EERC-79/10 "The Design of Steel Energy Absorbing Restrainers and Their Incorporation into Nuclear Power Plants for Enhanced Safety: Volume 4 - A Review of Energy-Absorbing Devices," by J.M. Kelly and M.S. Skinner - Feb. 1979(UCB/EERC-79/10)A04

UCB/EERC-79/11 "Conservatism In Summation Rules for Closely Spaced Modes," by J.M. Kelly and J.L. Sackman - May 1979(PB 301 328)A03

UCB/EERC-79/12 "Cyclic Loading Tests of Masonry Single Piers; Volume 3 - Height to Width Ratio of 0.5," by P.A. Hidalgo, R.L. Mayes, H.D. McNiven and R.W. Clough - May 1979(PB 301 321)A08

UCB/EERC-79/13 "Cyclic Behavior of Dense Course-Grained Materials in Relation to the Seismic Stability of Dams," by N.G. Banerjee, H.B. Seed and C.K. Chan - June 1979(PB 301 373)A13

UCB/EERC-79/14 "Seismic Behavior of Reinforced Concrete Interior Beam-Column Subassemblages," by S. Viwathanatepa, E.P. Popov and V.V. Bertero - June 1979(PB 301 326)A10

UCB/EERC-79/15 "Optimal Design of Localized Nonlinear Systems with Dual Performance Criteria Under Earthquake Excitations," by M.A. Bhatti - July 1979(PB 80 167 109)A06

UCB/EERC-79/16 "OPTDYN - A General Purpose Optimization Program for Problems with or without Dynamic Constraints," by M.A. Bhatti, E. Polak and K.S. Pister - July 1979(PB 80 167 091)A05

UCB/EERC-79/17 "ANSR-II, Analysis of Nonlinear Structural Response, Users Manual," by D.P. Mondkar and G.H. Powell July 1979(PB 80 113 301)A05

UCB/EERC-79/18 "Soil Structure Interaction in Different Seismic Environments," A. Gomez-Masso, J. Lysmer, J.-C. Chen and H.B. Seed - August 1979(PB 80 101 520)A04

UCB/EERC-79/19 "ARMA Models for Earthquake Ground Motions," by M.K. Chang, J.W. Kwiatkowski, R.F. Nau, R.M. Oliver and K.S. Pister - July 1979(PB 301 166)A05

UCB/EERC-79/20 "Hysteretic Behavior of Reinforced Concrete Structural Walls," by J.M. Vallenas, V.V. Bertero and E.P. Popov - August 1979(PB 80 165 905)A12

UCB/EERC-79/21 "Studies on High-Frequency Vibrations of Buildings - 1: The Column Effect," by J. Lubliner - August 1979 (PB 80 158 553)A03

UCB/EERC-79/22 "Effects of Generalized Loadings on Bond Reinforcing Bars Embedded in Confined Concrete Blocks," by S. Viwathanatepa, E.P. Popov and V.V. Bertero - August 1979(PB 81 124 018)A14

UCB/EERC-79/23 "Shaking Table Study of Single-Story Masonry Houses, Volume 1: Test Structures 1 and 2," by P. Gülkan, R.L. Mayes and R.W. Clough - Sept. 1979 (HUD-000 1763)A12

UCB/EERC-79/24 "Shaking Table Study of Single-Story Masonry Houses, Volume 2: Test Structures 3 and 4," by P. Gülkan, R.L. Mayes and R.W. Clough - Sept. 1979 (HUD-000 1836)A12

UCB/EERC-79/25 "Shaking Table Study of Single-Story Masonry Houses, Volume 3: Summary, Conclusions and Recommendations," by R.W. Clough, R.L. Mayes and P. Gülkan - Sept. 1979 (HUD-000 1837)A06

UCB/EERC-79/26 "Recommendations for a U.S.-Japan Cooperative Research Program Utilizing Large-Scale Testing Facilities," by U.S.-Japan Planning Group - Sept. 1979(PB 301 407)A06

UCB/EERC-79/27 "Earthquake-Induced Liquefaction Near Lake Amatitlan, Guatemala," by H.B. Seed, I. Arango, C.K. Chan, A. Gomez-Masso and R. Grant de Ascoli - Sept. 1979(NUREG-CR1341)A03

UCB/EERC-79/28 "Infill Panels: Their Influence on Seismic Response of Buildings," by J.W. Axley and V.V. Bertero Sept. 1979(PB 80 163 371)A10

UCB/EERC-79/29 "3D Truss Bar Element (Type 1) for the ANSR-II Program," by D.P. Mondkar and G.H. Powell - Nov. 1979 (PB 80 169 709)A02

UCB/EERC-79/30 "2D Beam-Column Element (Type 5 - Parallel Element Theory) for the ANSR-II Program," by D.G. Row, G.H. Powell and D.P. Mondkar - Dec. 1979(PB 80 167 224)A03

UCB/EERC-79/31 "3D Beam-Column Element (Type 2 - Parallel Element Theory) for the ANSR-II Program," by A. Riahi, G.H. Powell and D.P. Mondkar - Dec. 1979(PB 80 167 216)A03

UCB/EERC-79/32 "On Response of Structures to Stationary Excitation," by A. Der Kiureghian - Dec. 1979(PB 80166 929)A03

UCB/EERC-79/33 "Undisturbed Sampling and Cyclic Load Testing of Sands," by S. Singh, H.B. Seed and C.K. Chan Dec. 1979(ADA 087 298)A07

UCB/EERC-79/34 "Interaction Effects of Simultaneous Torsional and Compressional Cyclic Loading of Sand," by P.M. Griffin and W.N. Houston - Dec. 1979(ADA 092 352)A15

UCB/EERC-80/01 "Earthquake Response of Concrete Gravity Dams Including Hydrodynamic and Foundation Interaction Effects," by A.K. Chopra, P. Chakrabarti and S. Gupta - Jan. 1980(AD-A087297)A10

UCB/EERC-80/02 "Rocking Response of Rigid Blocks to Earthquakes," by C.S. Yim, A.K. Chopra and J. Penzien - Jan. 1980 (PB80 166 002)A04

UCB/EERC-80/03 "Optimum Inelastic Design of Seismic-Resistant Reinforced Concrete Frame Structures," by S.W. Zagajeski and V.V. Bertero - Jan. 1980(PB80 164 635)A06

UCB/EERC-80/04 "Effects of Amount and Arrangement of Wall-Panel Reinforcement on Hysteretic Behavior of Reinforced Concrete Walls," by R. Iliya and V.V. Bertero - Feb. 1980(PB81 122 525)A09

UCB/EERC-80/05 "Shaking Table Research on Concrete Dam Models," by A. Niwa and R.W. Clough - Sept. 1980(PB81 122 368)A06

UCB/EERC-80/06 "The Design of Steel Energy-Absorbing Restrainers and their Incorporation into Nuclear Power Plants for Enhanced Safety (Vol 1A): Piping with Energy Absorbing Restrainers: Parameter Study on Small Systems," by G.H. Powell, C. Oughourlian and J. Simons - June 1980

UCB/EERC-80/07 "Inelastic Torsional Response of Structures Subjected to Earthquake Ground Motions," by Y. Yamazaki April 1980(PB81 122 327)A08

UCB/EERC-80/08 "Study of X-Braced Steel Frame Structures Under Earthquake Simulation," by Y. Ghanaat - April 1980 (PB81 122 335)A11

UCB/EERC-80/09 "Hybrid Modelling of Soil-Structure Interaction," by S. Gupta, T.W. Lin, J. Penzien and C.S. Yeh May 1980(PB81 122 319)A07

UCB/EERC-80/10 "General Applicability of a Nonlinear Model of a One Story Steel Frame," by B.I. Sveinsson and H.D. McNiven - May 1980(PB81 124 877)A06

UCB/EERC-80/11 "A Green-Function Method for Wave Interaction with a Submerged Body," by W. Kioka - April 1980 (PB81 122 269)A07

UCB/EERC-80/12 "Hydrodynamic Pressure and Added Mass for Axisymmetric Bodies," by F. Nilrat - May 1980(PB81 122 343)A08

UCB/EERC-80/13 "Treatment of Non-Linear Drag Forces Acting on Offshore Platforms," by B.V. Dao and J. Penzien May 1980(PB81 153 413)A07

UCB/EERC-80/14 "2D Plane/Axisymmetric Solid Element (Type 3 - Elastic or Elastic-Perfectly Plastic) for the ANSR-II Program," by D.P. Mondkar and G.H. Powell - July 1980(PB81 122 350)A03

UCB/EERC-80/15 "A Response Spectrum Method for Random Vibrations," by A. Der Kiureghian - June 1980(PB81 122 301)A03

UCB/EERC-80/16 "Cyclic Inelastic Buckling of Tubular Steel Braces," by V.A. Zayas, E.P. Popov and S.A. Mahin June 1980(PB81 124 885)A10

UCB/EERC-80/17 "Dynamic Response of Simple Arch Dams Including Hydrodynamic Interaction," by C.S. Porter and A.K. Chopra - July 1980(PB81 124 000)A13

UCB/EERC-80/18 "Experimental Testing of a Friction Damped Aseismic Base Isolation System with Fail-Safe Characteristics," by J.M. Kelly, K.E. Beucke and M.S. Skinner - July 1980(PB81 148 595)A04

UCB/EERC-80/19 "The Design of Steel Energy-Absorbing Restrainers and their Incorporation into Nuclear Power Plants for Enhanced Safety (Vol 1B): Stochastic Seismic Analyses of Nuclear Power Plant Structures and Piping Systems Subjected to Multiple Support Excitations," by M.C. Lee and J. Penzien - June 1980

UCB/EERC-80/20 "The Design of Steel Energy-Absorbing Restrainers and their Incorporation into Nuclear Power Plants for Enhanced Safety (Vol 1C): Numerical Method for Dynamic Substructure Analysis," by J.M. Dickens and E.L. Wilson - June 1980

UCB/EERC-80/21 "The Design of Steel Energy-Absorbing Restrainers and their Incorporation into Nuclear Power Plants for Enhanced Safety (Vol 2): Development and Testing of Restraints for Nuclear Piping Systems," by J.M. Kelly and M.S. Skinner - June 1980

UCB/EERC-80/22 "3D Solid Element (Type 4-Elastic or Elastic-Perfectly-Plastic) for the ANSR-II Program," by D.P. Mondkar and G.H. Powell - July 1980(PB81 123 242)A03

UCB/EERC-80/23 "Gap-Friction Element (Type 5) for the ANSR-II Program," by D.P. Mondkar and G.H. Powell - July 1980 (PB81 122 285)A03

UCB/EERC-80/24 "U-Bar Restraint Element (Type 11) for the ANSR-II Program," by C. Oughourlian and G.H. Powell July 1980(PB81 122 293)A03

UCB/EERC-80/25 "Testing of a Natural Rubber Base Isolation System by an Explosively Simulated Earthquake," by J.M. Kelly - August 1980(PB81 201 360)A04

UCB/EERC-80/26 "Input Identification from Structural Vibrational Response," by Y. Hu - August 1980(PB81 152 308)A05

UCB/EERC-80/27 "Cyclic Inelastic Behavior of Steel Offshore Structures," by V.A. Zayas, S.A. Mahin and E.P. Popov August 1980(PB81 196 180)A15

UCB/EERC-80/28 "Shaking Table Testing of a Reinforced Concrete Frame with Biaxial Response," by M.G. Oliva October 1980(PB81 154 304)A10

UCB/EERC-80/29 "Dynamic Properties of a Twelve-Story Prefabricated Panel Building," by J.G. Bouwkamp, J.P. Kollegger and R.M. Stephen - October 1980(PB82 117 128)A06

UCB/EERC-80/30 "Dynamic Properties of an Eight-Story Prefabricated Panel Building," by J.G. Bouwkamp, J.P. Kollegger and R.M. Stephen - October 1980(PB81 200 313)A05

UCB/EERC-80/31 "Predictive Dynamic Response of Panel Type Structures Under Earthquakes," by J.P. Kollegger and J.G. Bouwkamp - October 1980(PB81 152 316)A04

UCB/EERC-80/32 "The Design of Steel Energy-Absorbing Restrainers and their Incorporation into Nuclear Power Plants for Enhanced Safety (Vol 3): Testing of Commercial Steels in Low-Cycle Torsional Fatigue," by P. Spencer, E.R. Parker, E. Jongewaard and M. Drory

UCB/EERC-80/33 "The Design of Steel Energy-Absorbing Restrainers and their Incorporation into Nuclear Power Plants for Enhanced Safety (Vol 4): Shaking Table Tests of Piping Systems with Energy-Absorbing Restrainers," by S.F. Stiemer and W.G. Godden - Sept. 1980

UCB/EERC-80/34 "The Design of Steel Energy-Absorbing Restrainers and their Incorporation into Nuclear Power Plants for Enhanced Safety (Vol 5): Summary Report," by P. Spencer

UCB/EERC-80/35 "Experimental Testing of an Energy-Absorbing Base Isolation System," by J.M. Kelly, M.S. Skinner and K.E. Beucke - October 1980(PB81 154 072)A04

UCB/EERC-80/36 "Simulating and Analyzing Artificial Non-Stationary Earthquake Ground Motions," by R.F. Nau, R.M. Oliver and K.S. Pister - October 1980(PB81 153 397)A04

UCB/EERC-80/37 "Earthquake Engineering at Berkeley - 1980," - Sept. 1980(PB81 205 874)A09

UCB/EERC-80/38 "Inelastic Seismic Analysis of Large Panel Buildings," by V. Schricker and G.H. Powell - Sept. 1980 (PB81 154 338)A13

UCB/EERC-80/39 "Dynamic Response of Embankment, Concrete-Gravity and Arch Dams Including Hydrodynamic Interaction," by J.F. Hall and A.K. Chopra - October 1980(PB81 152 324)A11

UCB/EERC-80/40 "Inelastic Buckling of Steel Struts Under Cyclic Load Reversal," by R.G. Black, W.A. Wenger and E.P. Popov - October 1980(PB81 154 312)A08

UCB/EERC-80/41 "Influence of Site Characteristics on Building Damage During the October 3, 1974 Lima Earthquake," by P. Repetto, I. Arango and H.B. Seed - Sept. 1980(PB81 161 739)A05

UCB/EERC-80/42 "Evaluation of a Shaking Table Test Program on Response Behavior of a Two Story Reinforced Concrete Frame," by J.M. Blondet, R.W. Clough and S.A. Mahin

UCB/EERC-80/43 "Modelling of Soil-Structure Interaction by Finite and Infinite Elements," by F. Medina - December 1980(PB81 229 270)A04

UCB/EERC-81/01 "Control of Seismic Response of Piping Systems and Other Structures by Base Isolation," edited by J.M. Kelly - January 1981 (PB81 200 735)A05

UCB/EERC-81/02 "OPTNSR - An Interactive Software System for Optimal Design of Statically and Dynamically Loaded Structures with Nonlinear Response," by M.A. Bhatti, V. Ciampi and K.S. Pister - January 1981 (PB81 218 851)A09

UCB/EERC-81/03 "Analysis of Local Variations in Free Field Seismic Ground Motions," by J.-C. Chen, J. Lysmer and H.B. Seed - January 1981 (AD-A099508)A13

UCB/EERC-81/04 "Inelastic Structural Modeling of Braced Offshore Platforms for Seismic Loading," by V.A. Zayas, P.-S.B. Shing, S.A. Mahin and E.P. Popov - January 1981(PB82 138 777)A07

UCB/EERC-81/05 "Dynamic Response of Light Equipment in Structures," by A. Der Kiureghian, J.L. Sackman and B. Nour-Omid - April 1981 (PB81 218 497)A04

UCB/EERC-81/06 "Preliminary Experimental Investigation of a Broad Base Liquid Storage Tank," by J.G. Bouwkamp, J.P. Kollegger and R.M. Stephen - May 1981(PB82 140 385)A03

UCB/EERC-81/07 "The Seismic Resistant Design of Reinforced Concrete Coupled Structural Walls," by A.E. Aktan and V.V. Bertero - June 1981(PB82 113 358)A11

UCB/EERC-81/08 "The Undrained Shearing Resistance of Cohesive Soils at Large Deformations," by M.R. Pyles and H.B. Seed - August 1981

UCB/EERC-81/09 "Experimental Behavior of a Spatial Piping System with Steel Energy Absorbers Subjected to a Simulated Differential Seismic Input," by S.F. Stiemer, W.G. Godden and J.M. Kelly - July 1981

UCB/EERC-81/10 "Evaluation of Seismic Design Provisions for Masonry in the United States," by B.I. Sveinsson, R.L. Mayes and H.D. McNiven - August 1981 (PB82 166 075)A08

UCB/EERC-81/11 "Two-Dimensional Hybrid Modelling of Soil-Structure Interaction," by T.-J. Tzong, S. Gupta and J. Penzien - August 1981(PB82 142 118)A04

UCB/EERC-81/12 "Studies on Effects of Infills in Seismic Resistant R/C Construction," by S. Brokken and V.V. Bertero - September 1981 (PB82 166 190)A09

UCB/EERC-81/13 "Linear Models to Predict the Nonlinear Seismic Behavior of a One-Story Steel Frame," by H. Valdimarsson, A.H. Shah and H.D. McNiven - September 1981(PB82 138 793)A07

UCB/EERC-81/14 "TLUSH: A Computer Program for the Three-Dimensional Dynamic Analysis of Earth Dams," by T. Kagawa, L.H. Mejia, H.B. Seed and J. Lysmer - September 1981(PB82 139 940)A06

UCB/EERC-81/15 "Three Dimensional Dynamic Response Analysis of Earth Dams," by L.H. Mejia and H.B. Seed - September 1981 (PB82 137 274)A12

UCB/EERC-81/16 "Experimental Study of Lead and Elastomeric Dampers for Base Isolation Systems," by J.M. Kelly and S.B. Hodder - October 1981 (PB82 166 182)A05

UCB/EERC-81/17 "The Influence of Base Isolation on the Seismic Response of Light Secondary Equipment," by J.M. Kelly - April 1981 (PB82 255 266)A04

UCB/EERC-81/18 "Studies on Evaluation of Shaking Table Response Analysis Procedures," by J. Marcial Blondet - November 1981 (PB82 197 278)A10

UCB/EERC-81/19 "DELIGHT.STRUCT: A Computer-Aided Design Environment for Structural Engineering," by R.J. Balling, K.S. Pister and E. Polak - December 1981 (PB82 218 496)A07

UCB/EERC-81/20 "Optimal Design of Seismic-Resistant Planar Steel Frames," by R.J. Balling, V. Ciampi, K.S. Pister and E. Polak - December 1981 (PB82 220 179)A07

UCB/EERC-82/01 "Dynamic Behavior of Ground for Seismic Analysis of Lifeline Systems," by T. Sato and A. Der Kiureghian - January 1982 (PB82 218 926)A05

UCB/EERC-82/02 "Shaking Table Tests of a Tubular Steel Frame Model," by Y. Ghanaat and R. W. Clough - January 1982 (PB82 220 161)A07

UCB/EERC-82/03 "Behavior of a Piping System under Seismic Excitation: Experimental Investigations of a Spatial Piping System supported by Mechanical Shock Arrestors and Steel Energy Absorbing Devices under Seismic Excitation," by S. Schneider, H.-M. Lee and W. G. Godden - May 1982 (PB83 172 544)A09

UCB/EERC-82/04 "New Approaches for the Dynamic Analysis of Large Structural Systems," by E. L. Wilson - June 1982 (PB83 148 080)A05

UCB/EERC-82/05 "Model Study of Effects of Damage on the Vibration Properties of Steel Offshore Platforms," by F. Shahrivar and J. G. Bouwkamp - June 1982 (PB83 148 742)A10

UCB/EERC-82/06 "States of the Art and Practice in the Optimum Seismic Design and Analytical Response Prediction of R/C Frame-Wall Structures," by A. E. Aktan and V. V. Bertero - July 1982 (PB83 147 736)A05

UCB/EERC-82/07 "Further Study of the Earthquake Response of a Broad Cylindrical Liquid-Storage Tank Model," by G. C. Manos and R. W. Clough - July 1982 (PB83 147 744)A11

UCB/EERC-82/08 "An Evaluation of the Design and Analytical Seismic Response of a Seven Story Reinforced Concrete Frame - Wall Structure," by F. A. Charney and V. V. Bertero - July 1982(PB83 157 628)A09

UCB/EERC-82/09 "Fluid-Structure Interactions: Added Mass Computations for Incompressible Fluid," by J. S.-H. Kuo - August 1982 (PB83 156 281)A07

UCB/EERC-82/10 "Joint-Opening Nonlinear Mechanism: Interface Smeared Crack Model," by J. S.-H. Kuo - August 1982 (PB83 149 195)A05

UCB/EERC-82/11 "Dynamic Response Analysis of Techi Dam," by R. W. Clough, R. M. Stephen and J. S.-H. Kuo - August 1982 (PB83 147 496)A06

UCB/EERC-82/12 "Prediction of the Seismic Responses of R/C Frame-Coupled Wall Structures," by A. E. Aktan, V. V. Bertero and M. Piazza - August 1982 (PB83 149 203)A09

UCB/EERC-82/13 "Preliminary Report on the SMART 1 Strong Motion Array in Taiwan," by B. A. Bolt, C. H. Loh, J. Penzien, Y. B. Tsai and Y. T. Yeh - August 1982 (PB83 159 400)A10

UCB/EERC-82/14 "Shaking-Table Studies of an Eccentrically X-Braced Steel Structure," by M. S. Yang - September 1982

UCB/EERC-82/15 "The Performance of Stairways in Earthquakes," by C. Roha, J. W. Axley and V. V. Bertero - September 1982 (PB83 157 693)A07

UCB/EERC-82/16 "The Behavior of Submerged Multiple Bodies in Earthquakes," by W.-G. Liao - Sept. 19[illegible] (PB83 158 709)A07

UCB/EERC-82/17 "Effects of Concrete Types and Loading Conditions on Local Bond-Slip Relationships," by A. D. Cowell, E. P. Popov and V. V. Bertero - September 1982 (PB83 153 577)A04

UCB/EERC-82/18 "Mechanical Behavior of Shear Wall Vertical Boundary Members: An Experimental Investigation," by M. T. Wagner and V. V. Bertero - October 1982 (PB83 159 764)A05

UCB/EERC-82/19 "Experimental Studies of Multi-support Seismic Loading on Piping Systems," by J. M. Kelly and A. D. Cowell - November 1982

UCB/EERC-82/20 "Generalized Plastic Hinge Concepts for 3D Beam-Column Elements," by P. F.-S. Chen and G. H. Powell - November 1982

UCB/EERC-82/21 "ANSR-III: General Purpose Computer Program for Nonlinear Structural Analysis," by C. V. Oughourlian and G. H. Powell - November 1982

UCB/EERC-82/22 "Solution Strategies for Statically Loaded Nonlinear Structures," by J. W. Simons and G. H. Powell - November 1982

UCB/EERC-82/23 "Analytical Model of Deformed Bar Anchorages under Generalized Excitations," by V. Ciampi, R. Eligehausen, V. V. Bertero and E. P. Popov - November 1982 (PB83 169 532)A06

UCB/EERC-82/24 "A Mathematical Model for the Response of Masonry Walls to Dynamic Excitations," by H. Sucuoğlu, Y. Mengi and H. D. McNiven - November 1982 (PB83 169 011)A07

UCB/EERC-82/25 "Earthquake Response Considerations of Broad Liquid Storage Tanks," by F. J. Cambra - November 1982

UCB/EERC-82/26 "Computational Models for Cyclic Plasticity, Rate Dependence and Creep," by B. Mosaddad and G. H. Powell - November 1982

UCB/EERC-82/27 "Inelastic Analysis of Piping and Tubular Structures," by M. Mahasuverachai and G. H. Powell - November 1982

UCB/EERC-83/01 "The Economic Feasibility of Seismic Rehabilitation of Buildings by Base Isolation," by J. M. Kelly - January 1983

UCB/EERC-83/02 "Seismic Moment Connections for Moment-Resisting Steel Frames," by E. P. Popov - January 1983

UCB/EERC-83/03 "Design of Links and Beam-to-Column Connections for Eccentrically Braced Steel Frames," by E. P. Popov and J. O. Malley - January 1983

UCB/EERC-83/04 "Numerical Techniques for the Evaluation of Soil-Structure Interaction Effects in the Time Domain," by E. Bayo and E. L. Wilson - February 1983

UCB/EERC-83/05 "A Transducer for Measuring the Internal Forces in the Columns of a Frame-Wall Reinforced Concrete Structure," by R. Sause and V. V. Bertero - May 1983

UCB/EERC-83/06 "Dynamic Interactions between Floating Ice and Offshore Structures," by P. Croteau - May 1983

UCB/EERC-83/07 "Dynamic Analysis of Multiply Tunnelled and Arbitrarily Supported Secondary Systems," by T. Igusa and A. Der Kiureghian - June 1983

UCB/EERC-83/08 "A Laboratory Study of Submerged Multi-body Systems in Earthquakes," by G. R. Ansari - June 1983

UCB/EERC-83/09 "Effects of Transient Foundation Uplift on Earthquake Response of Structures," by C.-S. Yim and A. K. Chopra - June 1983

UCB/EERC-83/10 "Optimal Design of Friction-Braced Frames under Seismic Loading," by M. A. Austin and K. S. Pister - June 1983

UCB/EERC-83/11 "Shaking Table Study of Single-Story Masonry Houses: Earthquake Performance under Three Component Simulated Seismic Input and Recommendations," by G. C. Manos, R. W. Clough and R. L. Mayes - June 1983

UCB/EERC-83/12 "Experimental Error Propagation in Pseudodynamic Testing," by P. B. Shing and S. A. Mahin - June 1983

UCB/EERC-83/13 "Experimental and Analytical Predictions of the Mechanical Characteristics of a 1/5-scale Model of a 7-story R/C Frame-Wall Building Structure," by A. E. Aktan, V. V. Bertero, A. A. Chowdhury and T. Nagashima - August 1983

UCB/EERC-83/14 "Shaking Table Tests of Large-Panel Precast Concrete Building System Assemblages," by M. G. Oliva and R. W. Clough - August 1983

UCB/EERC-83/15 "Seismic Behavior of Active Beam Links in Eccentrically Braced Frames," by K. D. Hjelmstad and E. P. Popov - July 1983